

71-12,556

CHIU, Chen-hwa, 1939-

LIQUID DENSITY, EXCESS PROPERTIES, AND THE
STATISTICAL THERMODYNAMICS OF ARGON, KRYPTON,
AND XENON BINARY LIQUID MIXTURES AT LOW
TEMPERATURE AND SATURATION PRESSURE.

The University of Oklahoma, Ph.D., 1970
Engineering, chemical

University Microfilms, A XEROX Company, Ann Arbor, Michigan

THE UNIVERSITY OF OKLAHOMA
GRADUATE COLLEGE

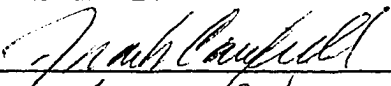
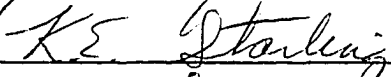
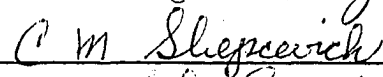
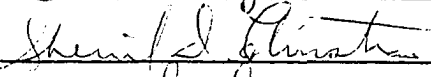
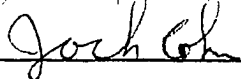
LIQUID DENSITY, EXCESS PROPERTIES, AND THE STATISTICAL
THERMODYNAMICS OF ARGON, KRYPTON, AND XENON BINARY
LIQUID MIXTURES AT LOW TEMPERATURE
AND SATURATION PRESSURE

A DISSERTATION
SUBMITTED TO THE GRADUATE FACULTY
in partial fulfillment of the requirements for the
degree of
DOCTOR OF PHILOSOPHY IN CHEMICAL ENGINEERING

BY
CHEN-HWA CHIU
Norman, Oklahoma
1970

LIQUID DENSITY, EXCESS PROPERTIES, AND THE STATISTICAL
THERMODYNAMICS OF ARGON, KRYPTON, AND XENON BINARY
LIQUID MIXTURES AT LOW TEMPERATURE
AND SATURATION PRESSURE

APPROVED BY

DISSERTATION COMMITTEE

TO
MY FATHER AND MY MOTHER

ACKNOWLEDGEMENTS

I would like to express my sincere gratitude to the following persons and organizations:

Dr. Frank B. Canfield -- for his able guidance and assistance in all phases of the experimental and theoretical work. His patience and encouragement helped to bring this work to its fruition.

Dr. Sherril . Christian -- for his advice as my thesis advisory committee member and for his hospitality in serving as my host family during my not too brief stay in Norman.

Dr. Cedomir M. Sliepcevich, Dr. Kenneth E. Starling, and Dr. Jack Cohn -- for their advice and willingness to serve in my thesis advisory committee.

Dr. M. Y. Shana'a -- for his help in the initial stage of this work.

Mr. Richard Bates, Mr. Gene J. Scott, and Mr. Ron Stermer -- for their prompt actions and skillful help in remodeling the experimental apparatus.

Phillips Petroleum Company and School of Chemical Engineering and Materials Science at The University of Oklahoma -- for their financial assistance through fellowship.

Allied Chemical Corporation and E. I. duPont de Nemours -- for their donation of monochlorotrifluoromethane needed for the bath fluid.

Directorate of Chemical Sciences, Air Force Office of Scientific Research -- for support of this work with a research grant.

Dr. Lewis C. Yen, Dr. L. Michael Shipman, and the Chemical Engineering Data Department of The Lummus Company-- for support of computer time and assistance in the final stage of this work.

Dr. L. A. K. Staveley of the Inorganic Chemistry Laboratory, Oxford University -- for his discussions and communications.

Dr. Chen-yen Cheng -- for his first introducing me to the versatility of thermodynamics and phase rules while at the National Taiwan University.

Mr. Jerry L. Haluska, Mr. Luther Davis Clements, and Mr. Norman F. Carnahan -- for their help in proofreading the dissertation reading copy.

Misses Mary Anne Matthews and Margaret Williford -- for typing the dissertation final copy.

My father and my mother -- for their encouragement, understanding, and patience.

ABSTRACT

An experimental apparatus was remodeled and constructed with novel design considerations. The apparatus was operable between 77°K and 300°K and pressure up to 200 psia for determining cryogenic liquid and liquid mixture densities with extremely high accuracy and reproducibility.

Liquid density data of argon and krypton at 115.77°K and at saturation pressure up to 138.1 psia were determined in full composition range. Liquid density data of krypton and xenon at 161.36°K and at saturation pressure up to 159.5 psia were also determined over the full composition range. The accuracy of data was established by an error analysis. The largest error is within 6×10^{-4} gm/cm³. The liquid density of argon and xenon at 115.77°K with 0.875 argon mole fraction also was determined.

The excess volume, V^E , and the excess Gibbs energy, G^E , were extracted from the experimental density - total pressure data with an iterative method based on thermodynamic analysis. The results confirmed the V^E , and G^E values of argon and krypton mixture at 115.77°K obtained by Staveley and co-workers at Oxford University. The asymmetry, though small, in both the (V^E, X_1) and (G^E, X_1)

curves was confirmed for both the Ar + Kr and Kr + Xe systems (where X_1 denotes the mole fraction of the more volatile component in the binary mixture). The results in Kr + Xe system did not agree with those obtained by Staveley, et al. Comparisons between the Ar + Kr and Kr + Xe systems showed that the results obtained in this investigation are consistent while those of Staveley, et al. are not.

Statistical thermodynamics of the binary liquid mixtures of argon, krypton, and xenon were studied and compared with the present experimental results in three different approaches.

In the average potential model approach, the van der Waals two liquid model in conjunction with the Srivastava and Madan rule for the length parameter and Canfield's rule for the energy parameter gives better prediction in both V^E and G^E . However, the model approach predicts only very slight asymmetry in the excess function versus composition curves.

The perturbation equation of state approach was studied in its simplified version. The liquid mixture equation of state as given by Longuet-Higgins, Widom, and Lebowitz was used to calculate excess properties and pure liquid density. The equation of state parameters were determined at the normal boiling temperature. This approach did predict G^E quantitatively and also

presented the asymmetry in both the (V^E, X_1) and (G^E, X_1) curves. However, the equation of state parameters were responsible for poor liquid density predictions when the system temperature was not close to that of the normal boiling point of the pure component.

A generalized equation of state was proposed and examined in its flexibility of accommodating the empiricism on the hard sphere repulsive part of the equation of state. The Longuet-Higgins and Widom equation of state again fared better in the context of Lorentz-Berthelot mixture. This approach is essentially the one fluid principle of corresponding states approach. However, it was found that both the inability of the equation of state in predicting Z_c and the temperature dependency of the equation of state parameters may be responsible for its present weakness.

TABLE OF CONTENTS

	Page
LIST OF TABLES	xiii
LIST OF ILLUSTRATIONS.	xvii
 Chapter	
I. INTRODUCTION	1
II. REVIEW OF PREVIOUS WORK	4
Density Date of Liquid Argon. Krypton, Xenon and Their Mixtures.	4
Previous Density Experiments.	6
III. EXPERIMENTAL APPARATUS.	8
Cryostat and Temperature Control.	8
High Pressure Weighing Bomb and Weighing Equipment	17
Pycnometer and Periscope Assembly	21
Temperature and Pressure Measurements	30
Valves, Tubings, and Vacuum Systems	30
Transfer Line Between the Weighing Bomb and the Pycnometer.	32
IV. MATERIALS USED.	34
Bath Fluid.	34
Research Grade Heavy Rare Gases	35
Research Grade Hydrocarbons	40
V. EXPERIMENTAL PROCEDURE AND PROBLEM.	42
Cool Down the Cryostat to Operating Temperature	42
Charging and Weighing of the High Pressure Sample Bomb	46

Chapter	Page
Condensation of Gas Sample into the Pycnometer.	48
Condensation Process in a Pure Component Run	49
Condensation Process in a Mixture Run	50
Liquid Volume Reading Procedure by Using the Cryogenic Periscope in Conjunction with a Cathetometer	51
Experimental Run of the Argon and Xenon Mixture	52
Completion of the Experimental Runs	53
VI. DATA AND APPLICATIONS	54
Experimental Results.	54
Argon and Xenon Mixture	59
Accuracy of Experimental Results.	68
Application of Experimental Results, Calculation of Excess Volume.	74
Calculation of Excess Gibbs Energy from the Experimental Data	85
Excess Gibbs Energy for the Heavy Rare Gas Liquid Mixtures	88
VII. MODIFIED AVERAGE POTENTIAL MODEL OF LIQUID MIXTURES.	97
Previous Methods and Present Methods.	97
Mixing Rules of Force Constants	109
Kihara Spherical Core Potential and Three Parameter Principle of Corresponding States.	113
Results of the Average Potential Model Calculations.	115
VIII. PERTURBATION APPROACH BASED ON HARD SPHERE EQUATION OF STATE	127
The Percus - Yevick Equation of State	128
Perturbation Approach, Single Component	131
Perturbation Approach for Mixtures.	134
Fundamental Equations for Hard Sphere Model of Binary Liquid Mixtures	135
Calculation of Excess Properties for Binary Liquid Mixture of Argon and Krypton, and Krypton and Xenon.	137

Chapter	Page
IX. CALCULATION OF THE BINARY LIQUID MIXTURE PROPERTIES BASED ON THE GENERALIZED EQUATION OF STATES.	148
Characteristic Constants of the Generalized Equation of State	153
Derivations of the Equations for Calculating Excess Thermodynamic Functions from the Equation of State	155
Excess Functions According to the Generalized Equation of State	158
Results of Calculation and the Temperature Dependency of Parameters.	161
X. CONCLUSIONS AND RECOMMENDATION FOR FURTHER WORK.	168
Conclusions	168
Recommendation for Further Work	169
BIBLIOGRAPHY.	171
APPENDICES	
A. CALIBRATION OF PYCNOMETER	178
The Density of Liquid Water	178
Calibration of Pycnometer by Differential Weighing with Distilled Water	180
Recalibration of Fused Quartz Pycnometer.	182
Calibration of the Pyrex Pycnometer	189
Calibration of Pyrex Pycnometer at Operation Temperatures Against the Quartz Pycnometer	191
Pressure Effect on Pycnometer Volume.	198
B. TEMPERATURE MEASUREMENT AND MASS MEASUREMENT	200
Temperature Measurement	200
Mass Measurement.	201
The Effect of the Variations in the Buoyancy Correction	204
C. ERROR ANALYSIS.	206
Estimation of the Partial Derivatives	207
Estimation of Errors Incurred in Each Individual Measurement.	207

Chapter	Page
D. TRANSFER LINE GAS CALCULATIONS.	214
Determination of the Volume of the Transfer Line	214
Determination of the Sample Gas Trapped inside the Transfer Line and the Dead- Space in Pycnometer	218

LIST OF TABLES

Table	Page
1. Some Characteristic Properties of Mono-chlorotrifluoromethane.	36
2. Saturated Liquid Density and Molar Volume of the Pure Components Argon, Krypton, and Xenon	56
3. Saturated Densities of Liquefied Heavy Rare Gases.	57
4. Saturated Vapor Pressures of Argon, Krypton, and Xenon, and Their Binary Mixtures Expressed in Terms of Antoine Constants . .	60
5. Saturated Liquid Density and Molar Volume of the Binary Mixtures Argon + Krypton, Krypton + Xenon, and Argon + Xenon.	64
6. Saturated Liquid Density and Molar Volume of the Pure Components Argon, Krypton, Xenon .	66
7. Saturated Liquid Density and Excess Volume of the Binary Liquid Mixtures of Argon, Krypton, and Xenon.	67
8. Comparison of Experimental Liquid Molar Volume with Results of Staveley and co-Workers.	71
9. Least Square Fit Constants for Excess Volume of Binary Liquid Mixtures of Argon and Krypton, and of Krypton and Xenon to the Equation.	79
10. Smoothed Experimental Excess Volumes of Argon and Krypton Mixtures at 115.77°K.	80

Table	Page
11. Smoothed Experimental Excess Volumes of Krypton and Xenon Mixtures at 161.36°K. . .	81
12. Data Used for the Iterative Calculations of the Excess Gibbs Energy for Binary Liquid Mixtures of Argon and Krypton, and Krypton and Xenon	89
13. Excess Gibbs Energy of Argon and Krypton Binary Liquid Mixtures at 115.77°K.	90
14. Excess Gibbs Energy of Krypton and Xenon Binary Liquid Mixtures at 161.36°K.	93
15. Least Square Fit Constants for Excess Gibbs Energy of Binary Liquid Mixtures of Argon and Krypton, and of Krypton and Xenon to Redlich-Kister Equation $G^E/(RTx_1x_2) = A+B(x_1-x_2)+C(x_1-x_2)^2$	94
16. Comparison of Excess Gibbs Energy for the Equimolar Mixtures of Argon + Krypton, and of Krypton + Xenon.	96
17. Pure Components Data used in the Average Potential Model Calculations.	116
18. Comparison of Mixing Rules of Force Constants	116
19. Comparison of Calculation Results for Equimolar Liquid Mixture of Argon and Krypton at 115.77°K Based on Average Potential Model Approaches (Simon Equation for $w(\tilde{T})$).	117
20. Comparison of Calculation Results for Equimolar Liquid Mixture of Krypton and Xenon at 161.36°K Based on Average Potential Model Approaches (Simon Equation for $w(\tilde{T})$).	118
21. Equation of State Parameters for the Pure AR, KR, and XE.	138
22. Normal Boiling Temperature Data for the Pure Components in Equation of State Study . . .	139

Table	Page
23. Excess Properties and Liquid Densities of Argon and Krypton Mixture at 115.77°K According to the Longuet-Higgins, Widom, and Lebowitz Equation of State.	141
24. Excess Properties and Liquid Densities of Krypton and Xenon Mixture at 161.36°K According to the Longuet-Higgins, Widom, and Lebowitz Equation of State.	142
25. Characterization of the Generalized Equation of State.	152
26. Comparison of Equation of State Parameters Based on Critical Conditions.	156
27. Critical Constants Used in the Generalized Equation of State Calculations.	162
28. Comparison of Calculated Liquid Molar Volumes of Argon, Krypton, and Xenon Based on Parameters Obtained at Critical Conditions	163
29. Excess Properties of Equimolar Liquid Mixture of Ar + Kr, and of Kr + Xe Calculated Based on Parameters Obtained at Critical Condition	165
30. Reduced Parameters for the Generalized Equation of State Based on Normal Boiling Temperature Data.	167
A-1. Calibration Readings of the Fused Quartz Pycnometer.	187
A-2. Calibration Readings of the Pyrex Pycnometer .	192
A-3. Thermal Expansion Data of Various Materials Related to Pycnometer Calibrations.	193
A-4. Ethane Densities at 161.36°K and at 115.77°K Determined by Using Quartz Pycnometer and by Using Pyrex Pycnometer	194
B-1. Calibration of Class-M Standards	202

Table		Page
C-1.	Partial Derivatives for the Error Analysis.	208
C-2.	Evaluation of the Partial Derivatives for the Pure Component Runs	209
C-3.	Evaluation of the Partial Derivatives for the Binary Mixture Runs	210
C-4.	Errors in Individual Measurement	211
C-5.	Absolute Accuracy of the Experimental Liquid Density Results	213

LIST OF ILLUSTRATIONS

Figure	Page
1. Photograph of the Experimental Apparatus . . .	9
2. Schematic Diagram of the Experimental Apparatus	10
3. Schematic Diagram of the Experimental Piping Arrangement	11
4. Schematic Diagram of the Cryostat.	13
5. Wiring Diagram of the Control Circuit.	18
6. Apparatus for Filling the Weighing Bomb with the Sample Gas.	20
7. Pyrex Pycnometer - Cryogenic Periscope Top Plate Seal.	23
8. Schematic Diagram of Pyrex Pycnometer.	25
9. Fused Quartz Pycnometer Top Plate Seal	27
10. Schematic Diagram of Cryogenic Periscope	29
11. Saturated Liquid Density of Argon and Krypton Mixture at 115.77°K	62
12. Saturated Liquid Density of Krypton and Xenon Mixture at 161.36°K	63
13. Excess Volume of Argon + Krypton Mixture at 115.77°K.	77
14. Total Vapor Pressure of Argon and Krypton Mixture at 115.77°K	78
15. Excess Volume of Krypton + Xenon Mixture at 161.36°K.	82

Figure	Page
16. Total Vapor Pressure of Krypton and Xenon Mixture at 161.36°K	84
17. Excess Gibbs Energy of Argon + Krypton Mixture at 115.77°K	91
18. Excess Gibbs Energy of Krypton + Xenon Mixture at 161.36°K	95
19. Comparison of Excess Volume Calculated from vdW-2 Model for Ar + Kr at 115.77°K	120
20. Comparison of Excess Volume Calculated from vdW-2 Model for Kr + Xe at 161.36°K	121
21. Comparison of Excess Gibbs Energy Calculated from vdW-2 Model for Ar + Kr at 115.77°K. .	122
22. Comparison of Excess Gibbs Energy Calculated from vdW-2 Model for Kr + Xe at 161.36°K. .	123
23. Comparison of Saturated Liquid Density of Ar + Kr at 115.77°K	144
24. Comparison of Saturated Liquid Density of Kr + Xe at 161.36°K	145
25. Comparison of Excess Gibbs Energy of Ar + Kr at 115.77°K	146
26. Comparison of Excess Gibbs Energy of Kr + Xe at 161.36°K	147

LIQUID DENSITY, EXCESS PROPERTIES, AND THE STATISTICAL
THERMODYNAMICS OF ARGON, KRYPTON, AND XENON BINARY
LIQUID MIXTURES AT LOW TEMPERATURE
AND SATURATION PRESSURE

CHAPTER I

INTRODUCTION

The objectives of this dissertation are two-fold. The first objective was to obtain liquid density data of pure heavy rare gases argon, krypton, and xenon at their saturation pressures and at low temperatures. The experimental temperatures for argon and krypton were at the krypton triple point 115.8°K and at the xenon triple point 161.4°K for krypton and xenon. Saturated liquid mixture density data were obtained at the following conditions: full composition range of argon+krypton at 115.8°K, full composition range of krypton+xenon at 161.4°K and one composition of xenon+argon at 115.8°K. Excess volume and excess Gibbs functions of argon+krypton and krypton+xenon were extracted from density data. These were compared with other investigations and theoretical interpretations developed in this dissertation. The second objective was

to improve the average potential model and also to examine the extension of the perturbation equation of state approach based on hard sphere radial distribution function to liquid mixtures. The pycnometer method which was adopted by Shana'a [71,72] was used for the experimental investigation. The absolute accuracy of measurement is presented in Appendix C.

Novel design modifications on the experimental apparatus originally designed and constructed for low pressure hydrocarbon liquids density measurements have been accomplished to obtain the objectives mentioned below:

- (1) A compact setup of neat equipment arrangement.
- (2) A shorter transfer line between the high pressure weighing bomb and the pycnometer to reduce the undesired dead volume considerably.
- (3) A new liquid level controller in the cryostat's outer dewar and a new transfer arrangement for the liquid nitrogen refrigerant.
- (4) A new top plate insulation using balsa wood and a pycnometer-periscope arrangement which guarantees frost-proof experimental observations.
- (5) A Pyrex pycnometer for measuring cryogenic liquid density at pressure up to 20 atmosphere.
- (6) A separate apparatus was built for filling the high pressure weighing bomb with high purity sample gases.

All these features are closely linked to achieving the claimed accuracy of data reported.

In recent years, considerably efforts have been expended in developing liquid state theories. Most interests have been centered around the prediction of thermodynamic properties of liquid mixtures in terms of molecular parameters of constituent pure components. Various statistical thermodynamic formulations have been proposed. The average potential models developed by Prigogine and co-workers [62] have met mediocre success, but fail even in the simple system such as argon+krypton [21]. Another approach is based on a perturbation of a rigorous equation of state for hard spheres by radial distribution function formalism [4]. This work has attempted to modify the average potential model for liquid mixtures. Also a liquid mixture theory was developed based on the perturbation approach. Both theories were used to interpret the experimental data obtained in this work. The conclusion is that the average potential model approach is inferior to the rigorous approach which provides a more sound foundation for a complete liquid mixture theory.

CHAPTER II

REVIEW OF PREVIOUS WORK

This review of previous work is to present a comprehensive account of experimental work on liquid density. Because Shana'a [71] has given a review on experimental work up to 1966, it is thus unnecessary to repeat them. The review on experimental data will be centered on those obtained after 1966. However, the liquid density data of argon, krypton, xenon and their mixtures will be presented including those obtained before 1966. The comprehensive reviews on the statistical thermodynamics theory of liquid and liquid mixtures, and on the excess thermodynamic functions for the heavy rare gas systems are postponed and will be given in their proper places in those chapters that deal with the theoretical interpretations and experimental results.

Density Data of Liquid Argon, Krypton, Xenon and Their Mixtures

Leadbetter and Thomas [44] have measured the density of liquid xenon in the temperature range 162-273°K under its saturated vapor pressure. The experimental method is to condense a known mass of xenon gas into a volume-calibrated glass capillary tube. The total probable error in the mass

of liquid is about 0.1%, and in the volume about 0.05% (or an accuracy of a few parts per thousand in density as claimed by the authors).

Patterson, Cripps, and Whytlaw-Gray [59] have made density measurements for liquid xenon from 206°K to the critical point, 289.7°K. The results of Leadbetter and Thomas are consistently 4-5% lower than those of Patterson et al.

Van Witzenburg and Stryland [90] measured the equation of state of liquids and soft liquids of argon experimentally in the temperature range from 96 to 154°K and at pressures about 100 to 2000 Kg/cm². The liquid data determine the PVT surface to within 0.1% for each of the variables.

Terry, Lynch, Bunclark, Mansell, and Staveley [84] measured the densities of liquid argon (86 to 118°K), krypton (118 to 164°K), xenon (164 to 219°K), oxygen (80 to 121°K), nitrogen (78 to 105°K), carbon monoxide (78 to 111°K), methane (92 to 151°K), and carbon tetrafluoride (91 to 185°K) along the orthobaric liquid curve with a precision of a few parts in 10⁴. A Pyrex pycnometer of 9 cm³ volume was used in the measurements.

Theeuwes and Bearman [85] measured the P-V-T behavior of liquid and dense gaseous krypton in the temperature range of 130 to 240°K at pressure from the vapor pressure to 280 atm at reduced density from 0.6

to 2.6. The mass of gas was measured by a gasometer. A pipet vessel was used to measure the liquid volume.

Previous Density Measurements

In this section some previous density measurements not covered by Shana'a and not involving the systems studied in this work will be surveyed.

Knobler and Pings [38] used a cylinder copper pycnometer with a volume of 22.45 cm^3 at 20°C for measuring the saturated liquid density of carbon tetrafluoride at 16 temperatures between 90° and 150°K . The estimated accuracy of the density determination is 0.1%.

Streett [83] has measured the densities of the pure components and of seven mixtures of the system neon-nitrogen at 100.78°K , at pressures from 68 up to 544 atm by the method of gas expansion. The estimated accuracy of the densities for mixtures and for pure neon is $\pm 0.5\%$. It is to be emphasized that while pure nitrogen is a liquid at the experimental conditions pure neon is above its critical point. Agreement between the average potential model prediction and experimental excess volume is generally poor.

Streett and Staveley [81] have measured the PVT behavior of liquid nitrogen at eight temperatures in the range 77.35° to 120.23°K and at pressures from just above saturation to 690 atm by the method of gas expansion. The estimated accuracy of the final results is $\pm 0.1\%$.

Mastinu [51] used a densitometer which was used to determine the ratio of the number of moles in the mixture and the number of moles in the solvent by means of the gasification of two equal liquid volumes of mixture and solvent. The excess volumes of the system N_2-H_2 at 77.4°K and 12 atm, with hydrogen concentration between 0.5% and 2%, were determined.

Fuks and Bellemans [27,28] measured the vapor pressure and density of methane and krypton, and nitrogen and methane liquid systems. The excess Gibbs energy and excess volume were calculated from these measurements.

Streett [80] has measured the liquid-vapor phase compositions for the system neon and argon at temperatures between 95.82°-129.92°K. The density of liquid phase was measured in the compressed liquid region at temperatures of 101.94°, 110.78°, and 121.36°K, at pressures up to 8,000 psia.

El Hardi, Durieax, and Van Dijk [24] measured the density of liquid 4He under a pressure slightly higher than its saturated vapor pressure between 1.2 and 5.1°K. The amount liberated from the pycnometer on warming was measured at room temperature. A copper pycnometer reservoir with a volume of about 17 cm³ was used.

CHAPTER III

EXPERIMENTAL APPARATUS

The experimental apparatus was originally designed and constructed for obtaining cryogenic liquid density with temperature range between 77°K and 273°K and pressure at below atmospheric inside the pycnometer. Considerable inconvenience had been experienced in controlling the liquid nitrogen level in the outside dewar and also in taking the pycnometer liquid level readings while the cryostat was being clouded by frost. The original apparatus as described in Shana'a's work [71] was taken apart and rebuilt with modifications. Those parts that were described in detail before by Shana'a will be mentioned briefly, while greater emphasis is being placed upon the major modifications. The experimental apparatus is shown in the laboratory photograph in Figure 1, and explained in Figure 2, and Figure 3.

Cryostat and Temperature Control

The cryostat shown in Figure 4, is a concentrically mounted double dewar setup. The inner dewar was used to contain the bath fluid, Freon-13. The outer dewar was used to contain the refrigerant, liquid nitrogen. The inner dewar wall has an evacuation port.

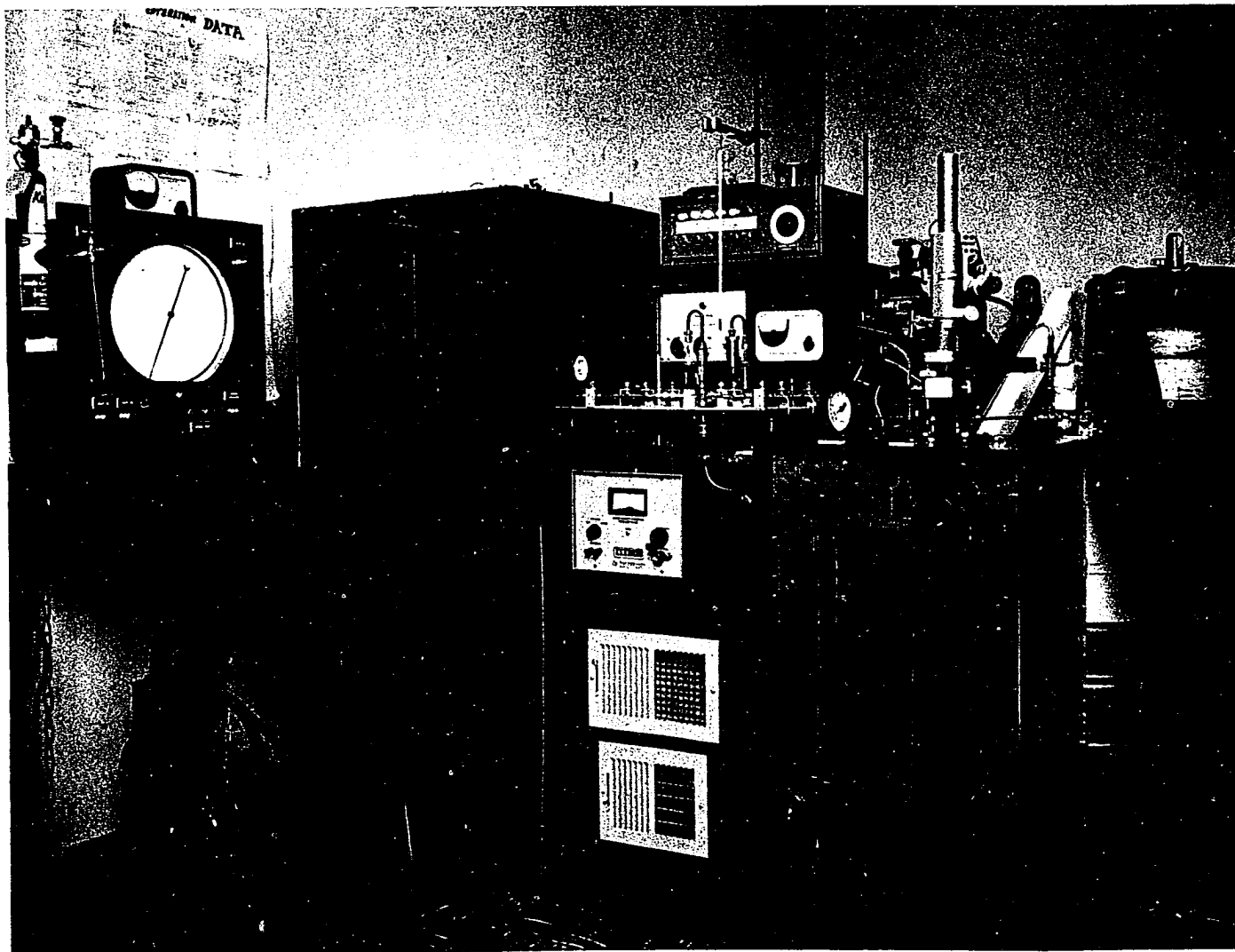


Figure 1. Photograph of the Experimental Apparatus

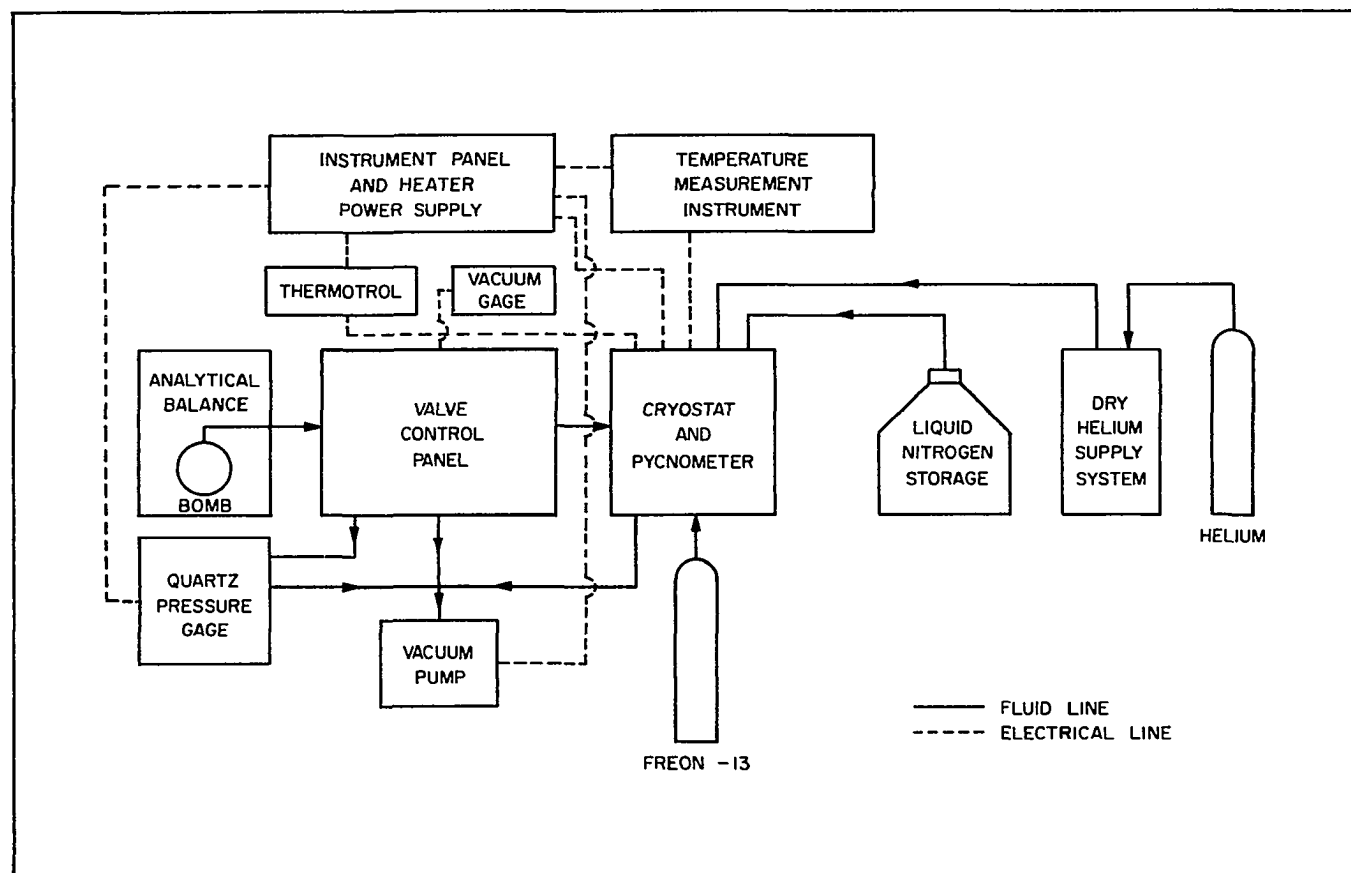


Figure 2. Schematic Diagram of the Experimental Apparatus

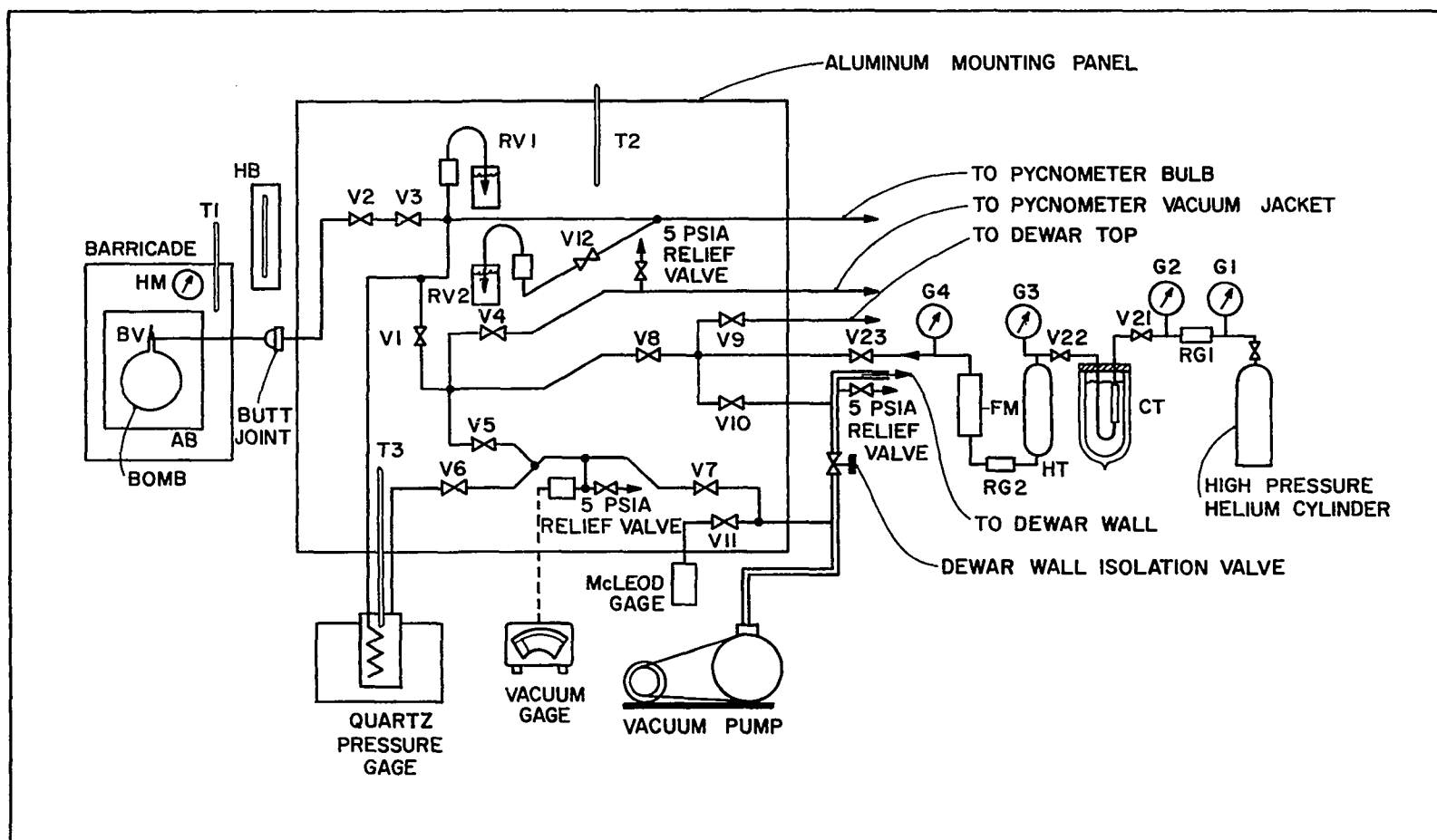


Figure 3. Schematic Diagram of the Experimental Piping Arrangement

LEGEND FOR FIGURE 3

AB	Analytical Balance
BV	Bomb Valve
CT	Cold Trap
FM	Flow Meter
G1	High Pressure Gauge
G2	Low Pressure Gauge
G3	100 psig Pressure Gauge
G4	5 psig Pressure Gauge
HB	Barometer
HM	Hygrometer
HT	Dry Helium Storage Tank
RG1	Helium Pressure Regulator
RG2	Low Pressure Regulator
RV1	250 psig Water Relief Valve
RV2	5 psig Water Relief Valve
T1	Barricade Thermometer
T2	Piping Panel Thermometer

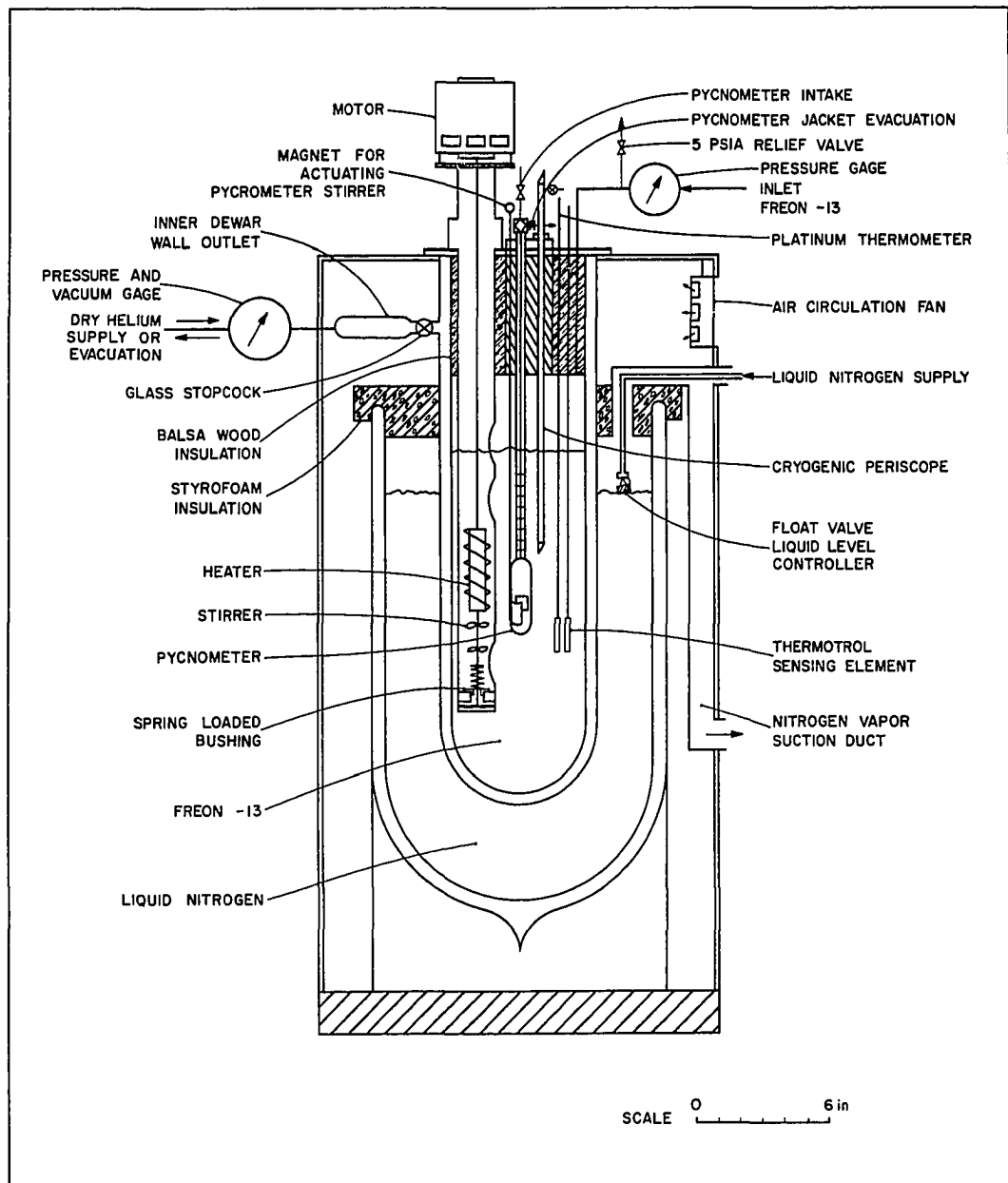


Figure 4. Schematic Diagram of the Cryostat

The cryostat has a top plate consisting of a 1/8 inch brass plate connected with a 6-inch thick balsa wood. (In a preliminary run it was found that Freon-21, which was used as the bath fluid then, can attack both urethane and styrofoam.) Three long metal rods were threaded on to the brass plate. The balsa wood insulation plates were then bolted on. The main feature of the cryostat is essentially the same as before. However, for safety's sake, the outer dewar flask was mounted on a metal frame and sealed with aluminum plates 3/8-inch thick on three sides. The front plate was mounted with three 6-inch military side-viewing right angle mirrors. Thus, the pycnometer can be viewed from the outside by a right angle. To eliminate hazardous operation conditions, propane was not used as the bath fluid anymore. Instead, Freon-13 (a duPont trademark of CClF_3 , Monochlorotrifluoromethane) was used. Freon-13 was classified in group 6 in Underwriters' Laboratories' classification of comparative life hazard of gases and vapors. Its boiling point is 191.8°K and its freezing point is 92.2°K. Freon-13 was used as the bath fluid in all the experimental runs.

Constant temperature was maintained in the cryostat to within $\pm 0.002^\circ\text{K}$ by closely controlling the liquid nitrogen level, an optimum vacuum inside the inner dewar wall, and a combined heating-stirring effect in the bath fluid. Liquid nitrogen used as the refrigerant was kept at a constant level to within ± 0.5 cm inside the outer dewar flask. A float valve was used to regulate the flow rate of liquid nitrogen. A

positive pressure around 2 to 5 psig was maintained in the 50-liter storage dewar. This pressure was sufficient to cause the liquid nitrogen to flow through a vacuum insulated glass transfer line to the cryostat's outside flask when the float valve was slightly opened due to lowering liquid level. The transfer line was a 6 mm O.D. glass tubing sticking out from the storage dewar with 30 degree angle and measured 21 3/8 inches long outside. This outside tubing was vacuum sealed permanently with a 15 mm O.D. glass tubing to reduce liquid nitrogen loss. The length of transfer tubing inside the storage dewar is 29 inches. The glass transfer line was broken during an experiment. Another liquid nitrogen transfer line was built. This time 3/18 inch Invar thin wall tubing was used with an urethane insulation block glued on to reduce heat transfer. A sintered glass filter was glued by silicon rubber on the tip of the tubing which sticks into the 50-liter liquid nitrogen storage dewar. This arrangement ensured an unobstructed transfer of liquid nitrogen toward the cryostat outer dewar. A multipurpose Teflon pressuring head was installed on the storage dewar. This device allowed the dewar to be refilled from the 110-liter pressurized dewars while continuously transferring the liquid nitrogen into the cryostat. A nylon pressuring head was used initially, but it cracked due to excessive stress generated upon rapid cooling. A 5 psig Circle Seal relief valve and a small pressure gauge were mounted on this pressuring head. The above arrangement of a float valve assembly, and insulated Invar transfer line, and a

pressuring head ensured a constant refrigerant effect for the cryostat without any interruption.

To solve the problem of accumulating too much frost around the cryostat's nitrogen inlet, an aluminum duct 2 1/8 inch by 1 1/2 inch with a blower mounted on the other end was glued to the nitrogen inlet opening with silicon rubber. Thus, vaporized nitrogen was pulled out from the cryostat at a constant rate. With the help of another blowing fan to circulate the air, only a small amount of frost was formed during prolonged experimental runs.

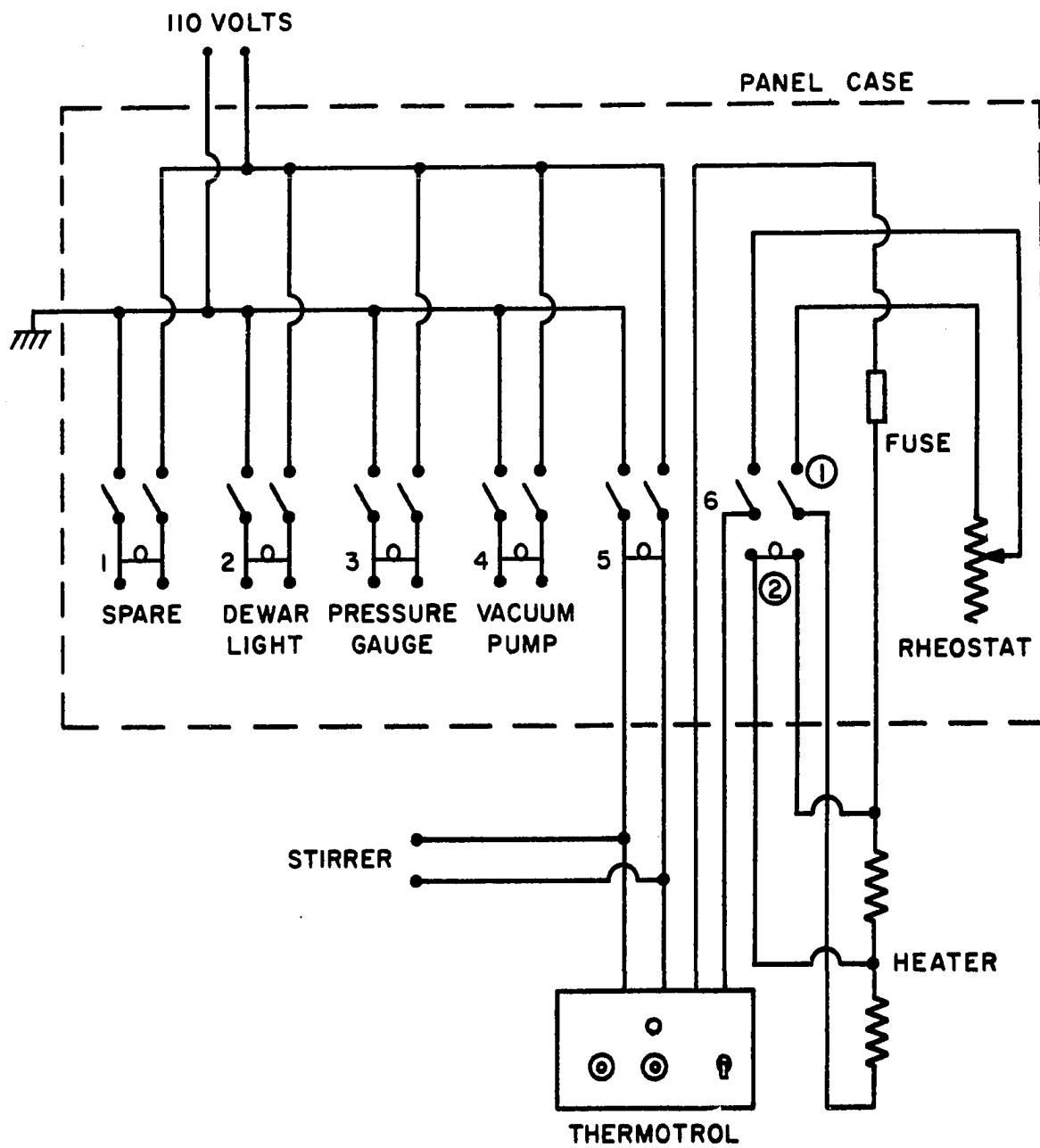
A bare wire control heater was made of 30 gauge Nichrome wire, with a 6.82 ohms per foot resistance, wound around a 5-inch diameter phenolic frame. The wiring was divided into two equal length parts to be used in either series or parallel connection. The total length of wiring gave a resistance of 210 ohms. In series the wattage may be varied from 9.2 to 65.2 watts by means of a 350 ohm external rheostat. The heater leads made from 20 gauge copper wires insulated by Teflon spaghetti tubing were soldered on three 1/8 inch diameter rods sticking out around the upper shaft base of the stirrer-heater assembly. With three small plugs the heater was connected to a power line which can be connected to the control panel. The series connection used for control heater was connected to a Hallikainen Model 1053A Thermotrol with proportional plus reset control. The sensor is a Rosemont Model 104N48AAC thermometer. The parallel connection was used as a quick heater and can

dissipate 261 watts. The electrical wiring diagram is shown in Figure 5.

The stirrer was driven by an induction motor at 1750 rpm and was essentially the same as that used before. However, some slight adjustments were made. In the course of preliminary runs it was found that the two bearings on both ends of the shaft wore out very fast and started making loud noises when this happened. A piano wire was coiled around the lower part of the shaft to push down a bushing. This bushing exerts a slight load on the top of the lower bearing to ward off its wobbling movement and so preventing unnecessary wear. Further, around the shaft just above the upper bearing it was discovered that the Teflon bushings used as seal were not functioning properly. Therefore, these were replaced by three V-shaped Chevron bushings made from Teflon. The stirring effect was such that there was no significant vertical temperature gradient inside the cryostat bath fluid.

High Pressure Weighing Bomb and Weighing Equipment

The high pressure weighing bombs constructed before were used in this investigation. Detailed information is available [71] and will not be repeated. Briefly, these bombs were constructed from PH 15-7 Mo Stainless steel of Armco Steel Corp. with 0.028 inch thickness. Two bombs were heat treated and one was not. The empty bomb weighs 215 grams including a silver-soldered 35 gram AISI 303 stainless steel specially designed valve. The fact that these bombs are



POSITION ① : CONTROL HEATER

POSITION ② : QUICK HEATER

Ⓛ : LIGHT

Figure 5. Wiring Diagram of the Control Circuit

capable of storing 20 grams of sample gas at around 750 psi. (a safety factor of 4.75) put design restrictions on the new Pyrex glass pycnometer. Calibration of the bomb volume as a function of its internal pressure were presented elsewhere [71]. This information was required for accounting accurately the change of air buoyance effect on the bomb in the weighing process.

The weighing equipment is a 300 gram capacity Right-A-Weigh analytical balance of Wm. Ainsworth and Sons, Inc. The balance was securely housed inside a pressure barricade. By using a vernier-scale readout to obtain readings in the 0.1 mg range, the balance has a sensitivity of 0.1 milligram. A thermometer that is accurate to $\pm 0.01^{\circ}\text{C}$ and a Lufft Durotherm-hygrometer were placed inside the pressure barricade. The information of temperature, relative humidity, and the barometric pressure was used to calculate the air buoyancy effect for each weighing. A set of class M standards calibrated by the National Bureau of Standards was used for the substitution weighing of materials.

For filling the high pressure bomb with the sample gas from the gas cylinder, a separate filling apparatus was built. This apparatus is a mobile unit complete with its own vacuum gauge, pressure gauge, and the vacuum pump. As shown in Figure 6, there is a 1,000 psia Heise Model C, H49488, bourdon tube gauge with a Circle Seal 850 psia relief valve for preventing overpressurizing the bomb. A low pressure Circle Seal 5 psia relief valve was also installed in conjunction with a Consolidated Vacuum Corporation GTC 100

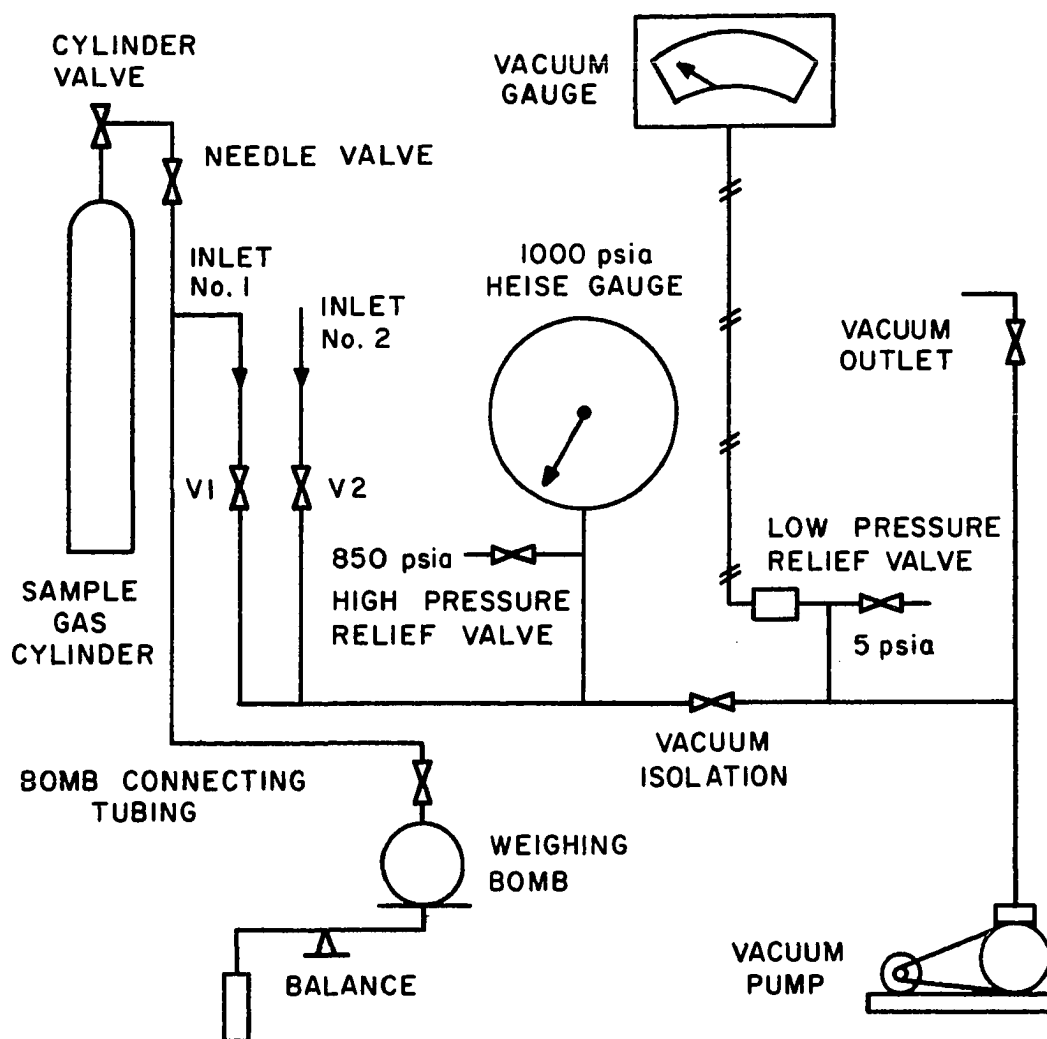


Figure 6. Apparatus for Filling the Weighing Bomb with the Sample Gas

thermocouple vacuum gauge. Inlet number one and inlet number two were spare outlets for extra evacuation and filling. The vacuum outlet may be used either for evacuating other systems or for calibrating the vacuum gauge with a McLeod gauge. This apparatus thus served the purpose of a mobile vacuum generating unit also. Here a scale type balance was used for weighing roughly. The gas cylinder can be securely chained and held at the side of the upper left side of the apparatus. A separate bomb connecting tubing, which has a butt joint pressure seal connection on the other end from the bomb, was made for this unit. This apparatus considerably improved the efficiency of experimentation, because a sample bomb may be evacuated and filled with sample gas without using any instrument in the main experimental apparatus.

Pycnometer and Periscope Assembly

Due to the higher pressure at around 200 psia encountered in this experiment, it was necessary to redesign a pycnometer. There were the following considerations concerning the new pycnometer design.

1. The pycnometer must be capable of withstanding an internal pressure of about 700 psia at room temperature, a safety factor of 2.9. The pycnometer should stand a 200 psia internal pressure at low temperature.
2. The high pressure weighing bomb has a volume of 589 cm³ and a capacity of containing 75 gm of

sample gas due to the range of the analytical balance. This restriction should be carefully evaluated with respect to all three gas samples: argon, krypton, and xenon for designing the pycnometer volume.

3. A new design of the vacuum jacket evacuation port and a new design of a pycnometer top plate should be achieved to accommodate the concept of using a cryogenic periscope for viewing the pycnometer readings.

Pyrex was chosen as the material of pycnometer because it was difficult to fabricate a heavy wall pycnometer out of fused quartz. The outside diameter of the pycnometer bulb cylinder was limited at 1 inch by the consideration of working space available. From the information of the high pressure weighing bomb and the PVT properties of argon, krypton, and xenon [19], it was calculated that the pycnometer volume should be set at 20 cm^3 . Although theoretical calculation was done it was decided to pressure test the pycnometer bulb experimentally at the bulb thickness of 5/32 inch. Three dummy bulbs were made from Pyrex glass at the designed size of the pycnometer bulb and pressure tested to 1,300 psia with water without any sign of failure. After the Pyrex glass pycnometer was built it was pressure tested with vacuum pump oil to 700 psia twice and 500 psia once. The results showed that both the pycnometer top plate fittings as shown in Figure 7 and the Pyrex pycnometer

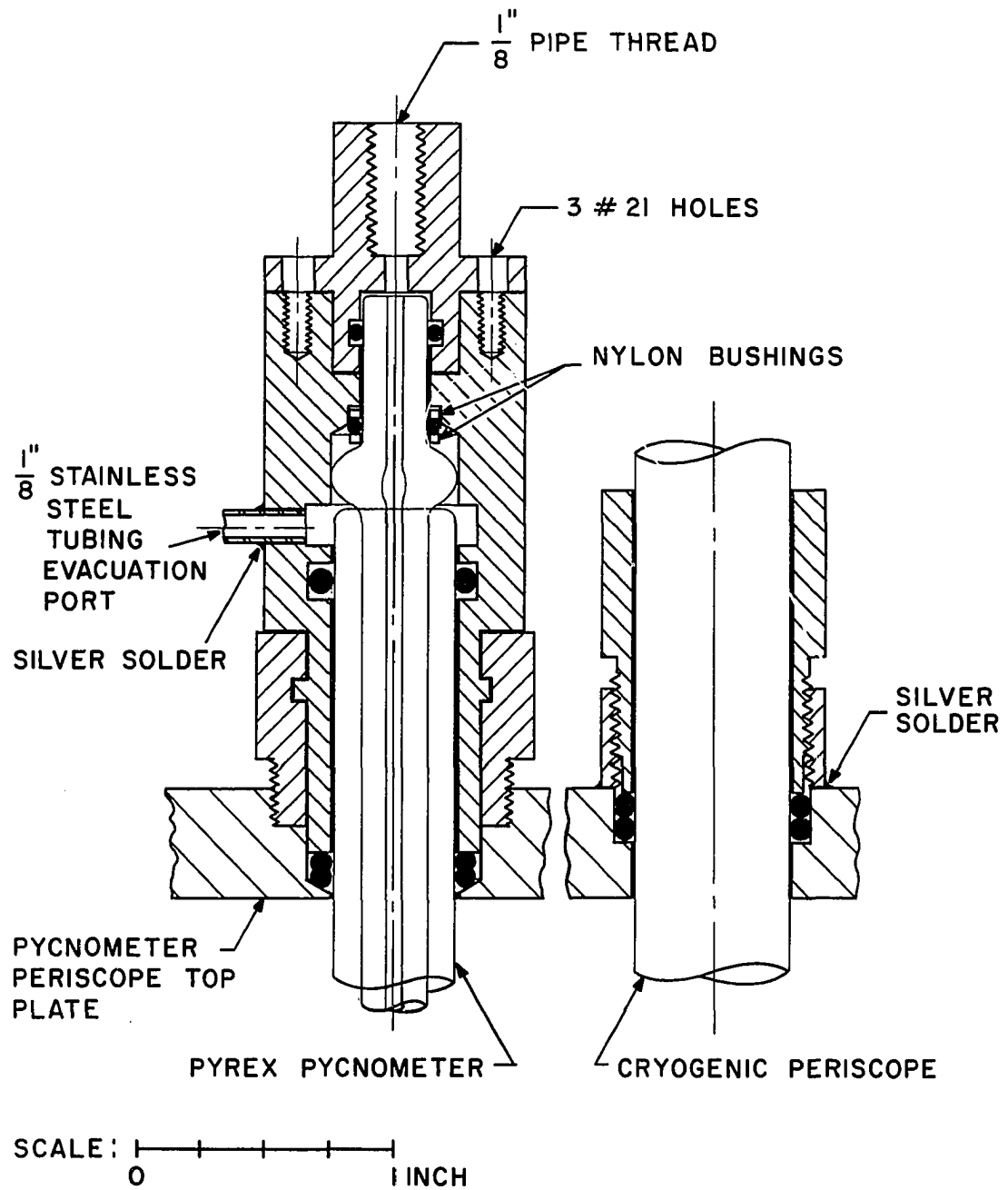
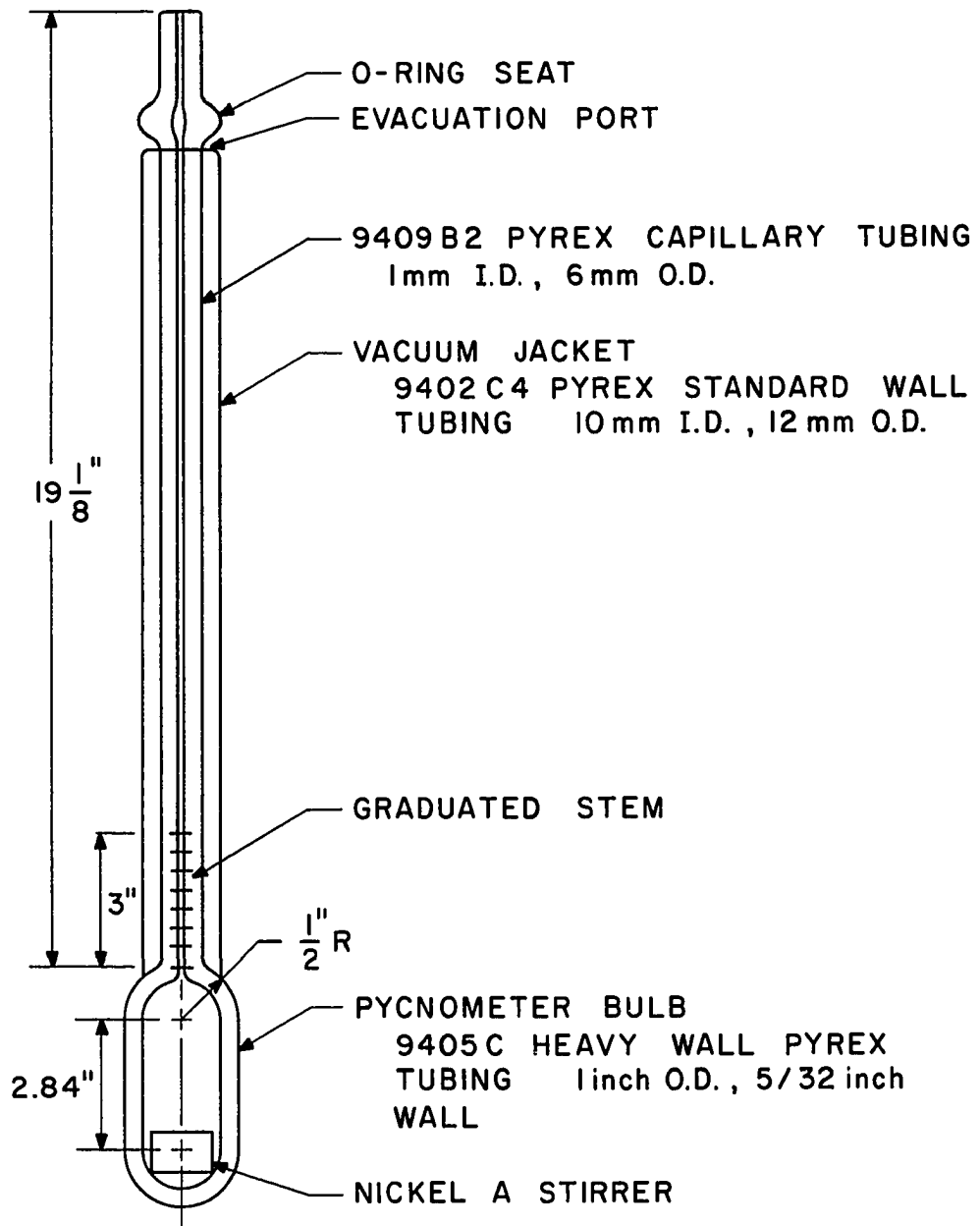


Figure 7. Pyrex Pycnometer - Cryogenic Periscope Top Plate Seal

designed as shown in Figure 8 were capable of withstanding the pressure to be encountered in actual experiments.

It can be seen that the evacuation port of the Pyrex pycnometer was different from that of the fused quartz pycnometer used before. The idea of using the space originally occupied by the evacuation port of the quartz pycnometer for the cryogenic periscope suggested that a new design concept must be sought. At first a pycnometer was built without the evacuation port arm but with a tiny hole 0.15 inch I.D. and 5/16 inch below the upper edge of the pycnometer vacuum jacket. The idea then led to the construction of a fitting such that it accommodated both the pycnometer gas input and the jacket evacuation. In the process of pressure testing it was found that the rigidity of the vacuum jacket relative to the center capillary stem rendered it difficult to have a good pressure seal on the pycnometer top and thus enhancing the chance of breaking the top part of the pycnometer.

The pycnometer was designed so that the upper edge of the vacuum jacket was not sealed around the capillary. A small bulge was made on the capillary directly above the jacket opening and served as an O-ring seat. Two nylon bushings positioned this O-ring above the glass seat. The capillary was graduated and a Nickel-A stirrer was enclosed inside the pycnometer bulb. Three oversized bolt holes drilled into the pycnometer top plate fitting permitted slight adjustment of the fitting to the position of the



NOTE: NOT TO SCALE

Figure 8. Schematic Diagram of Pyrex Pycnometer

capillary. The calibration of the pycnometer is presented in Appendix A. A separate set of top plate fillings were designed and fabricated for the quartz pycnometer. This top plate seal is shown in Figure 9.

The inability to view clearly the pycnometer because of the frosting of the cryostat necessitated the use of a cryogenic periscope. The following factors were considered in the design of the periscope:

1. The periscope must transmit the true image of the graduated capillary stem to the cathetometer.
2. The contribution to the heat leakage into the cryostat by the periscope must be as small as possible.
3. The periscope must be adjustable so that experimental readings can be made along the entire length of the graduated stem of the pycnometer.

A simple periscope was constructed. An optical glass rod with square cross section 0.5 inch by 0.5 inch and 20-inches long was cut on each end to have two parallel slant surfaces 45° to the axis of the rod. The surfaces of the rod except the two viewing surfaces were silvered. However, this periscope which was constructed by the Gertner Optical Co. at Chicago transmitted only multiple dim images. A second attempt was to construct a periscope which used two small prisms ($\frac{1}{2}$ -inch x $\frac{1}{2}$ -inch x $\frac{1}{2}$ -inch). A brass tubing with square cross section was chemically treated to blacken its inside surface. Prisms were clamped on each end of the brass tubing by the

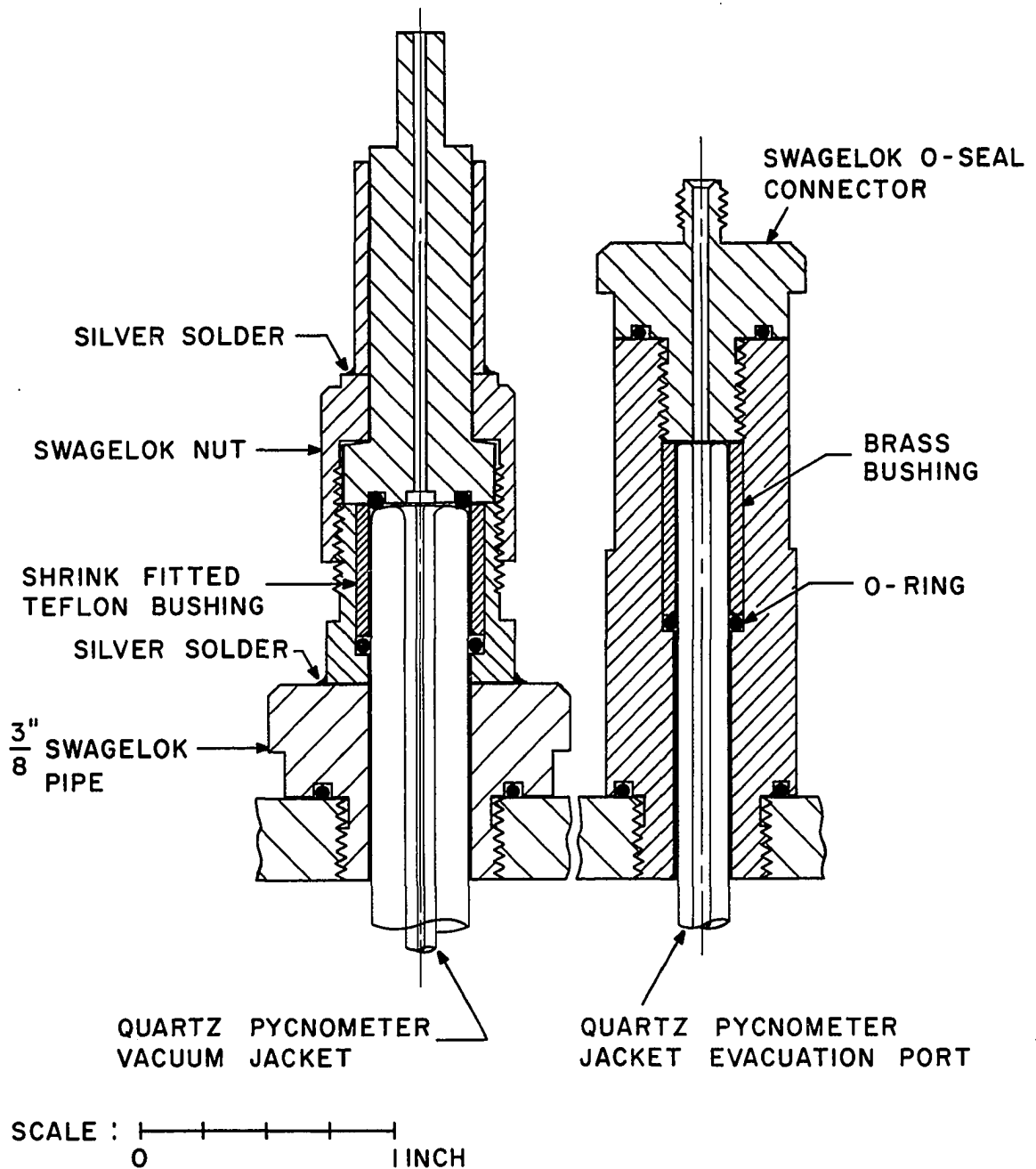


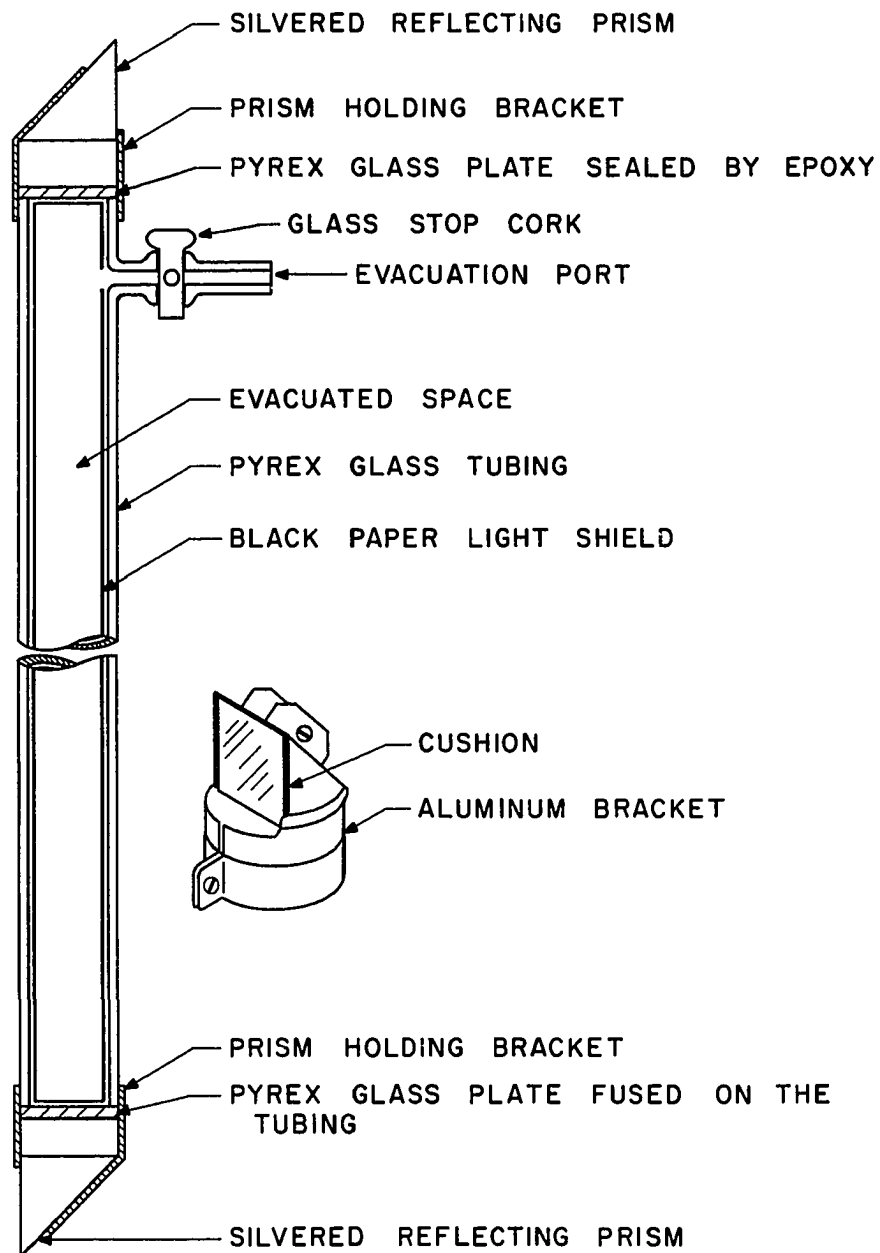
Figure 9. Fused Quartz Pycnometer Top Plate Seal

square tubing itself. This periscope was then vacuum sealed inside a special glass tubing. However, it was found that the glass tubing wall distorted the transmitted image. No improvement was achieved on this design. Finally a simple yet workable design was made.

As shown in Figure 10, the main part of the periscope consists of two prisms and a glass tubing. The tubing was built with an evacuation port. On the top end of the tubing a circular piece of Pyrex glass plate 1/16-inch thick was cemented by epoxy. A similar circular glass plate was fused on the bottom end of the tubing. To eliminate undesirable light, a cylindrical sheet of black paper was fitted coaxially inside the tubing. A glass stop cock was installed on a side evacuation port to permit evacuating the periscope tubing. The vacuum served to decrease the heat leakage and to prevent moisture from condensing inside the periscope tubing.

Right angle silvered surfaced prisms 21 mm x 15 mm x 15 mm supplied by the Edmund Scientific Co. were mounted on each end of the glass tubing. Aluminum brackets were used to fasten the prisms to the tubing. Rubber gaskets served as cushions between the top prism and the bracket and between the bracket and the glass tubing. Because the lower prism was immersed in the Freon-13 bath fluid cork wood gaskets were used. The periscope fitting can be manually manipulated to finger tight for positioning the periscope.

It should be noted that the Pyrex pycnometer, the horse-shoe magnet, and the cryogenic periscope were all



NOTE: NOT TO SCALE

Figure 10. Schematic Diagram of Cryogenic Periscope

mounted on the same top plate. This pycnometer-periscope assembly can be removed from the cryostat as a separate entity. The detail of using a cathetometer to take the pycnometer readings by means of this periscope is explained in Chapter V.

Temperature and Pressure Measurements

The temperature and pressure measurement instruments were essentially the same as those used before [71] with small changes. A Leeds and Northrup Model 8164 capsule type platinum thermometer was used with a Leeds and Northrup G-2 Mueller bridge and galvanometer to measure the temperature of the bath fluid. This thermometer was calibrated by the National Bureau of Standards and the reader is referred to Shana'a's work [71].

The absolute pressure in the pycnometer and the transfer line was measured by a Texas Instrument Fused Quartz Pressure Gauge, Model 140. A new bourdon tube capsule was purchased from and calibrated by the Texas Instruments. The capsule is a type 1 model with operating pressure range of 0 to 200 psia. The absolute accuracy was claimed at 0.015% plus 0.002% of Standard Readout.

Valves, Tubings, and Vacuum Systems

Most valves used in the system are the Whitey valves. Special attention was exercised in positioning the valve seat so that high pressure side is always in contact with the needle tip when the valve is closed. The main control valves shown in

Figure 3 were mounted on an aluminum panel, which was securely mounted horizontally, and is removable. To cut down the possibility of contamination of sample gases, the system tubings were built by using 1/8" stainless steel tubings. The tubings were cleaned first by using toluene and acetone. After the tubings were assembled, the whole system was cleaned using trichloroethylene and acetone. The dry helium gas supply line was built using 1/8" copper tubings. Because the valves and the Swagelok fittings were brass, the front ferrels used were Zytel and the back ferrels were brass. This arrangement insured tightness of the system.

Relief valves were mounted to protect various delicate parts of the system. A 5 psig Circle Seal relief valve was mounted next to the thermocouple vacuum gauge sensing element. Another 5 psig Circle Seal relief valve was mounted in the dry gas supply line to the cryostat inner dewar wall. To prevent overpressurizing the pycnometer vacuum jacket, a similar 5 psig Circle Seal relief valve was mounted in the line. In order to maintain a 2 psig positive helium atmosphere on top of the cryostat bath fluid, a 5 psig relief valve was also mounted on the cryostat top plate to prevent overpressurizing the cryostat. Special water relief valves in the transfer line between the weighing bomb and the pycnometer are to be described later in the following section.

A two-stage, oil-lubricated vacuum pump was used to evacuate the system including the pycnometer, the pycnometer

jacket, the transfer line, the cryostat inner dewar wall, and the pressure gauge reference port. A dry helium supply system incorporating a cold trap and a storage tank was used to supply the dry helium gas used inside the cryostat dewar wall, the pycnometer vacuum jacket, the cryostat top space and for general purging purposes. A Consolidated Vacuum Corporation GTC 100 type thermocouple vacuum gauge was used to indicate the system vacuum. It has a range of 0 to 1,000 microns. This gauge was periodically checked with a swing-type McLeod gauge to insure proper readings.

Transfer Line Between the Weighing Bomb and the Pycnometer

The transfer line between the weighing bomb and the pycnometer is very important in the sense that it traps the sample gas which is in contact with the sample liquid condensed in the pycnometer during the experimental runs. This transfer line volume needs to be as small as possible and its volume should be known precisely in order to achieve the required accuracy of the experimental data.

As shown in Figure 3, the transfer line begins at the bomb valve. The line between the bomb and V2 is removable. It was disconnected from the system and from the bomb when the bomb was removed from within the pressure barricade. Right after V2, a metering valve V3 was used for metering minute amounts of gas for a slow condensation process. The line then branches to the pressure gauge bourdon tube, to the high

pressure Circle Seal 250 psig relief valve, and to the pycnometer. No valve was placed between the pressure gauge bourdon tube and the transfer line such that the pressure in the transfer line can be checked at all times. The relief valve in the transfer line also protected the bourdon tube from being overpressurized. In the present investigation, part of the calibrations of the Pyrex pycnometer was done by measuring the liquid density of ethane both in the Pyrex pycnometer and in the quartz pycnometer, which served as a standard, at the same operation temperature. Therefore, it was necessary to install a 5 psig Circle Seal relief valve for protecting the low pressure quartz pycnometer. This was accomplished by branching the transfer line between the 250 psig water relief valve and the pycnometer with a tee. A valve was placed between the transfer line and the low pressure water relief valve for operations. The pycnometer valve, PV, served to isolate the pycnometer from the transfer line. During the remodeling process, special attention was paid to shortening of the transfer line.

Calibration of the transfer line volume and the dead space between PV and the liquid surface inside the pycnometer was done with the Burnett-type expansion between the unknown transfer line volume and an evacuated bomb whose volume was known precisely. Dry helium gas was used as the expansion gas. Details of the calibration are presented in Appendix D. The calibration was performed for both the low pressure quartz pycnometer setup and the high pressure Pyrex pycnometer setup at room temperatures.

CHAPTER IV

MATERIALS USED

Selection of bath fluid and selection of high purity research grade sample gases are essential to the success of the present investigation. Monochlorotrifluoromethane was used as a bath fluid. High purity research grade heavy rare gases and research grade hydrocarbons were used in the experiment. These materials are discussed in the following sections.

Bath Fluid

The following criteria were used in selecting a bath fluid:

1. The material should not be toxic or explosive.
2. The material should be a liquid between 100°K and 180°K.
3. The material should not react with metal or elastomers.

After a survey of available bath fluids, monochlorotrifluoromethane was chosen as a suitable fluid. This material is marketed under the trade name Freon-13 by du Pont and Genetron-13 by Allied Chemicals. Both these companies have generously donated this material for the present investigation.

Some characteristics of this material are presented in Table 1.

Besides being less hazardous than propane, which was the bath fluid used by Shana'a [71], Freon-13 possessed another important advantage: it can be condensed faster than propane. Using Freon-13 the condensing process required two hours as opposed to eleven hours when using propane.

Research Grade Heavy Rare Gases

The research grade heavy rare gases, with the exception of one cylinder of argon, were purchased from the Linde Division of Union Carbide Corporation. The gases were prepared from the procedure adopted by Linde Division, and stored into XA cylinder having a water volume of 0.43 liters and ICC 1,800 psig rating. The maximum pressure, approximate quantity of each gas contained are as follows:

	<u>Maximum Cylinder Pressure</u>	<u>Approximate Volume Contained</u>
Argon	1,800 psig	59 liters (97.3 gm.)
Krypton	1,800 psig	72 liters (246 gm.)
Xenon	900 psig	55 liters (296 gm.)

The Linde Division analyzed the rare gases from the bulk containers. Small baked cylinders were then filled from the analyzed bulk containers. All air constituents were then reanalyzed via gas chromatography to assure no contamination on filling. Approximately one-half liter sample volume was required for the reanalysis. All of the impurities in the

TABLE 1

SOME CHARACTERISTIC PROPERTIES OF
MONOCHLOROTRIFLUOROMETHANE*

	"FREON-13"
Chemical Formula	CClF_3
Molecular Weight	104.47
Boiling Point at 1 atm.	-81.4°C (191.8°K)
Freezing Point	-181°C (92.2°K)
Critical Temperature	28.9°C
Critical Pressure	38.2 atm.
Liquid Density	1.298 g/cc. at -30°C
Density, Saturated Vapor at Boiling Point	7.01 gm/liter
Heat of Vaporization at Boiling Point	35.47 cal/gm.
Toxicity	probably Group 6**

*Information supplied by the E. I. duPont de Nemours and Co. (Inc.) "Freon" Product Division.

**Result based on preliminary toxicological data. Estimated by Underwriters' Laboratories to belong to group 6, i.e.: gases or vapors which in concentrations up to at least about 20% by volume for durations of exposure of the order or 2 hours do not appear to produce injury.

bulk containers were analyzed by the methods indicated below to one parts per million (PPM) by volume or better:

<u>Impurity</u>	<u>Method</u>
Oxygen	Trace electrolytic oxygen analyzer
Carbon Dioxide	Non-dispersive infrared
Moisture	Electrolytic Hygrometer
Total Hydrocarbons	Total hydrocarbon flame ionization detector
Helium	All the following impurities are analyzed for using gas chromatography and thermal conductivity, flame ionization, and photo-ionization detectors except for nitrogen in argon. The nitrogen in argon is analyzed via a high voltage spectroanalyzer.
Hydrogen	
Argon	
Nitrogen	
Methane	
Carbon Monoxide	
Nitrous Oxide	
Krypton	Chromatographic columns used are Linde SA Molecular Sieves, Por-O-Pak Q, and regular Silica Gel.
Xenon	

The above analytical procedures were confirmed by this investigator on a plant visit. Due to the high cost of the research grade heavy rare gases it was absolutely necessary to estimate closely the amount of gases to be purchased. A prudent decision was made to purchase part of the total gases required: three cylinders of argon, two cylinders of krypton, and one cylinder of xenon. Their compositions are as follows:

<u>Argon Gas Composition</u>	<u>Cylinder #A169, A146, A400</u>
Hydrogen	< 1 ppm
Neon	< 1 ppm
Nitrogen	< 2 ppm
Oxygen	< 1 ppm
Carbon Dioxide	< 1 ppm
Total Hydrocarbons	< 2 ppm
Moisture	< 3 ppm
Argon	Balance
<u>Krypton Gas Composition</u>	<u>Cylinder #A401, A220</u>
Hydrogen	< 1 ppm
Argon	< 1 ppm
Oxygen	< 1 ppm
Nitrogen	< 5 ppm
Xenon	< 30 ppm
Total Hydrocarbons	< 1 ppm
Moisture	< 3 ppm
Krypton	Balance

<u>Xenon Gas Composition</u>	<u>Cylinder #A213</u>
Krypton	< 11 ppm
Nitrogen	< 5 ppm
Argon	< 3 ppm
Oxygen	< 2 ppm
Total Hydrocarbons	< 1 ppm
Moisture	< 1 ppm
Xenon	Balance

The one cylinder of argon gas purchased from Cryogenic Rare Gas Laboratories, Inc., 730 South 13th Street, Newark, N. J. in March, 1968 has the following composition, analyzed for from the bulk container, as claimed by the supplier:

R.G.L. Argon Gas
Composition

Oxygen	ND	3 ppm
Nitrogen		3 ppm
Neon	ND	1 ppm
Hydrogen	ND	1 ppm
Argon		Balance

where ND, the not detectable figures shown were limits of gas chromatography as claimed by the supplier. The argon gas was filled into a 0.4 liter cylinder from a stock cylinder of 9,000 liters on April 8, 1968. This cylinder of ultra high purity (UHP) argon was also sent to the U. S. Department of the Interior, Bureau of Mines, Helium Research Center, at Amarillo, Texas for reanalysis. The chromatography analysis did not show any impurity. However, the lower

detectable limit for each impurity was as follows:

$\frac{\text{He}}{<4\text{ppm}}$	$\frac{\text{Ne}}{<9\text{ppm}}$	$\frac{\text{H}_2}{<3\text{ppm}}$	$\frac{\text{O}_2}{<34\text{ppm}}$	$\frac{\text{N}_2}{<62\text{ppm}}$
----------------------------------	----------------------------------	-----------------------------------	------------------------------------	------------------------------------

The argon was also analyzed, using a mass spectrometer, for the following components: He, H₂, Ne, N₂, O₂, CO₂, Xe, and Kr. None were detected.

One cylinder of krypton gas was purchased during the course of the experiment, it has the following certified analysis supplied by the Linder Division:

<u>Krypton Gas Composition</u>	<u>Cylinder #A-338</u>
Hydrogen	< 1 ppm
Oxygen	< 1 ppm
Nitrogen	< 22 ppm
Methane	< 1 ppm
Moisture	< 1 ppm
Total Hydrocarbons	< 1 ppm
Xenon	< 1 ppm
Krypton	Balance

Research Grade Hydrocarbons

Research grade ethane supplied by Phillips Petroleum Company was used in the pycnometer calibration runs. The composition of ethane was obtained from the Phillips Petroleum Company and previous investigator's analysis [71]:

<u>Ethane Gas Composition</u>		<u>Method of Analysis</u>
C_2H_6	99.99 Wt.%	Infrared and Gas Chromatography
C_2H_4	< .01 Wt.%	
$C_3H_6+C_3H_8$	< .01 Wt.%	
Air	< 25 ppm.	

CHAPTER V

EXPERIMENTAL PROCEDURE AND PROBLEM

In this chapter the experimental procedure is described. The experimental problems confronted during investigation are described and their solutions and implications are presented.

Cool Down the Cryostat to Operating Temperature

To cool the cryostat, the inner dewar was purged with dry helium at 2 psig a few times. Then the inner dewar was held at 2 psig of dry helium while the outside dewar was filled with liquid nitrogen (LN_2). It was important to prevent any moisture from condensing on and thus damaging the platinum thermometer. The dewar wall was filled with helium at 2 psig to enhance heat transfer. The side fan and the blower for withdrawing the nitrogen vapor from the cryostat LN_2 inlet were turned on. The LN_2 was controlled at the desired level which was about even with the upper opening of the stirrer-heater assembly. The Freon-13 storage cylinder then was connected to the Freon inlet opening. Freon was charged into the inside dewar at 2 psig positive pressure. It took about 2 hours to condense the Freon to about one inch above the upper opening of the stirrer-heater assembly. Then the heater-thermotrol-stirrer mechanism was turned on. By adjusting the

dewar wall vacuum, electrical heating, and controlling the LN_2 level, it was possible to bring the cryostat temperature up to the operating temperature.

In order to transfer LN_2 to the cryostat it was necessary to have a slight positive pressure inside the 50 liter storage dewar. The venting valve of the 50 liter dewar was opened slightly to prevent excessive pressure build-up. If the venting valve was closed the initial pressure may be 2 psig, but when the pressure built up, the float-valve LN_2 liquid level controller could not prevent LN_2 from flowing into the outside cryostat. Thus LN_2 level was increased and overflow occurred. This was very undesirable, because it upset the temperature control and also might damage the cryostat by forcing the LN_2 through the styro-foam insulation cover between the two dewars. It was expedient to increase the LN_2 consumption somewhat by keeping the venting valve slightly open instead of risking damage to the cryostat.

The above method was adopted for the period of using a failing 50 liter storage dewar. Eventually this 50 liter storage dewar failed and took the glass LN_2 transfer line with it. Another 50 liter storage dewar was used with a new Invar LN_2 transfer line. The situation of excessive pressure build up never occurred again. Thus even putting another 10 psig relief valve in place of the venting valve in the multiple-purpose Teflon dewar head was proven to be unnecessary. The venting valve was closed all the time except when refilling the 50 liter storage dewar.

Another critical factor is to keep a positive pressure helium atmosphere above the Freon-13 bath fluid. In the initial stage of remodeling the system, a gas bath cryostat was contemplated and tried out. Besides the problem of bad temperature control in the gas bath cryostat another serious problem was the leakage of dry helium from the inside dewar. In the present experiment, it was found that the main leakage passage was around the stirrer shaft. Although the stirrer shaft packings were replaced, using Teflon Chevron bushings, the problem still was not solved. To cut down the dry helium consumption, a positive helium atmosphere on the order of 0.05 psig was maintained above the bath fluid. The dry helium stored in small storage tanks at 40 psig pressure lasted about 12 hours.

Due to the unusually large consumption of dry helium caused by the leakage of the dewar top, it was decided to use dry nitrogen gas as the inert atmosphere above the bath fluid. This approach was adopted after the stirrer-heater assembly shaft packing reinforced with a 1/4" style 380 twisted asbestos and rubber stem packing failed to prevent the leak. A line was branched out from the 50 liter dewar's Teflon head with a needle valve. This line was then connected with a flexible Tycon tubing to the cryostat dewar top. The needle valve was cracked a bit such that at all times a 1 psig positive pressure dry nitrogen atmosphere was maintained above the cryostat bath fluid.

Since the situation now was a dynamic one as the dry nitrogen gas was actually flowing into and leaking out at the same time. Therefore, it was absolutely necessary to keep the 50 liter storage dewar from completely emptying during the experimental runs.

Another task was that of condensing the Freon-13 to a desired level of about 1 inch above the upper opening of the stirrer. This was accomplished with the following procedures:

1. An approximate amount of Freon-13 was condensed into the inner dewar just about even with the upper stirrer opening.
2. By controlling the temperature at about the higher operating temperature, the bath level was maintained at the desired height by charging Freon from the Freon cylinder.
3. When the operating temperature was lowered from 161.36°K to 115.77°K, the Freon level was lowered on the order of an inch. Then additional Freon was charged into the inner dewar to make up the original level.

The above procedure was adopted because it was extremely difficult to remove the Freon if the operating level was exceeded. If the Freon were condensed at the lower operating temperature to the desired level, the Freon level would be too high at the upper temperature. This would

create a stagnant layer of Freon which could not be removed by the stirring action, thus making temperature control somewhat more difficult.

It was necessary to add the Freon-13 bath fluid after each experimental run to make up the original bath fluid level.

The temperature of the cryostat was controlled to within $\pm 0.001^\circ\text{K}$ after an optimum controlling combination was found by a trial and error procedure. Then the cryostat was controlled at the operating temperature for a period of not less than 24 hours before an experimental run.

Charging and Weighing of the High Pressure

Sample Bomb

There are three sample bombs which were used in this experiment. Two were heat treated and one was not. The one which has more dark marks left from the heat treatment was denoted as No. 4 bomb, while the other one which has less dark marks was denoted as No. 1 bomb. The one which was not heat treated was denoted as No. 3 bomb. Bomb No. 4 was used to contain argon and to contain xenon, while the bomb No. 1 was used to contain krypton.

As mentioned before, a separate apparatus was built for the purpose of filling the sample bomb with experimental gas. When the bomb was first used, it was evacuated down to below 2μ and then purged with the sample gas and then re-evacuated down to below 2μ . The amount of gas sample

required was estimated and the corresponding bomb pressure calculated. The sample bomb was then filled with the sample gas to the estimated pressure.

In weighing the sample bomb, proper account of the change of buoyancy effect due to the volume changes caused by the change in the internal pressure of the bomb must be made. The pressure effects on the bomb volumes are represented in the following equation:

$$V = V_o + aP \quad (P \text{ in psia})$$

<u>Bomb No. .</u>	<u>V_o (cm³)</u>	<u>$a \times 10^3$</u>
1	587.69	1.68
3	587.72	2.36
4	586.39	1.70

The substituting weighing method described in Appendix B was used in the weighing of the bombs. In handling the sample bomb care was taken not to use bare hands, but by using the gloves to keep the bomb from any finger prints. The bomb was kept scrupulously clean during the experiment. The bomb valve was closed or opened with a specially made extended nut. Each time when closing the valve a torque wrench was used to make sure that a 15 inch-pound torque was applied. The bomb was weighed before being connected to the transfer line. During the run, the bomb stays connected to the system. Because of that, the line connecting the bomb and the system is also included in the transfer line calculations. After one pure component run,

or after the one component was condensed, or the second compound condensed and the mixture run finished, the bomb was disconnected from the system and weighed. In the weighing process, the readings of humidity, the barricade temperatures, and the barometric pressures were recorded. This procedure permits the accurate calculations of the mass measurements by taking into account the various correction factors.

Condensation of Gas Sample into the Pycnometer

The condensation process can be best described in two parts. First, the one component process is described, then the binary mixture process is described.

After connecting the bomb to the system, the pycnometer valve was closed and the connecting line was evacuated down to 2μ . The cryostat was controlled at about 1°K above the operating temperature. This condensation process is the most critical phase in all the experimental operation. The intriguing problems it poses are: (1) how to condense the right amount of sample gases so that the liquid level inside the pycnometer could be measured at around the operating temperature; (2) how not to overpressurize the system during the condensation process; and (3) how to insure the tightness of the system. In view of the highly expensive gases used in this experiment, these problems cannot be overlooked and were tackled with extra care during this investigation.

Condensation Process in a Pure Component Run

In the pure component run, the pycnometer, the transfer line, and the pressure gauge were evacuated to 2μ . Then the pycnometer valve PV was closed. The sample bomb which had been weighed was then connected to the system next to V2. After V2 was opened, the transfer line was reevacuated to 2μ before PV was opened. The cryostat temperature was controlled at about one degree centigrade above the operating temperature. The system isolation valve V1 was then closed.

The pycnometer vacuum jacket and the pressure gauge vacuum port were being continuously evacuated. Before opening the bomb valve, the V2 and the metering valve V3 were closed. Then the bomb was opened by using a special extending fitting. The valves V2 and V3 were then slightly adjusted to allow the sample gas to flow into the pycnometer. Care must be taken not to overpressurize the system and hence jeopardize both the Pyrex pycnometer and the fused quartz pressure gauge. The water relief valve was watched closely to make sure that no leakage occurred through the relief valve. The condensation process usually took about three to four hours.

At the impending stage of filling up the pycnometer, the valves V2 and V3 were slightly closed to prevent any rapid pressure build up. After the bomb valve was closed, the cryostat temperature was lowered

to operating temperature to draw the liquid in the capillary stem back to the pycnometer bulb. The pycnometer jacket was then filled with dry helium gas. The above procedure was repeated until sufficient amount of gas was condensed.

Condensation Process in a Mixture Run

The less volatile component was condensed first in the binary mixture run. The amount of gas to be condensed was estimated first for a specific mixture composition. When the estimated height of the liquid level inside the pycnometer bulb was reached the bomb valve was closed.

The pycnometer valve PV was closed and the pressure reading and the tubing panel temperature reading were taken. These data were used in part of the transfer line gas calculations. The valve V2 was closed. The sample bomb was disconnected and weighed.

Condensation of the more volatile compound was done in a similar fashion to that of the pure component run. However, there were some steps that deserved special attention. The pycnometer content was continuously stirred during this condensation process to maintain an homogeneous liquid composition. After the bomb valve was closed, the cryostat temperature was lowered several degrees below the operating temperature. The liquid was drawn back from the capillary into the pycnometer bulb. The mixture was stirred again. The temperature was then raised slowly. The stirring action was stopped when the

liquid level barely reached the capillary stem. Otherwise, the liquid in the capillary might be segmented with entrapped vapor space, thus rendering it impossible for undertaking the liquid volume readings. The above procedure of mixing was repeated for a couple of hours to ensure the homogeneous liquid composition. It also served to create the saturation vapor atmosphere above the liquid. Afterwards, the pycnometer content was not stirred during the volumetric reading period.

Liquid Volume Reading Procedure by Using the
Cryogenic Periscope in Conjunction with
a Cathetometer

The cathetometer was balanced and aligned with the periscope for viewing the pycnometer capillary stem graduations. The cryostat temperature was stabilized at a specific temperature for at least one and a half hours. During this period, two sets of readings of temperature and liquid level were taken about thirty minutes apart. The readings were recorded when they stayed constant. The corresponding system pressure and the tubing panel temperature were recorded. Otherwise, additional time was allowed for stabilization.

The temperature was then raised gradually so that the liquid level was raised gradually and stabilized at about ten graduations above its previous reading. In several runs, after the liquid level reached the highest

reading, one more reading was taken by lowering the temperature. This reading served to check if there was any inconsistency or leakage of gas. By this method, a leakage of gas was promptly detected in Run Number 11, when the fused quartz pressure gauge bourdon tube sealing failed. The pressure gauge was dismantled from the system. The bourdon tube capsule was taken apart and the sealing repaired. The tube was then recalibrated inside the pressure gauge. It cannot be overemphasized that a leak-free system is essential to the success of this kind of experiment. During the experiment the valve stem positions of V2, V3, and PV were maintained at exactly the same positions as those during the calibration of the transfer line volume.

Experimental Run of the Argon and Xenon Mixture

The sole run on argon and xenon mixture was made at 115.77°K. The pure xenon was at solid state at this temperature. First, the composition of the mixture was decided to be $x_{Xe} < 0.25$ by using Heastie's paper [34]. It was estimated that the mixture would stay liquid. Extreme care must be exercised not to solidify the xenon in the process of condensation. It was found that once xenon was solidified, it was almost impossible to dissolve it in the liquid solution. Thus xenon was condensed at a temperature slightly higher than its triple point. The cryostat temperature was maintained at this temperature while argon gas was allowed to flow into the pycnometer at

a pressure above 100 psia. While at this high pressure, the cryostat temperature was gradually lowered and the pycnometer bulb content continuously stirred. In this way, the solidification problem was avoided. The volume reading procedure was the same as that mentioned before.

Completion of the Experimental Runs

At the end of each run, the pressure gauge evacuation port valve, the pycnometer vacuum jacket isolation valve, and the dewar wall evacuation valve were closed. The valve V2 was closed before disconnecting the bomb from the system for weighing. Then with the pycnometer valve opened, the system isolation valve V1 was opened for evacuating the liquified rare gases from the pycnometer bulb.

When the whole system required a temporary shut down, or at the end of the whole experiment, it was necessary to vaporize the bath fluid from the cryostat dewar. This was accomplished by the following procedure:

1. keeping the system opened at the vacuum pump.
2. stop transferring liquid nitrogen into the 50 liter storage dewar.
3. turning off the stirrer-heater assembly switch.
4. connecting a Tycon tubing to a dewar top hole for venting the Freon-13 vapor into the hood.

CHAPTER VI

DATA AND APPLICATIONS

The experimental results are presented in this chapter. The pure component liquid density of argon, krypton, and xenon are treated first. In order to calculate the liquid mixture density, the pure component vapor pressure and molar volume were obtained from the pure component experimental results. The details of data treatment are given in Appendix D. The accuracies of the data are established in Appendix C. The liquid density data and saturation pressure data are compared with literature data. Further, the excess volume and the excess Gibbs free energy were derived from the experimental results for argon + krypton liquid mixture at 115.77°K and for krypton + xenon liquid mixture at 161.36°K.

Experimental Results

Because the liquid density values were measured as a function of temperature in a small temperature range, around either 115.77°K or 161.36°K, extrapolations or interpolations of treated data were required. The liquid density data of pure components was fit by least square

method to the equation:

$$\rho = a + bt \quad (1)$$

where ρ is liquid density in gm/ml., t is temperature in °C. The saturated liquid density, the saturated vapor pressure, and the liquid molar volume of the pure components are reported in Table 2. The constants a and b in Equation (1) for the pure components are presented in Table 3. It can be seen that the equation will reproduce the liquid density within the experimental accuracy.

In order to treat liquid mixture density data, pure component liquid molar volume was obtained by using Equation (1). The pure component vapor pressures have been reported in some correlated equations given by Garside and Smith [29], Thodos, et al. [33], and Bowman, et al. [10].

Although the vapor pressures predicted by the Garside and Smith equation were used first, it was found that the predicted vapor pressures for argon at 115.77°K are 5.4 psia too high. In other cases, the deviations are consistently on one side of the experimental data. The pure component saturation vapor pressures obtained in this investigation were fitted by non-linear least square method to the Antoine equation:

$$\ln P = C + \frac{A}{B + T} \quad (2)$$

TABLE 2
SATURATED LIQUID DENSITY AND MOLAR VOLUME OF THE
PURE COMPONENTS ARGON, KRYPTON, AND XENON

COMPONENT (RUN NO.)	TEMPERATURE °C	PRESSURE psia	DENSITY gm/ml	MOLAR VOLUME ml/gm-mole
Argon (6)	-157.6327	136.088	1.200017	33.2862
	-157.5530	136.677	1.199391	33.3036
	-157.4862	137.194	1.198861	33.3183
	-157.3964	138.024	1.198157	33.3379
	-157.3034	138.757	1.197435	33.3579
	-157.2178	139.514	1.196773	33.3764
	-157.1510	140.009	1.196270	33.3904
Krypton (5)	-157.3782	10.593	2.449646	34.2090
	-157.2811	10.673	2.448928	34.2190
	-157.1822	10.765	2.448198	34.2293
	-157.0722	10.866	2.447386	34.2406
	-156.9477	10.976	2.446504	34.2530
	-156.8047	11.109	2.445410	34.2683
	-156.6572	11.249	2.444341	34.2833
	-156.4905	11.408	2.443134	34.3002
Krypton (19)	-157.4120	10.633	2.449795	34.2069
	-157.2682	10.762	2.448736	34.2217
	-157.1492	10.869	2.447825	34.2345
	-156.9522	11.048	2.446378	34.2547
	-156.7718	11.214	2.445075	34.2730
	-156.5940	11.380	2.443771	34.2913
	-156.4566	11.509	2.442735	34.3058
Krypton (18)	-112.1518	157.038	2.061305	40.6539
	-112.0218	157.940	2.059880	40.6820
	-111.9042	158.739	2.058684	40.7056
	-111.8017	159.425	2.057598	40.7271
	-111.6897	160.207	2.056487	40.7491
	-111.6324	160.606	2.055876	40.7612
	-111.5750	161.010	2.055248	40.7737
Xenon (13)	-111.7697	11.907	2.969355	44.2184
	-111.6192	12.017	2.968342	44.2334
	-111.4357	12.130	2.967063	44.2525
	-111.2448	12.262	2.965783	44.2716
	-111.0180	12.428	2.964236	44.2947
	-110.7752	12.604	2.962598	44.3192
	-110.5446	12.778	2.961109	44.3415

TABLE 3

SATURATED DENSITIES OF LIQUEFIED HEAVY RARE GASES

 X_{AR} = Argon Mole Fraction, X_{KR} = Krypton Mole Fraction

 $\rho = a + b \cdot t$, t in degree centigrades, ρ in gm/ml

 X' = overall composition

COMPONENT (RUN NO.)	a	b	TEMPERATURE RANGE, °C	DEVIATION	
				MAXIMUM $\times 10^5$	MINIMUM $\times 10^6$
Argon (6)	-0.2774306 (-1)	-0.7788685 (-2)	-157.6327 -157.1510	1.434	- 3.470
Krypton (5)	+0.1294079 (+1)	-0.7342581 (-2)	-157.3782 -156.4905	2.374	0.004
Krypton (19)	+0.1289519 (+1)	-0.7370884 (-2)	-157.4120 -156.4566	1.584	9.818
Krypton (18)	+0.9017157 (+0)	-0.1033884 (-1)	-112.1581 -111.5750	2.897	4.078
Xenon (13)	+0.2214650 (+1)	-0.6752164 (-2)	-111.7697 -110.5446	4.352	-10.54
Argon+Krypton (7) $X'_{Ar} = 0.49556$	+0.7092217 (+0)	-0.7342636 (-2)	-158.5574 -157.7161	-2.424	0.480
Argon+Krypton (8) $X'_{Ar} = 0.72102$	+0.3961676 (+0)	-0.7495145 (-2)	-157.3356 -156.6820	2.803	0.044

TABLE 3
(CONTINUED)

COMPONENT (RUN NO.)	a	b	TEMPERATURE RANGE, °C	DEVIATION	
				MAXIMUM x 10 ⁵	MINIMUM x 10 ⁶
Argon+Krypton (9) $X'_{Ar} = 0.88067$	+0.1544783 (+0)	-0.7637121 (-2)	-158.5893 -158.0392	-1.746	2.538
Krypton+Xenon (12) $X'_{Kr} = 0.68435$	+0.1415827 (+1)	-0.8717321 (-2)	-112.0829 -111.2890	2.116	0.196
Krypton+Xenon (15) $X'_{Kr} = 0.21245$	+0.2004375 (+1)	-0.7171072 (-2)	-112.3707 -111.2871	-2.706	5.972
Krypton+Xenon (16) $X'_{Kr} = 0.27852$	+0.1932535 (+1)	-0.7333469 (-2)	-112.3378 -111.1986	1.468	2.293
Krypton+Xenon (17) $X'_{Kr} = 0.82649$	+0.1213469 (+1)	-0.9246239 (-2)	-112.0415 -111.2843	-2.509	2.947
Argon+Xenon (20) $X'_{Ar} = 0.87617$	+0.3296460 (+0)	-0.7617794 (-2)	-157.7792 -157.1849	1.211	-1.593

where P is the pressure in psia, A , B , C are Antoine constants, and T is the temperature in $^{\circ}\text{K}$. The Antoine constants determined from both the pure component and the mixture runs are given in Table 4.

The saturated vapor pressure, the liquid density, (shown in Figure 11 and in Figure 12) and the molar volume for the liquid mixtures are presented in Table 5.

The liquid density data, the molar volume data, and the saturated vapor pressure for the pure components argon and krypton at 115.77°K and for the pure components krypton and xenon at 161.36°K are obtained by either extrapolation or interpolation. The results are given in Table 6. Similar results for the binary mixtures argon and krypton at 115.77°K and krypton and xenon at 161.36°K are presented in Table 7. In calculating the liquid molar volume at the operating temperatures (115.77 or 161.36°K), the liquid phase compositions, x , were either extrapolated or interpolated from experimental data. The application of the experimental data will be discussed in a later section.

Argon and Xenon Mixture

One mixture run was done for argon and xenon mixture at 115.77°K . In order to calculate the liquid mixture density, it was necessary to obtain subcooled liquid volume of xenon. Pure xenon exists in solid state at 115.77°K . It was found that the equation for liquid xenon

TABLE 4
SATURATED VAPOR PRESSURES OF ARGON, KRYPTON, AND
XENON, AND THEIR BINARY MIXTURES EXPRESSED
IN TERMS OF ANTOINE CONSTANTS

COMPONENT (RUN NO.)	TEMPERATURE RANGE, °K	ANTOINE CONSTANTS	MAXIMUM DEVIATION psia	MINIMUM DEVIATION psia
Argon (6)	115.5173 115.9990	-0.23266935 (+3) -0.17806979 (+3) +0.11934638 (+1)	-0.053	-0.001
Krypton (5)	115.7718 116.6595	-0.19164569 (+3) -0.16406426 (+3) -0.16085438 (+1)	+0.005	+0.001
Krypton (19)	115.7380 116.6934	-0.19702868 (+3) -0.67749420 (+2) +0.64630124 (+1)	-0.005	+0.000
Krypton (18)	160.9919 161.5750	-0.22466584 (+2) -0.18418930 (+3) +0.40879653 (+1)	+0.013	+0.000
Argon+Krypton (7)	114.5926 115.4339	-0.15777204 (+2) -0.13224205 (+3) +0.33627298 (+1)	+0.081	+0.005
Argon+Krypton (8)	115.8144 116.4626	-0.34804939 (+3) -0.36838449 (+2) +0.90330291 (+1)	+0.072	-0.024
Argon+Krypton (9)	114.5607 115.1108	-0.25421627 (+2) -0.93465001 (+2) +0.59305723 (+1)	-0.041	-0.002
Krypton+Xenon (15)	160.7793 161.8629	-0.77685207 (-1) -0.16313673 (+3) +0.37695096 (+1)	+0.037	+0.002
Krypton+Xenon (16)	160.8122 161.9514	-0.30767964 (+2) -0.19376854 (+3) +0.30652320 (+1)	+0.052	-0.003

TABLE 4
(CONTINUED)

COMPONENT (RUN NO.)	TEMPERATURE RANGE, °K	ANTOINE CONSTANTS	MAXIMUM DEVIATION psia	MINIMUM DEVIATION psia
Krypton+Xenon (17)	161.1085 161.8657	-0.96045537 (+0) -0.16645957 (+3) +0.46931404 (+1)	+0.052	-0.003
Krypton+Xenon (12)	161.0671 161.7011	-0.26879658 (+3) +0.10127935 (+3) +0.63120438 (+1)	+0.094	-0.015
Krypton+Xenon (14)	160.4944 161.4697	-0.43589130 (-0) -0.16472516 (+3) 0.43610233 (+1)	-0.133	+1.002
Argon+Xenon (20)	115.3708 115.9651	-0.47915338 (+1) -0.12480006 (+3) +0.42780394 (+1)	-0.116	+0.003

Note: For Antoine Constant -0.233(+3) denotes $-0.233 \times 10^{+3}$.

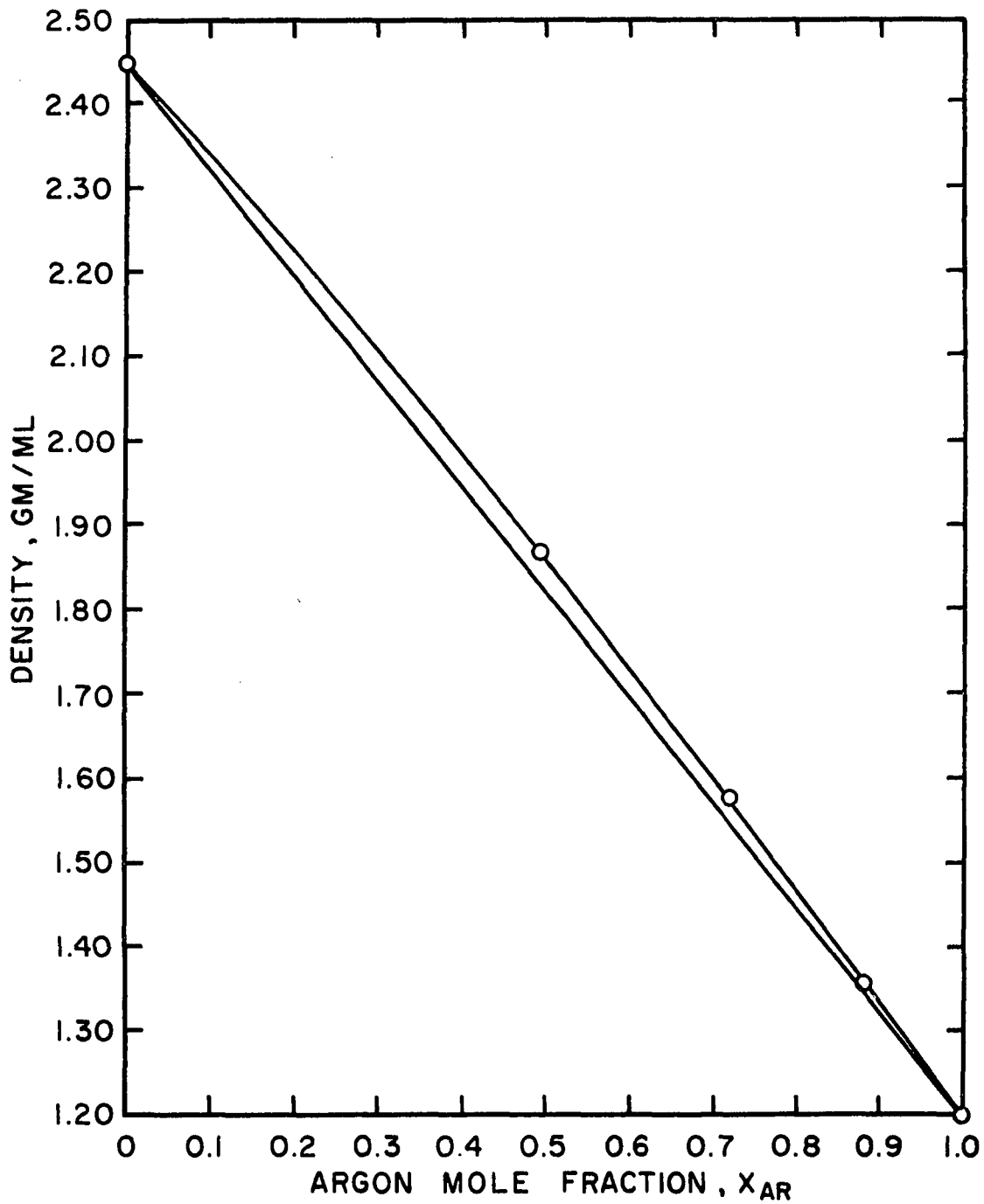


Figure 11. Saturated Liquid Density of Argon and Krypton Mixture at 115.77°K

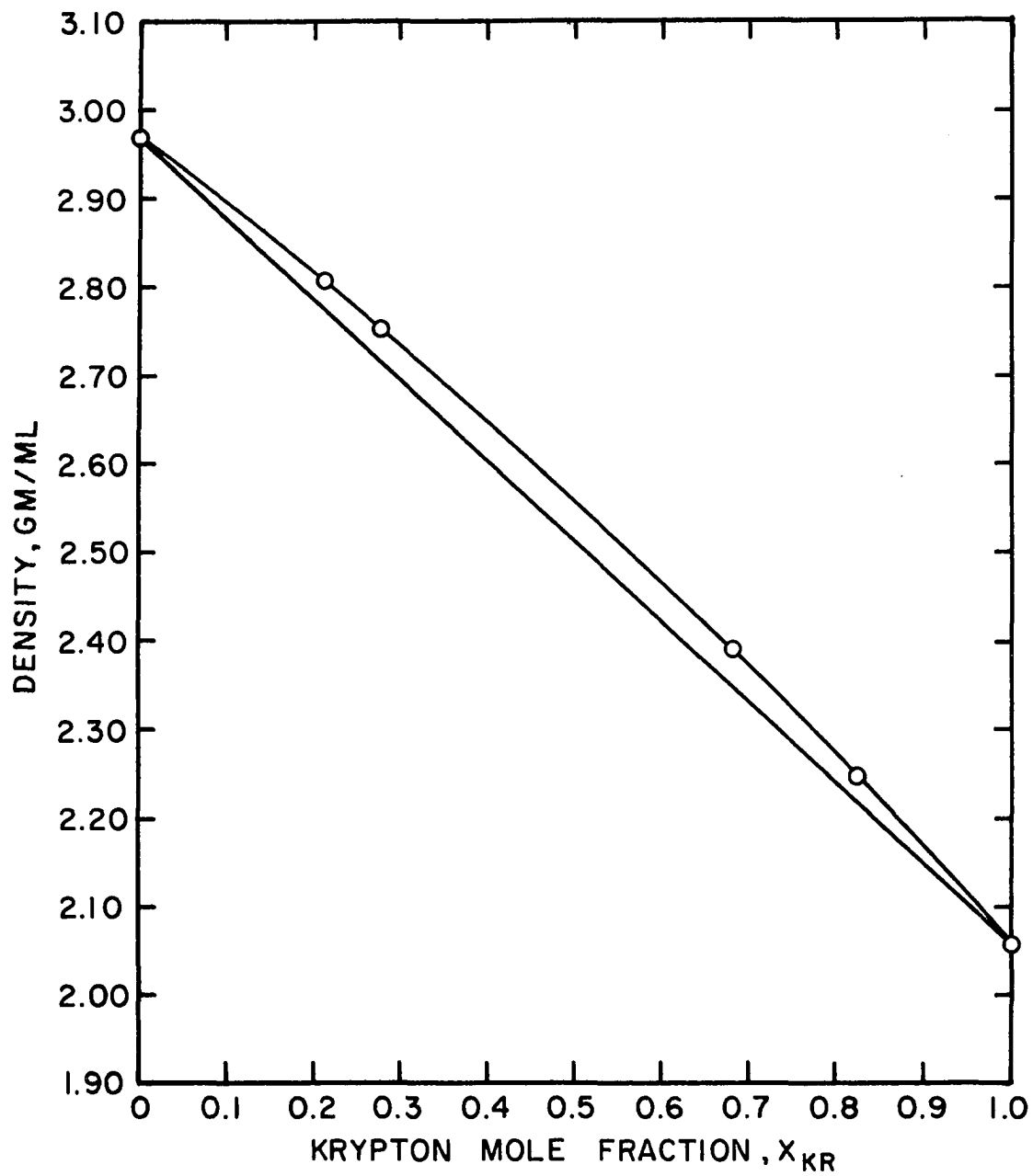


Figure 12. Saturated Liquid Density of Krypton and Xenon Mixture at 161.36°K

TABLE 5

SATURATED LIQUID DENSITY AND MOLAR VOLUME
OF THE BINARY MIXTURES ARGON+KRYPTON,
KRYPTON+XENON, AND ARGON+XENON

MIXTURE (RUN NO.)	TEMPERATURE °C	PRESSURE psia	DENSITY gm/ml	MOLAR VOLUME ml/gm-mole
Argon+Krypton (7) $x'_{Ar} = 0.49556$	-158.5574	70.535	1.873443	33.1696
	-158.4401	71.078	1.872591	33.1849
	-158.3495	71.301	1.871947	33.1964
	-158.2186	71.810	1.870956	33.2142
	-158.0768	72.336	1.869898	33.2333
	-157.9651	72.814	1.869106	33.2475
	-157.8708	73.181	1.868419	33.2599
	-157.7646	73.594	1.867628	33.2741
	-157.7161	73.808	1.867274	33.2805
Argon+Krypton (8) $x'_{Ar} = 0.72102$	-157.3356	102.068	1.575418	33.1597
	-157.2536	102.621	1.574810	33.1726
	-157.0960	103.518	1.573641	33.1975
	-157.0008	103.985	1.572889	33.2135
	-156.8927	104.617	1.572101	33.2303
	-156.7946	105.173	1.571359	33.2461
	-156.6820	105.938	1.570504	33.2645
	-156.6874	105.810	1.570590	33.2626
Argon+Krypton (9) $x'_{Ar} = 0.88067$	-158.5893	112.786	1.365488	33.1072
	-158.4941	113.415	1.364764	33.1248
	-158.3925	114.010	1.363966	33.1443
	-158.3074	114.602	1.363347	33.1594
	-158.2286	115.116	1.362713	33.1749
	-158.1371	115.669	1.362039	33.1915
	-158.0392	116.290	1.361287	33.2099
Krypton+Xenon (12) $x'_{Kr} = 0.68435$	-112.0829	114.681	2.392890	41.3293
	-111.9785	114.743	2.391963	41.3454
	-111.8656	114.868	2.391008	41.3619
	-111.7170	115.076	2.389696	41.3848
	-111.5778	115.141	2.388508	41.4055
	-111.4442	115.265	2.387321	41.4262
	-111.2890	115.583	2.385961	41.4499
	-111.4489	115.255	2.387357	41.4255

TABLE 5
(CONTINUED)

MIXTURE (RUN NO.)	TEMPERATURE °C	PRESSURE psia	DENSITY gm/ml	MOLAR VOLUME ml/gm-mole
Krypton+Xenon (15) $x'_{\text{Kr}} = 0.21245$	-112.3707	44.808	2.810181	43.1640
	-112.1610	44.958	2.808705	43.1866
	-111.9747	45.125	2.807339	43.2077
	-111.7847	45.269	2.806009	43.2281
	-111.5985	45.574	2.804671	43.2489
	-111.4122	45.809	2.803293	43.2702
	-111.2871	46.094	2.802429	43.2837
Krypton+Xenon (16) $x'_{\text{Kr}} = 0.27852$	-112.3378	54.531	2.756366	42.8736
	-112.1873	54.738	2.755252	42.8910
	-111.9531	55.157	2.753537	42.9179
	-111.7659	55.422	2.752157	42.9395
	-111.5684	55.758	2.750733	42.9619
	-111.3841	56.035	2.749351	42.9836
	-111.1986	56.417	2.748009	43.0048
Krypton+Xenon (17) $x'_{\text{Kr}} = 0.83649$	-111.9813	55.124	2.753750	42.9146
	-112.0415	130.677	2.249451	40.9467
	-111.8788	131.369	2.247930	40.9746
	-111.7923	131.800	2.247102	40.9898
	-111.6794	132.412	2.246073	41.0087
	-111.5571	133.065	2.244949	41.0294
	-111.4038	133.798	2.243545	41.0552
Argon+Xenon (20) $x'_{\text{Ar}} = 0.87617$	-111.2843	134.619	2.242437	41.0755
	-157.7792	119.848	1.531568	33.5190
	-157.6794	120.488	1.530827	33.5355
	-157.5851	121.160	1.530091	33.5518
	-157.4908	121.735	1.529381	33.5676
	-157.3966	122.467	1.528658	33.5838
	-157.2838	123.286	1.527803	33.6029
	-157.1849	124.001	1.527046	33.6198

TABLE 6

SATURATED LIQUID DENSITY AND MOLAR VOLUME OF THE
PURE COMPONENTS ARGON, KRYPTON, XENON

COMPONENT (RUN NO.)	TEMPERATURE °K	PRESSURE psia	DENSITY gm/ml	MOLAR VOLUME ml/gm-mole
Argon (6)	115.77	138.122	1.198040	33.3411
Krypton (5)	115.77	10.588	2.449654	34.2089
Krypton (19)	115.77	10.591	2.449549	34.2104
Krypton (18)	161.36	159.505	2.057495	40.7291
Xenon (13)	161.36	11.897	2.969475	44.2166

TABLE 7

SATURATED LIQUID DENSITY AND EXCESS VOLUME OF THE BINARY LIQUID
MIXTURES OF ARGON, KRYPTON, AND XENON

SYSTEM	COMPOSITION, X_1	TOTAL PRESSURE, psia	DENSITY, gm/cm ³	MOLAR VOLUME, cm ³ /gm-mole	EXCESS VOLUME, cm ³ /gm-mole
<u>Argon+Krypton at 115.77°K, $X_1 = X_{Ar}$</u>					
	0.0	10.588	2.449654	34.2089	0.0
	.49377	75.230	1.864805	33.3253	- .4551
	.71963	101.852	1.575753	33.1523	- .4321
	.87975	120.403	1.356251	33.3337	- .1116
	1.0	138.122	1.198040	33.3411	0.0
<u>Krypton+Xenon at 161.36°K, $X_1 = X_{Kr}$</u>					
	0.0	11.897	2.969475	44.2166	0.0
	.21056	45.297	2.806029	43.2276	- .2547
	.27629	55.402	2.752344	42.9366	- .3194
	.68217	114.963	2.390336	41.3736	- .4640
	.82509	131.826	2.247106	40.9897	- .3494
	1.0	159.505	2.057495	40.7291	0.0
<u>Argon+Xenon at 115.77°K, $X_1 = X_{Ar}$</u>					
	.87528	122.538	1.528534	33.5866	- .2477

given by Staveley, et al. cannot be used at this temperature. In data treatment, the Simon's equation, which was used in the average potential model, was used to calculate the sub-cooled liquid volume of xenon. The value obtained by this extrapolation was $33.3375 \text{ cm}^3/\text{gm-mole}$ at 115.7533°K . The average molar volume of solid xenon between 48 to 161.37°K was $38.3 \text{ cm}^3/\text{gm-mole}$ (value at 152°K) as reported by Ziegler [101]. The vapor pressure of xenon at 115.77°K was 0.00836 atm . obtained from interpolation of their tabulated values. The second virial coefficient was calculated from the equation given by Guggenheim. This equation was explained in Appendix D. The results of calculations are presented in Table 3 and Table 7.

Accuracy of the Experimental Results

The accuracy of the experimental results is established in Appendix C. The smoothness of the resultant experimental data can be judged from the results presented in the previous section. The inherent errors due to the experimental apparatus are discussed in Appendix C. Thus, further check on the accuracy of the experimental results can be obtained from a check on the reproducibility of the data and from the comparison with literature data.

The reproducibility of the experimental data was established from two independent runs on the liquid density of krypton at 115.77°K . It should be emphasized that the first run, run number 5, of krypton was made by using the

old pressure gauge calibration. The second run of krypton, run number 19, was made by using the new pressure gauge calibration after a leaky pressure gauge occurred and was detected during run number 11.

The experimental results of the two krypton runs at 115.77°K can be readily compared in Table 5 and in Table 6. The difference in the vapor pressure of the two runs at 115.77°K is 0.003 psia which is within the accuracy of the pressure gauge (0.05 in Hg). The difference in the saturated liquid density is 1×10^{-4} gm/ml at 115.77°K, which is within the accuracy of the pure component runs.

Recently, Staveley and co-workers have done similar investigations. First, they did the experimental and theoretical work on the thermodynamics of liquid mixtures of argon and krypton [21]. A distinct feature is that it was found that the excess volume curve of argon and krypton was not symmetrical with respect to the composition, instead, the curve showed a minimum at an argon mole fraction of approximately 0.6. Besides, there are discrepancies between Oxford's excess Gibbs function values and those reported by Göttingen's group, i.e., Schmidt [67] and Wilhelm and Schneider [97].

Staveley, et al. [84] further measured and reported the densities of liquid argon, krypton, xenon, oxygen, nitrogen, carbon monoxide, methane, and carbon tetrafluoride, along the orthobaric liquid curve. They reported the data

with a precision of a few parts in 10^4 . A Pyrex pycnometer with a wall thickness of 4 mm. and 9,000 cm³ bulb was used. They also fitted the experimental data to polynomials in $(T-T_r)$, T is the temperature in °K, T_r is a convenient reference temperature. For argon, krypton, and xenon that are concerned here T_r is the triple point temperature.

$$V = V_r + \sum_{i=1}^{i=5} A_i (T-T_r)^i \quad (3)$$

This polynomial reproduces Staveley's density data of argon, krypton, and xenon within a maximum deviation of 0.014 cm³/mole for argon molar volume 33.619 cm³/mole at 116.43°K. This information with the constants V_r , T_r , A_i , are presented in Table 2 of Terry, et al. [84].

The comparisons of the experimental pure component liquid molar volume data with those obtained by Staveley, et al. are given in Table 8. In the temperature range from 115.5173 to 115.9990°K, the present experimental data for argon was lower than their value by 0.319% to 0.338%. For krypton in the temperature range from 115.7718°K to 116.6595°K, the present experimental data was lower than their value by 0.313% to 0.306% (Run No. 5). For krypton in the temperature range from 161.4452°K to 162.3390°K the present experimental data was lower than their value by 0.390% to 0.497%. For xenon in the temperature range from

TABLE 8
COMPARISON OF EXPERIMENTAL LIQUID MOLAR VOLUME
WITH RESULTS OF STAVELEY AND CO-WORKERS

TEMPERATURE, °K	$V_{\text{expt.}}$ cm ³ /gm-mole	V_{Oxford} cm ³ /gm-mole	$V_{\text{expt.}} - V_{\text{Oxford}}$, cm ³ /gm-mole
<u>Run No. 6, Argon</u>			
115.5173	33.2826	33.3924	-.1062
115.5970	33.3036	33.4106	-.1071
115.6638	33.3183	33.4259	-.1077
115.7536	33.3379	33.4466	-.1087
115.8466	33.3579	33.4680	-.1101
115.9322	33.3764	33.4878	-.1114
115.9990	33.3904	33.5033	-.1129
<u>Run No. 5, Krypton</u>			
115.7718	34.2090	34.3161	-.1071
115.8689	34.2190	34.3258	-.1067
115.9678	34.2293	34.3356	-.1064
116.0778	34.2406	34.3466	-.1060
116.2023	34.2530	34.3591	-.1061
116.3453	34.2683	34.3734	-.1051
116.4928	34.2833	34.3883	-.1050
116.6595	34.3002	34.4051	-.1049
<u>Run No. 19, Krypton</u>			
115.7380	34.2069	34.3127	-.1058
115.8818	34.2217	34.3270	-.1053
116.0008	34.2345	34.3389	-.1044
116.1978	34.2547	34.3586	-.1039
116.3782	34.2730	34.3767	-.1038
116.5560	34.2913	34.3946	-.1034
116.6934	34.3058	34.4085	-.1027
<u>Run No. 10, Krypton</u>			
161.4452	40.6209	40.7711	-.1502
161.5938	40.6416	40.8008	-.1591
161.7444	40.6621	40.8310	-.1689
161.9034	40.6871	40.8630	-.1759
162.0567	40.7085	40.8940	-.1855
162.1960	40.7297	40.9222	-.1925
162.3390	40.7489	40.9513	-.2024

TABLE 8
(CONTINUED)

TEMPERATURE, °K	$V_{\text{expt.}}$ $\text{cm}^3/\text{gm-mole}$	V_{Oxford} $\text{cm}^3/\text{gm-mole}$	$V_{\text{expt.}} - V_{\text{Oxford}}$ $\text{cm}^3/\text{gm-mole}$
<u>Run No. 13, Xenon</u>			
161.3803	44.2184	44.3120	-.0937
161.5308	44.2334	44.3267	-.0933
161.7143	44.2525	44.3446	-.0921
161.9052	44.2716	44.3632	-.0916
162.1320	44.2947	44.3854	-.0907
162.3748	44.3192	44.4092	-.0900
162.6054	44.3415	44.4318	-.0903

161.3803°K to 162.3748°K, the present experimental data was lower than their value by 0.0212% to 0.0203%.

However, there were two major differences in their experimental setup and the present investigation method. First, in assessing the mass of liquified gases condensed into the pycnometer, they applied corrections for gaseous imperfection and for small change in the internal 8 dm^3 volume of the calibrated "globes", which was submerged in a $25^\circ\text{C} \pm 0.01^\circ\text{K}$ thermostat, with pressure. This method of mass determination was definitely inferior to the substitution weighing method adopted in this investigation. The more serious drawback was that their periscope was illuminated by an internal light source. They admitted that the light had an appreciable heating effect, even though it was switched on for the shortest possible time when readings were taken. These factors may account for their high liquid molar volumes obtained. Their liquid argon molar volumes were larger than the British Oxygen Company's data by 0.17% near the triple point temperature, by 0.11% at 110°K, and by 0.27% at 120°K. Although their argon value differ from the Leiden results of Mathias, Onnes and Crommelin [52] by less than 0.1%, their methane liquid molar volumes were 0.15% larger than those reported by Davenport, Rowlinson, and Saville [20]. Their carbon tetrafluoride liquid molar volumes were 0.25% higher than those reported by Knobler and Pings [38], and

carbon monoxide liquid molar volumes at 80°K were 0.8% higher than those reported by Mathias and Crommelin [53].

The present liquid molar volume of argon at 115.77°K was 33.3411 ml/gm-mole as compared with 33.301 ml/gm-mole, which was 0.123% too low, reported by Davies, Duncan Saville, and Staveley [21]. The liquid molar volume of krypton at 115.77°K was 34.2089 ml/gm-mole as compared with their value of 34.222 ml/gm-mole, which was 0.038% too high.

The density calculated by our least square equation gave the krypton liquid density of 2.05694 g/cm³, at 161.414°K, which was 0.04% lower than 2.0579 g/cm³ reported by Theeuwes and Bearman [85]. It was believed that the accuracy of the present experimental data was firmly established. The density data at 115.77°K and 161.36°K obtained by extrapolation or interpolation from the experimental data are given in Table 8.

Application of Experimental Results, Calculation of Excess Volume

The application of experimental results was to obtain the excess thermodynamic properties from the experimental density data. These data are the basis for checking the statistical thermodynamic theories of simple liquid mixtures.

First the excess volume function was obtained from the following equation:

$$V^E = V_m - \sum_{i=1}^2 x_i V_i \quad (4)$$

where V_m , V_i , are the liquid molar volume of the mixture and of the pure component i respectively. All the volumes are at the same temperature and pressure. However, due to the uncertainties of the liquid compressibility data, the liquid volumes were taken to be the saturated liquid volume instead of those corrected to the liquid volume at zero pressure. The difference between the excess volume at zero pressure and the excess volume at saturation pressure was only $0.001 \text{ cm}^3/\text{gm-mole}$ for argon and krypton mixture at 115.77°K . This was about 0.2% of the excess volume and hence was negligible. The same was assumed for the krypton and xenon mixture at 161.36°K . The excess volumes of argon and krypton at 115.77°K , of krypton and xenon at 161.36°K , and of argon and xenon at 115.77°K were presented in Table 8.

The system of argon and krypton has been studied by Davies, Duncan, Saville, and Staveley [21]. Their excess volume data were plotted for comparison with those obtained in this investigation. The agreement was good. The purpose of making the argon and krypton run was to check Staveley's results. Also the cost of experimental gas was too prohibitive to make too many runs. Two mixture points were planned originally. Although one more

run at $x_{\text{Ar}} = 0.88$ was made, it was suspected that the gauge was leaking during this run. The excess volumes of argon and krypton at 115.77°K were plotted in Figure 13 with Staveley's results. It can be seen that the minimum of both curves were at $x_{\text{Ar}} = 0.6$, although there was a difference of 0.05 cm³/mole between the minima.

Thus, the "skewness" of the excess volume curve was confirmed. The total pressures of this system were plotted in Figure 14. It can be seen that the agreement was good.

The readings taken from the smoothed v^E curve were used to obtain the least square fitted equation:

$$v^E/x_1x_2 = A + B (x_1-x_2) + C (x_1-x_2)^2 \quad (5)$$

where x_1 was the mole fraction of the more volatile component. The constants are given in Table 9 with Staveley's value. The smoothed excess volume data read from the curve in Figure 13, were given in Table 10 with those calculated from Equation 5. The number in the first column was the weight assigned to the observation for the least square fit program.

For krypton and xenon mixture at 161.36°K, the excess volume data are presented in Table 11, and compared with Staveley's [77] data in Figure 15. Staveley's data were kindly communicated to the author by Professor L. A. K. Staveley of the Oxford University prior to the release for publication. Data in Figure 15 were generated

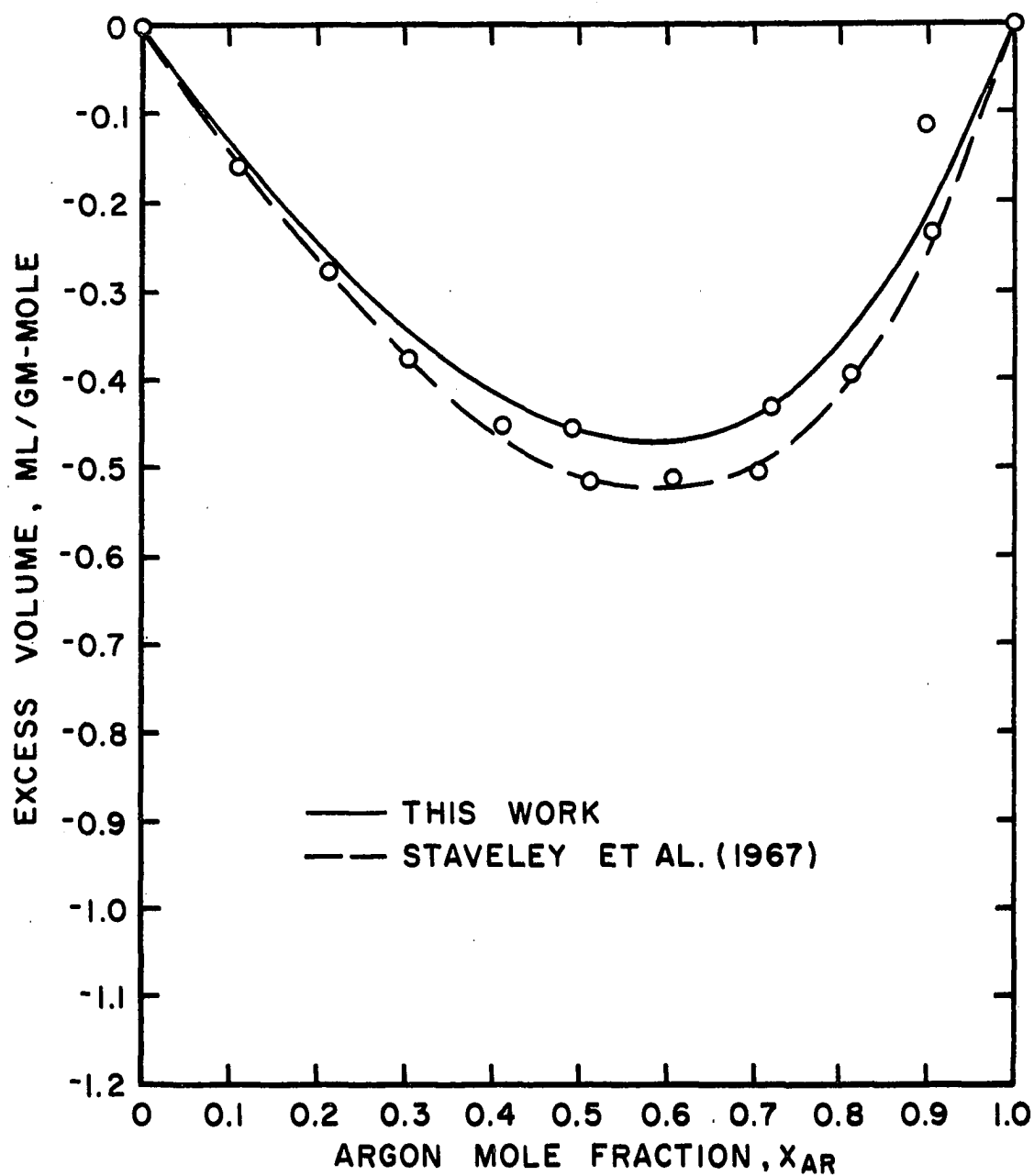


Figure 13. Excess Volume of Argon + Krypton Mixture at 115.77°K

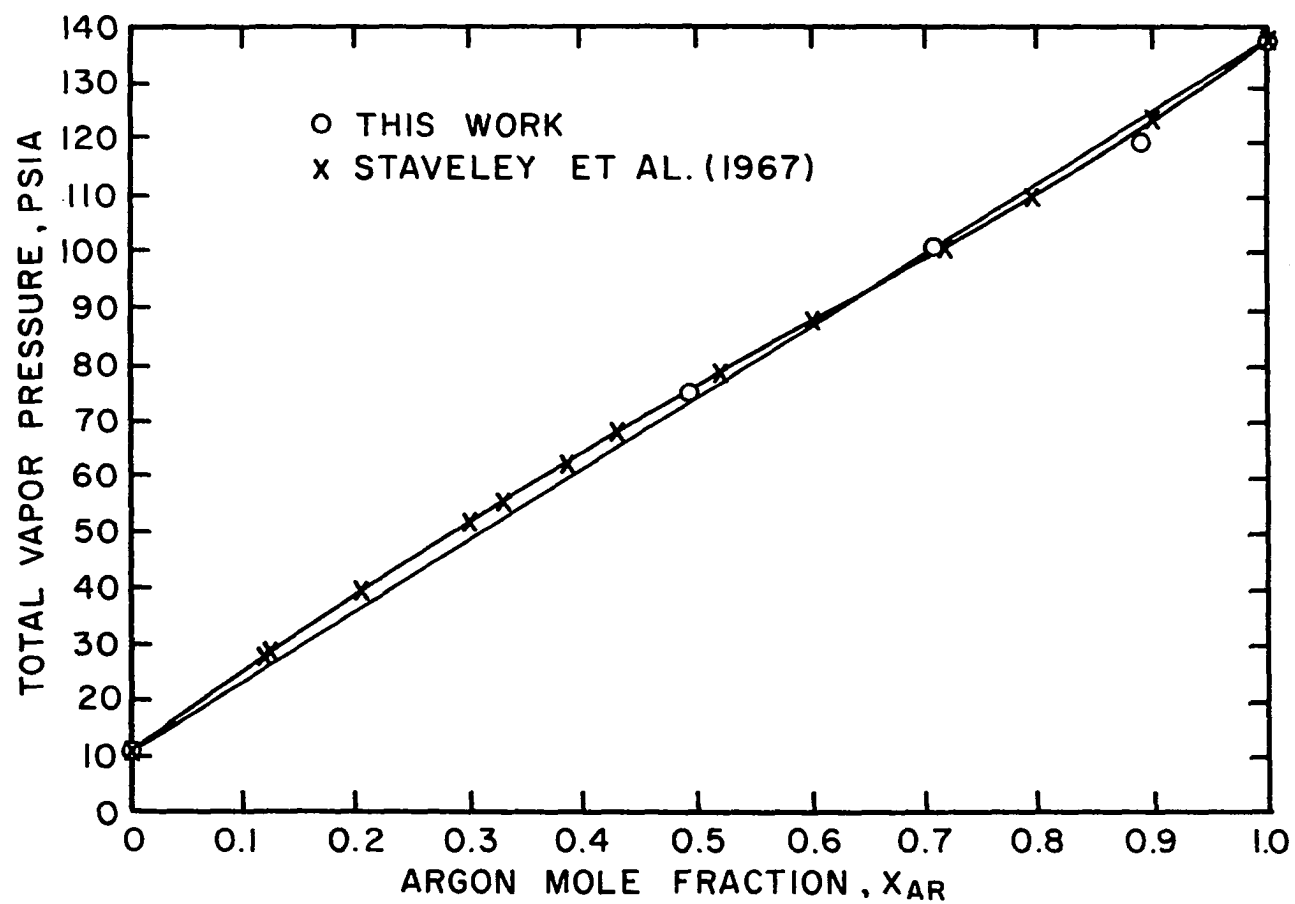


Figure 14. Total Vapor Pressure of Argon and Krypton Mixture at 115.77°K

TABLE 9

LEAST SQUARE FIT CONSTANTS FOR EXCESS VOLUME OF BINARY
LIQUID MIXTURES OF ARGON AND KRYPTON, AND OF KRYPTON
AND XENON TO THE EQUATION

$$V^E/x_1x_2 = A + B(x_1-x_2) + C(x_1-x_2)^2$$

SYSTEM	A	B	C	SOURCES
Argon+Krypton	-1.85557	-0.609870	-0.0326583	This work
at 115.77°K	-2.071	-0.734	0.	Staveley [21] (1967)
Krypton+Xenon	-1.83659	-0.694899	-0.349372	This work
at 161.36°K	-2.7806	+0.4397	-1.4314	Staveley [77] (1970)

TABLE 10

SMOOTHED EXPERIMENTAL EXCESS VOLUMES OF
ARGON AND KRYPTON MIXTURES AT 115.77°K

WEIGHT	COMPOSITION, $x_1 = x_{Ar}$	V^E/x_1x_2	$V^E, \text{ cm}^3/\text{gm-mole}$	$V_{\text{expt.}}^E - V_{\text{calc.}}^E,$ $\text{cm}^3/\text{gm-mole}$
	0.0		0.0	
1	.116	-1.375	-.141	.003
1	.121	-1.410	-.150	.000
1	.203	-1.533	-.248	-.005
1	.300	-1.652	-.347	-.007
1	.328	-1.670	-.368	-.004
1	.385	-1.727	-.409	-.002
2	.49377	-1.821	-.4551	.007
1	.430	-1.758	-.431	.003
1	.519	-1.859	-.464	.005
2	.602	-1.966	-.471	.004
2	.716	-2.139	-.435	-.003
2	.71963	-2.142	-.4321	-.002
1	.794	-2.262	-.370	-.006
1	.900	-2.333	-.210	.003
	1.0		0.0	

TABLE 11

SMOOTHED EXPERIMENTAL EXCESS VOLUMES OF
KRYPTON AND XENON MIXTURES AT 161.36°K

WEIGHT	COMPOSITION, $x_1 = x_{\text{Kr}}$	V^E/x_1x_2	$V^E, \text{ cm}^3/\text{gm-mole}$	$V_{\text{expt.}}^E - V_{\text{calc.}}^E,$ $\text{cm}^3/\text{gm-mole}$
	0.0		0.0	
1	.100	-1.500	-.135	.000
1	.200	-1.563	-.250	-.003
2	.21056	-1.532	-.2547	.003
2	.27629	-1.597	-.3194	-.000
1	.300	-1.647	-.345	-.006
1	.400	-1.721	-.413	-.002
2	.500	-1.836	-.459	.000
2	.600	-1.983	-.476	.001
2	.68217	-2.140	-.464	-.001
1	.700	-2.167	-.455	.001
1	.800	-2.375	-.380	.001
2	.82509	-2.421	-.3494	.002
1	.900	-2.644	-.238	-.003
	1.0		0.0	

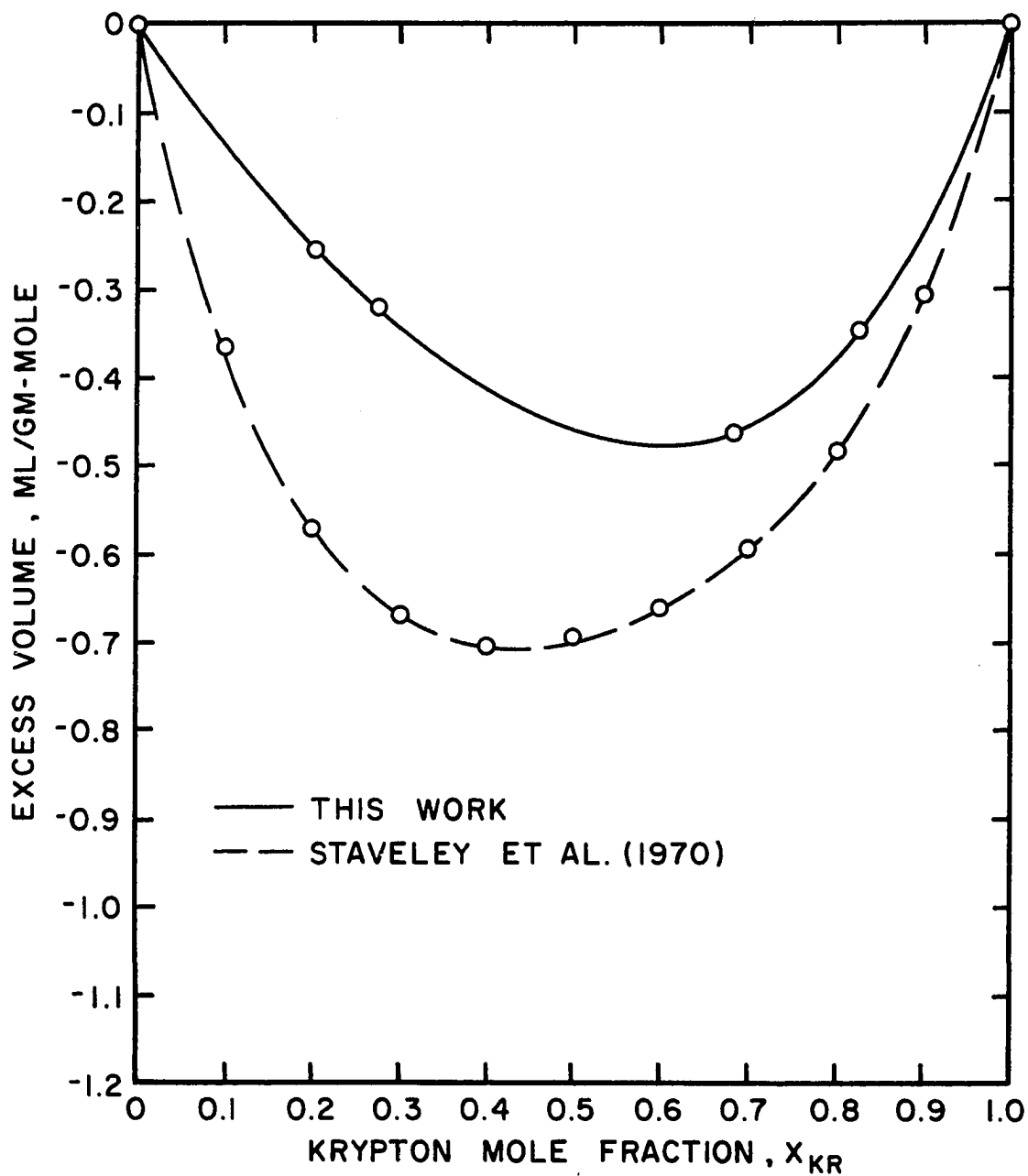


Figure 15. Excess Volume of Krypton + Xenon Mixture at 161.36°K

from the constants given in Table 9. As shown in the comparison, the minimum of the excess volume curve was at $x_{\text{Kr}} = 0.6$, while Staveley's results gave a minimum at $x_{\text{Kr}} = 0.4$. The maximum difference between two curves was at $x_{\text{Kr}} = 0.4$ with Staveley's result $0.29 \text{ cm}^3/\text{gm-mole}$ too negative.

However, comparison of the shapes of the total pressure versus composition curves of krypton and xenon system at 115.77°K , and of argon and krypton system at 161.36°K , which is shown in Figure 16, showed a striking similarity. That is, the inflection points of pressure-composition curves from a positive deviation from the ideal solution value to a negative deviation seems to be situated between 0.65 to $0.75 x_1$. Again, this point was similar to the "skewness" of the excess volume-composition curves in the present experimental results. While Staveley's V^E for krypton and xenon mixture seems to behave in the wrong way.

Further comparisons showed that at 115.77°K , the temperature was at the reduced temperature of 0.768 of the more volatile component, argon. At 161.36°K , the system temperature was at the reduced temperature of 0.771 of the more volatile component, krypton. Staveley, et al. gave an intuitive physical picture concerning the "asymmetry" of the excess volume-composition curve. Because the system temperature was about half-way to the

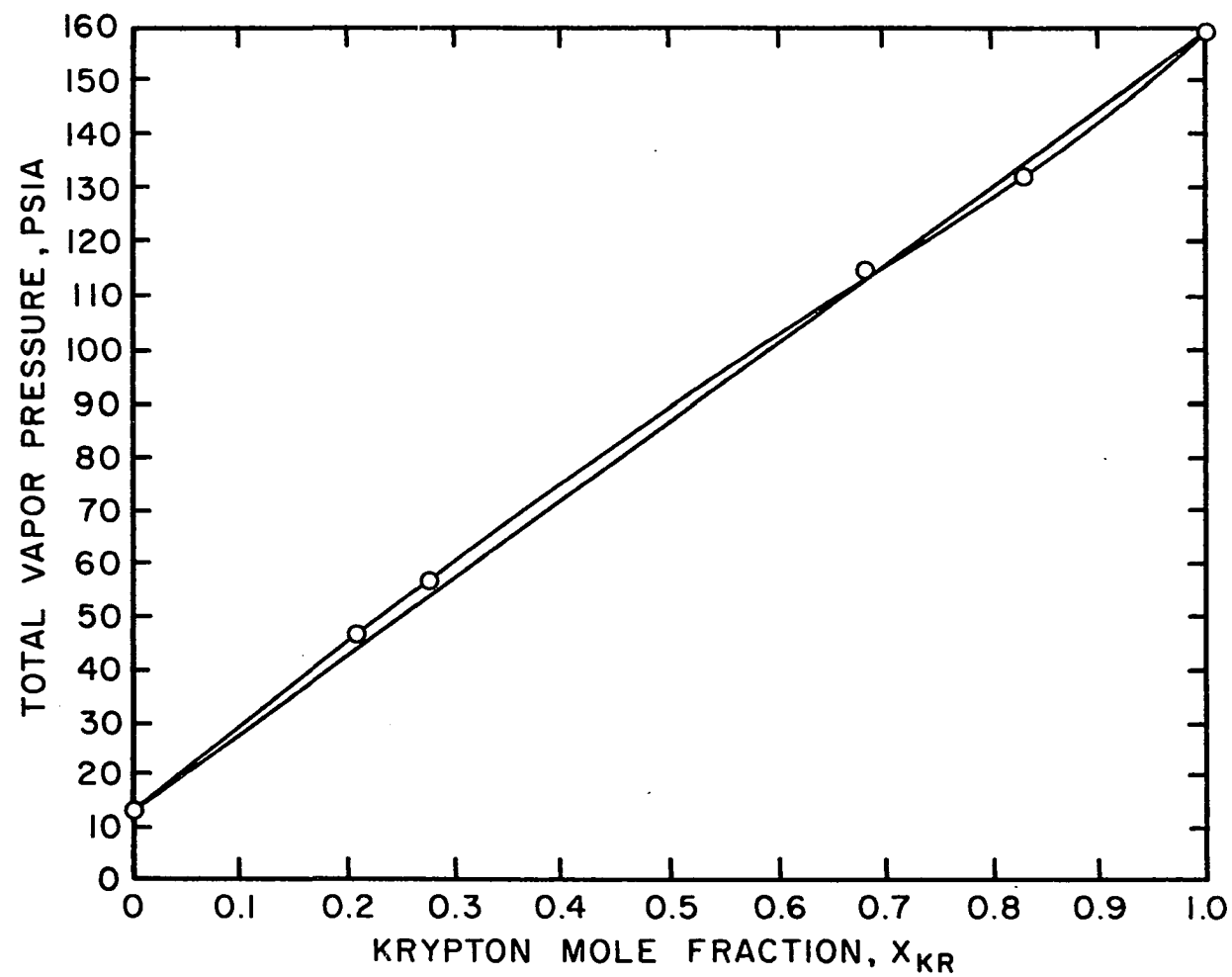


Figure 16. Total Vapor Pressure of Krypton and Xenon Mixture at 161.36°K

critical temperature of the more volatile component, the "clustering" in the more volatile component liquid may begin to be significant. This would provide cavities in the liquid which tends to make the excess volume both negative and to be asymmetric function of composition in the observed direction. This may serve to explain that the total vapor pressure-composition curve would tend to be lower than the ideal situation when clustering occurs at high x_1 values.

Calculations of the Excess Gibbs Energy
from the Experimental Data

Barker's method [3] with modifications was used to extract excess Gibbs energy functions from the experimental data. As shown in Appendix D, the activity coefficient of liquid can be given as:

$$\begin{aligned} \gamma_i &= \text{Exp} \left(\frac{\mu_i^E}{RT} \right) = \frac{y_i P}{x_i P_i^\circ \beta_i} \\ &= \frac{y_i P}{x_i P_i^\circ} \text{Exp} \left\{ \frac{(B_{ii} - V_i^L)}{RT} - \frac{B_{ii}^2 (P^2 - P_i^{\circ 2})}{2 (RT)^2} + \frac{(1 - y_i)^2 \delta_{ij} P}{RT} \right. \\ &\quad \left. - \frac{(1 - y_i)^2 \Delta_i P^2}{2 (RT)^2} \right\}, \quad i = 1, 2 \end{aligned} \quad (6)$$

where μ_i^E is the excess partial molal Gibbs energy for component i , β_i is the reciprocal of the vapor phase fugacity coefficient and

$$\delta_{ij} = 2B_{12} - (B_{11} + B_{22}) \quad (7)$$

$$\Delta_1 = (1-y_2^2) \delta_{12}^2 + 2B_{22}\delta_{12} + B_{11}^2 + B_{22}^2 \quad (8)$$

$$\Delta_2 = (1-y_1^2) \delta_{12}^2 + 2B_{11}\delta_{12} + B_{11}^2 + B_{22}^2$$

the truncated virial equation was used:

$$\frac{PV}{RT} = 1 + \frac{BP}{RT} - \left(\frac{BP}{RT}\right)^2 \quad (9)$$

The equation given by Guggenheim [31] was used to calculate the second virial coefficients B_{11} , B_{22} , and B_{12} . This equation was explained in Appendix D. The interaction critical constants were calculated by using the arithmetic mean for $V_{c12}^{1/3}$, and the Srivastava and Madan rule [76] for T_{c12} . First, the Redlich-Kister form of γ was assumed:

$$\begin{aligned} \ln \gamma_1 &= Ax_2^2 + B(-x_2^2)(1-4x_1) + Cx_2^2(1-8x_1+12x_1^2) \\ \ln \gamma_2 &= Ax_1^2 + B(+x_1^2)(1-4x_2) + Cx_1^2(1-8x_2+12x_2^2) \end{aligned} \quad (10)$$

The constants A, B, and C were then obtained by iterations which minimized the pressure residuals $R = (P_{\text{exptl.}} - P_{\text{calc.}})$. The excess Gibbs energy at the system temperature and pressure was given by:

$$G^E(P=P_{\text{sat.}})/RT = \sum_{i=1}^2 x_i \left(\frac{\mu_i^E}{RT} \right) = x_1 x_2 \left[A + B(x_1 - x_2) + C(x_1 - x_2)^2 \right] \quad (11)$$

The function G^E at $P = 0$ was then calculated from:

$$G^E(P=0) = G^E(P=P_{\text{sat.}}) + V^E(0-P) \quad (12)$$

To start the iteration, constants B and C were set equal to zero. The total vapor pressure of the system was:

$$P = x_1 \gamma_1 P_1^\circ \beta_1 + x_2 \gamma_2 P_2^\circ \beta_2 \quad (13)$$

where β_1 and β_2 were set equal to zero also. In order to calculate γ_1 and γ_2 , the pressure estimated from the smoothed total vapor pressure-composition curve at $x = 0.5$, p^* , was used to calculate the initial value of constant A:

$$A = 4 \ln \left(2P^* (P_1^\circ + P_2^\circ)^{-1} \right) \quad (14)$$

Then β_1 and β_2 were calculated by first neglecting the vapor phase activity coefficient terms that involved

δ_{ij} and Δ_i . Then y_i was calculated and normalized by $y_i = \frac{y_i}{\sum_{i=1}^2 y_i}$. These were used again to calculate β_1 and

β_2 . This step was repeated until y_i stayed constant.

The changes δA , δB , δC in A, B, C which will minimize the pressure residuals were determined by least square fitting to the equation:

$$\left(\frac{dP}{dA} \right) \delta A + \left(\frac{dP}{dB} \right) \delta B + \left(\frac{dP}{dC} \right) \delta C = R \quad (15)$$

The amount of δA , δB , δC were added to the initial values

of A, B, C for improved approximations. The iteration was terminated when A, B, C did not change significantly. This set of constants A, B, C were used to calculate excess Gibbs energy at saturation pressures. The zero pressure G^E values were then least square fitted to the Redlich-Kister equation to obtain the corresponding A, B, and C for G^E at $P = 0$. The sets of constants obtained in different sources were given in Table 15.

Excess Gibbs Energy for the Heavy Rare Gas

Liquid Mixture

The data reduction and comparisons with results obtained in other investigations are presented here.

For argon and krypton mixture at 115.77°K, the set of physical properties given in Table 12 was used for iteration. Staveley's results were retreated. These results and those obtained in the present work were compared in Table 13 and Figure 17. In calculating G^E for the present work the total pressure readings taken from Staveley's measurements were combined with those of this work for the iteration. The agreement between G^E of this work, and Staveley's G^E was good.

The total pressure of the krypton and xenon mixture at 161.36°K was measured at four compositions in this work. The other points were read from a smoothed curve drawn through these points and the two end points. The results for G^E were given in Table 14. Staveley's G^E at 161.38°K were also given

TABLE 12

DATA USED FOR THE ITERATIVE CALCULATIONS OF THE
EXCESS GIBBS ENERGY FOR BINARY LIQUID MIXTURES
OF ARGON AND KRYPTON, AND KRYPTON AND XENON

SYSTEM	SUBSTANCE	VAPOR PRESSURE, psia	SECOND VIRIAL COEFFICIENTS, cm ³ /gm-mole	PURE LIQUID VOLUME, cm ³ /gm-mole	SOURCE
Argon + Krypton at 115.77°K	Argon Krypton	138.0606 10.5831	-145. -335. B ₁₂ =-219.	33.301 34.227	Staveley (1967) [21]
Argon + Krypton at 115.77°K	Argon Krypton	138.122 10.588	-141.3 -331.2 B ₁₂ =-215.6	33.3411 34.2089	This Work
Krypton + Xenon at 161.36°K	Krypton Xenon	159.505 11.897	-171.8 -421.0 B ₁₂ =-268.5	40.7291 44.2166	This Work

TABLE 13

EXCESS GIBBS ENERGY OF ARGON AND KRYPTON
BINARY LIQUID MIXTURES AT 115.77°K

COMPOSITION, $x_1 = x_{Ar}$	TOTAL PRESSURE, psia	$P_{exp} - P_{calc}$, psia	G^E cal/gm-mole	G^E_{Oxford} cal/gm-mole
0.0	(10.5831)		0.	0.
.11581	27.7404	.032	7.754	7.851
.12148	28.5098	.004	8.085	8.187
.20235	39.5163	-.028	12.315	12.479
.29973	52.0518	-.020	16.137	16.371
.32803	55.5254	-.054	16.981	17.234
.38495	62.5402	.030	18.309	
(.49377)	(75.230)	-.120	19.451	
.42999	68.0918	.194	19.005	19.325
.51899	78.1956	-.094	19.451	19.817
.60171	87.9592	.043	18.744	19.137
.71569	101.3297	.013	15.982	16.371
(.71963)	(101.852)	.057	15.849	
.79409	110.8478	.011	12.871	13.219
.90064	124.2571	-.157	7.057	7.278
1.0	(138.0606)		0.	0.

Note: the data in parentheses are original experimental data obtained in this work.

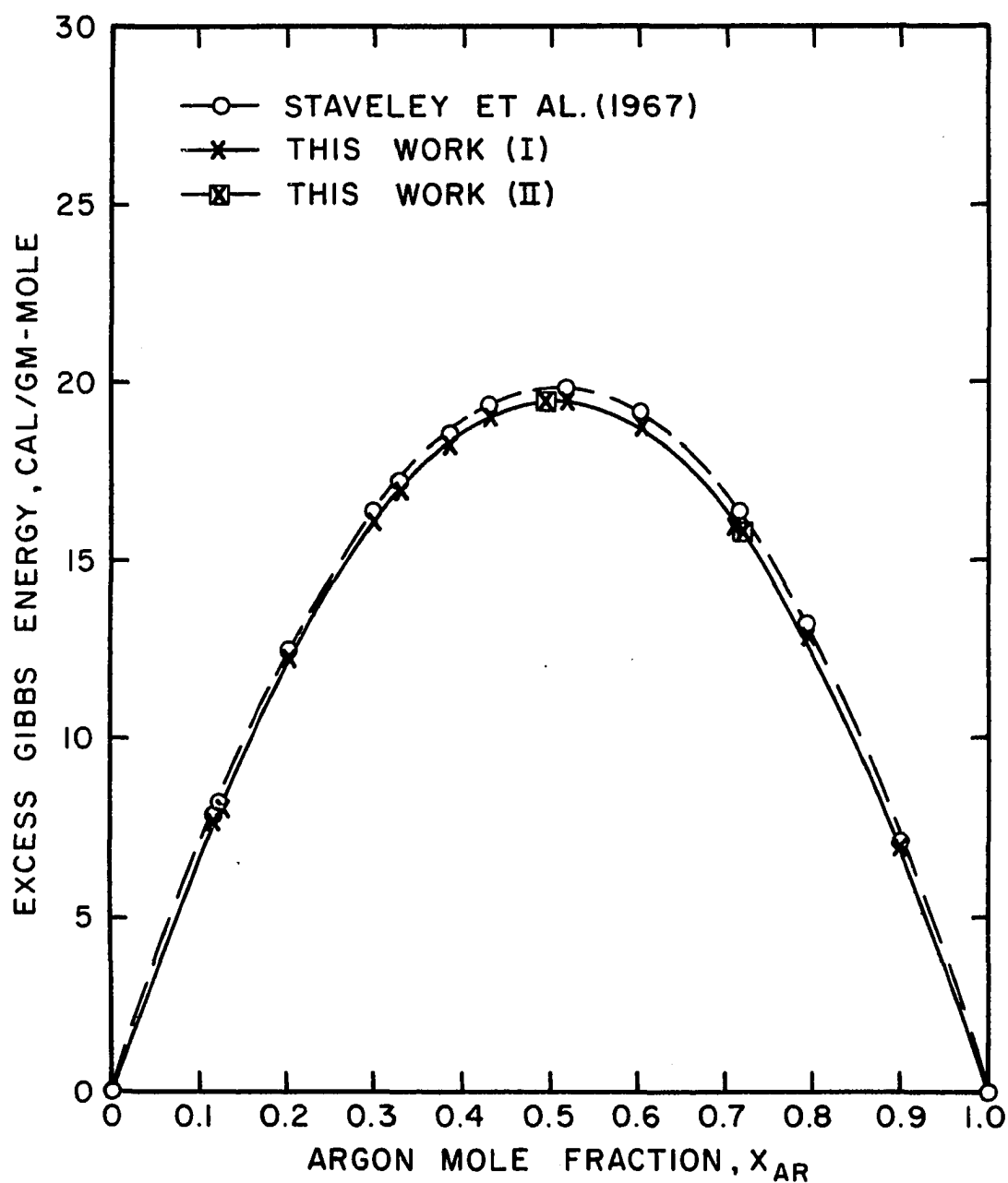


Figure 17. Excess Gibbs Energy of Argon + Krypton Mixture at 115.77°K

Note: This work (I) were obtained by using Staveley's (P,x) data with (v^E, x) obtained in this work. This work (II) were obtained by using the experimental (P,x) and (v^E, x) data obtained in this work.

in Table 14. They were calculated from the equation he privately communicated to this author. Both sets of results were compared in Figure 18. As can be seen that the maximum of G^E obtained in this work was at the composition $x_{Kr} = 0.6$, while Staveley's was at $x_{Kr} = 0.5$.

It must be pointed out that Staveley measured the total pressures of the mixture independent of the density measurement. When the total pressure measurements were made, the pycnometer bulb was filled with liquified rare gas half full only. The existence of asymmetry in G^E merits further investigation.

Comparisons shown above suggested that the discrepancies between the G^E reported by Staveley's group and those of the Göttingen group were resolved. The comparisons were also given in Table 15 and in Table 16. It can be seen that the work done at the University of Göttingen gave higher values of G^E for both Ar + Kr and Kr + Xe than the present results or the Staveley's results.

As mentioned by Staveley, the values of G^E for the equimolar mixture given by Schmidt's measurements at 88.05°K was close to that of 45 cal/mole obtained from Walling and Halsey's work [92] on solid solutions at 83°K. However, in the solid solutions, the molecular position is complicated by some degree of local crystal order, which tends to give G^E values larger than that in the liquid.

TABLE 14

EXCESS GIBBS ENERGY OF KRYPTON AND XENON
BINARY LIQUID MIXTURES AT 161.36°K

COMPOSITION, $x_1 = x_{Kr}$	TOTAL PRESSURE, P psia	$P_{exp} - P_{calc}$, psia	G^E cal/gm-mole	G^E_{oxford} cal/gm-mole (at 161.38°K)
0.0	(11.897)		0.	0.
.10	28.0	.41	5.757	9.811
.20	44.0	.27	11.782	17.313
(.21056)	(45.297)	-.103	12.401	
(.27629)	(55.402)	-.386	16.080	
.30	59.2	-.28	17.310	22.683
.40	74.5	-.23	21.675	26.023
.50	88.9	.16	24.327	27.363
.60	102.8	.44	24.820	26.660
(.68217)	(113.5) *	.20	23.367	
.70	116.0	.29	22.814	23.798
.80	129.0	-.26	18.076	18.587
(.82509)	(131.826)	-.849	16.440	
.90	143.0	-.63	10.480	10.766
1.0	159.505		0.	0.

Note: the data in parentheses are original experimental data obtained in this work; the one with * and other points were obtained from the smoothed (P,X) curve.

TABLE 15

LEAST SQUARE FIT CONSTANTS FOR EXCESS GIBBS ENERGY
OF BINARY LIQUID MIXTURES OF ARGON AND DRYPTON,
AND OF KRYPTON AND XENON TO REDLICH-KISTER EQUATION

$$G^E/(RT \cdot x_1 x_2) = A + B(x_1 - x_2) + C(x_1 - x_2)^2$$

SYSTEM	A	B	C	SOURCES
Argon+Krypton at 115.77°K	.3373872	.007692885	-.004365371	This work (P=P _{sat})
	77.8429	2.03225	-.942829	This work* (P=0.)
	.3434702	.01165431	-.002541371	Staveley (1967)[21] retreated in this work (P=P _{sat})
	.3488	.0191	.0051	Staveley (1967)[21] (P=0.)
Argon+Krypton at 103.94°K	.3818	.0058	.0170	Staveley (1967)[21] (P=0.)
Argon+Krypton at 88.05°K	.947	.121	0.0	Schmidt (1960)[67]
Argon+Krypton at 87.5°K	4.17	-1.93	0.0	Wilhelm and Schneider (1962)[97]
Krypton+Xenon at 161.36°K	.3026612	.1012205	-.03500696	This work (P=P _{sat})
	97.3073	32.7840	-11.1070	This work* (P=0.)
	.3413	.0207	.0237	Staveley (1970)[77]

Note: the constants in this work (*) are multiplied by (R·T);
Staveley's results of krypton and xenon are at 161.38°K.
R = 1.987 cal/mole°K.

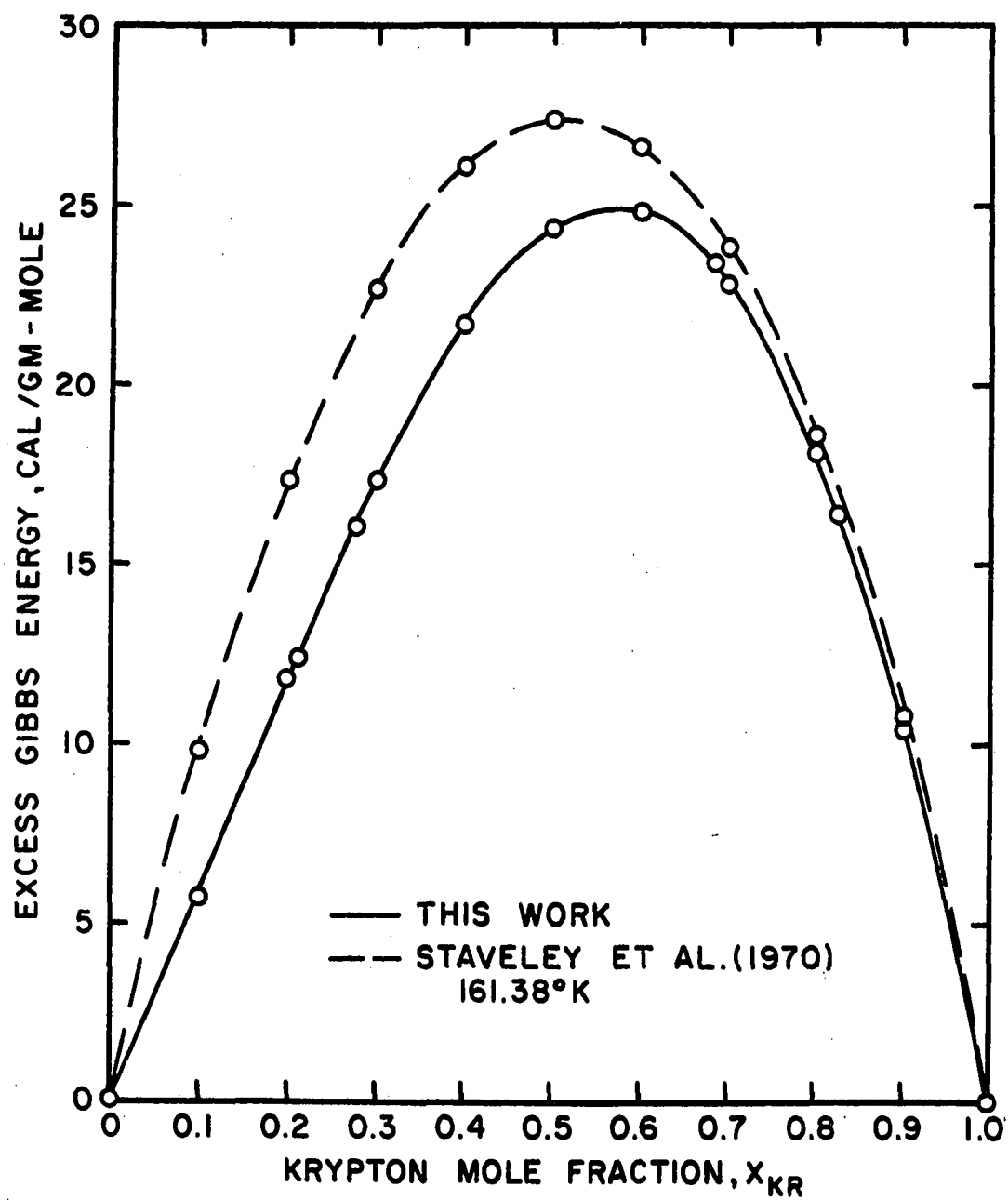


Figure 18. Excess Gibbs Energy of Krypton + Xenon Mixture at 161.36°K

TABLE 16
COMPARISON OF EXCESS GIBBS ENERGY FOR THE
EQUIMOLAR MIXTURES OF ARGON + KRYPTON,
AND OF KRYPTON + XENON

System	Temperature, °K	G^E cal./gm-mole	Sources
Argon + Krypton	117.	31.8	Köhler (1964) [39]
	115.77	19.46	This Work
	115.77	22.06 (± 0.10)	Staveley (1967) [21]
	103.94	19.71 (± 0.39)	Staveley (1967) [21]
($x_{Kr} = 0.13$) *	88.05	41.5 ($\pm 15.$)	Schmidt (1960) [67]
($x_{Kr} = 0.35$) *	87.5	180. ($\pm 21.$)	Wilhelm and Schneider (1962) [97]
(Solid Solution)	83.	45.	Walling and Halsey (1958) [92]
Krypton + Xenon	161.36	24.32	This Work
	161.38	27.36 ($\pm .31$)	Staveley (1970) [77]
	166.	34.66	Seemeyer (1965) [70]

Note: At 88.05°K and at 87.5°K, x_{Kr} indicates the upper limit of composition in experimental measurements, the values at $x_{Kr} = 0.5$ were extrapolated by Staveley (1967).

CHAPTER VII

MODIFIED AVERAGE POTENTIAL MODEL OF LIQUID MIXTURES

In this chapter, a review on the average potential model of liquid mixtures is given. A modified average potential model is examined. Although the model approach in liquid theory development is not as theoretically elegant and strict as those approaches started from first principles, it does give a link between the microscopic and macroscopic properties in predicting the mixture behavior. The average potential model as developed by Prigogine and co-workers [62] is reviewed and possible modifications are given. Their numerical results are compared with the experimental data obtained in the investigation.

Previous Methods and Present Method

Prigogine, Bellemans and Mathot [62] combined the basic ideas underlying the theory of conformal solutions [49] with those of the cell model of solutions and presented the average potential model (APM) in both crude and refined versions. Scott [68] independently developed a similar version with one liquid (crude version on Prigogine), two liquid

(refined version of Prigogine), and the three liquid models based on the principle of corresponding states. The series expansions of Prigogine involved higher derivatives, which are scarcely available experimentally and accurately. The series expression of excess function converges very slowly, especially for excess volume V^E [6,21].

Bellemans, Mathot, and Simon [6] presented a detailed and significant comparison of the APM with experimental data available to July, 1965, on simple mixtures. In their modified version, they used the full expressions instead of the expanded forms of the excess functions. Also, analytical expressions of reduced properties based on the principle of corresponding states were used as bases for calculating excess functions. Quantitative discussions of the following five systems were given: $\text{CO}+\text{CH}_4$, $\text{A}+\text{CH}_4$, N_2+O_2 , N_2+A , and O_2+A .

Bellemans and Vilcu [7] further extended their treatment to the following five other systems: CH_4+Kr , N_2+CH_4 , $\text{A}+\text{Kr}$, N_2+CO , and $\text{CO}+\text{A}$. Fuks and Bellemans [28] also obtained the excess free energies and volumes of the liquid systems: methane-krypton, and nitrogen-methane experimentally. The average potential model was also compared with these results. The conclusion was that the APM was still able to predict semi-quantitatively the excess properties of simple mixtures.

Vilcu and Bellemans [91] extended the average potential model of solutions to systems at moderate pressure. However, because the reduced equations of free energy and of volume were obtained between the ranges of $0.7 < T_r < 1.0$ and $0.0 < P_r < 0.9$, the validity of these extensions is thus limited.

Wheeler and Smith [95] extended the molecular corresponding states theory to highly nonideal liquid mixtures by using two flexibilities: first, the averaging procedure used to obtain effective pair-potential parameters for a mixture; second, the pair of exponent values used in a Lennard-Jones type of pair-potential function.

Street and Staveley [79] compared the various merits of the one-liquid, two-liquid, and three-liquid versions of the average potential models with eight binary liquid mixtures formed from the following substances: argon, krypton, methane, oxygen, nitrogen, and carbon monoxide. However, for the systems of argon-krypton and argon-methane, none of the three versions gave any reasonable agreement with the experimental value of V^E . These discrepancies were explained as follows:

1. The inadequacy of a two parameter principle of corresponding states in presenting a reasonable reduced equation of state of pure liquid volume.
2. The inadequacy of the Lennard-Jones (12:6) potential and hence the inadequacy of the force constants

were mentioned to be partially responsible for the lack of agreement between theory and experiment. In cases such as CO and N_2 , this Lennard-Jones potential can not take care of the directional forces such as quadrupole interactions.

3. The inadequacies of the mixing rule of force constants.

4. The erroneous assumption of random mixing.

Due to these failures, Street and Staveley [79] concluded that it is obviously desirable to obtain experimental information on simple liquid mixtures as Kr+Xe and Kr+CH₄.

Davies, Duncan, Saville, and Staveley [21] measured V^E for liquid mixtures of argon and krypton at 115.77°K, the triple point of krypton. The total vapor pressure of liquid mixtures has been measured over the whole range of composition at 115.77°K and from an argon mole fraction of ~0.4 to unity at 103.94°K. The excess Gibbs free energy G^E was evaluated for equimolar solutions at 115.77°K and 103.94°K. As far as several versions of average potential model are concerned, none of them was satisfactory for V^E when applied to the argon-krypton system. The experimental V^E is negative and has an unsymmetrical dependence on mole fraction. The skewness of V^E versus composition curve was explained as possibly caused by the clustering of argon molecules.

Leland, Rowlinson, and Sather [47] circumvented the random mixing assumption by proposing the usage of the

so-called van der Waals approximation. The random mixing assumption of Byers Brown, or the crude approximation of Prigogine, or the one-fluid model of Scott, all lead to a "singularity" in the average mixture force constants when the n in a Lennard-Jones (n,m) potential approaches infinity.

The average potential model was critically reviewed [6]. Their main features are presented here. The idea was to combine the concept of average potential involved in the cell model with the principle of corresponding states. First, the microscopic two parameter principle of corresponding states follows if the substance obeys an interaction potential of the form

$$u(r) = \epsilon \cdot f\left(\frac{r}{\sigma}\right) \quad (15)$$

where ϵ is the energy parameter, σ is the length parameter, u is the intermolecular potential, and r is the distance between two molecules. The configurational partition function is

$$Q(N,T,V) = \sigma^{3N} q(\tilde{T},\tilde{v})^N \quad (16)$$

where $q(\tilde{T},\tilde{v})$ is a universal partition function per molecule of the system, N is the Avogadro number, with the reduced quantities defined as

$$\tilde{p} = \frac{p\sigma^3}{\epsilon}, \quad \tilde{v} = \frac{V}{N\sigma^3}, \quad \tilde{T} = \frac{kT}{\epsilon} \quad (17)$$

Thus the configurational Helmholtz free energy is

$$\begin{aligned}\frac{F}{NkT} &= \ln Q = - \ln q(\tilde{T}, \tilde{v}) - 3 \ln \sigma \\ &= \xi(\tilde{T}, \tilde{v}) - 3 \ln \sigma\end{aligned}\quad (18)$$

and the Gibbs free energy is

$$\begin{aligned}\frac{G}{NkT} &= \xi(\tilde{T}, \tilde{v}) + \tilde{P}\tilde{v}/\tilde{T} - 3 \ln \sigma \\ &= \xi(\tilde{T}, \tilde{v}) - \tilde{v} \partial \xi(\tilde{T}, \tilde{v}) / \partial \tilde{v} - 3 \ln \sigma \\ &= \eta(\tilde{T}, \tilde{p}) - 3 \ln \sigma\end{aligned}\quad (19)$$

From the cell model of solutions, Prigogine used a single, but important feature. This feature is to introduce composition dependent averages for the interaction constants. By so doing, the sum of pair interactions was replaced by some average interaction depending on the mole fraction. The crude version takes an average over all kinds of pairs in the system, while the refined versions take separate average potentials for each kind of molecule in the solutions. The mixture was assumed to be described by one average potential as

$$\langle u(r) \rangle = \langle \epsilon \rangle f \left(\frac{r}{\langle \sigma \rangle} \right) \quad (20)$$

For a Lennard-Jones (12, 6) potential

$$u(r) = 4\epsilon \left[\left(\frac{\sigma}{r} \right)^{12} - \left(\frac{\sigma}{r} \right)^6 \right] \quad (21)$$

The following "methods" are possible in the averaging process:

1. One-liquid model

$$\langle u(r) \rangle = x_A^2 u_{AA}(r) + 2x_A x_B u_{AB}(r) + x_B^2 u_{BB}(r) \quad (22)$$

The potential parameters are given by

$$\langle \epsilon \rangle = \frac{x_A^2 \epsilon_{AA}^6 \sigma_{AA}^6 + 2x_A x_B \epsilon_{AB}^6 \sigma_{AB}^6 + x_B^2 \epsilon_{BB}^6 \sigma_{BB}^6}{x_A^2 \epsilon_{AA}^6 \sigma_{AA}^6 + 2x_A x_B \epsilon_{AB}^6 \sigma_{AB}^6 + x_B^2 \epsilon_{BB}^6 \sigma_{BB}^6} \quad (23)$$

$$\langle \sigma \rangle = \left(\frac{x_A^2 \epsilon_{AA}^6 \sigma_{AA}^6 + 2x_A x_B \epsilon_{AB}^6 \sigma_{AB}^6 + x_B^2 \epsilon_{BB}^6 \sigma_{BB}^6}{x_A^2 \epsilon_{AA}^6 \sigma_{AA}^6 + 2x_A x_B \epsilon_{AB}^6 \sigma_{AB}^6 + x_B^2 \epsilon_{BB}^6 \sigma_{BB}^6} \right)^{1/6} \quad (24)$$

Simon [73] has obtained, using the principle of corresponding states, an analytical expression of reduced volume $w(T)$ from the reduced experimental molecular volume of Ar, Kr, CO, N₂, and CH₄ as:

$$w(\tilde{T}) = 0.952596 - 0.705204 \tilde{T} + 0.834608 \tilde{T}^2 \quad (25)$$

where $w(T)$ was defined as

$$w(\tilde{T}) = \tilde{T} \left(\frac{\partial}{\partial \tilde{P}} \eta(\tilde{T}, \tilde{P}) \right)_{\tilde{P}=0} \quad (26)$$

It should be pointed out that in Equation (25) $w(T)$ is the molecular volume obtained by reducing the macroscopic volume with $(\sqrt{2} \cdot \sigma^3 \cdot N)$, where N is Avogadro's number. The corresponding reduced free energy function is defined as

$$\eta_0(\tilde{T}) = \eta(\tilde{T}, P=0) \quad (27)$$

and expressed as:

$$\eta_o(\tilde{T}) = -8.379308 \tilde{T}^{-1} - 4.59179 \ln \tilde{T} + 2.301041 \tilde{T} - 0.806469 \tilde{T}^2 + 3.558774 \quad (28)$$

Thus, the excess volume can be given as

$$\begin{aligned} v^E &= v_m - (x_A v_A + x_B v_B) \\ &= \langle \sigma \rangle^3 \omega(\langle \tilde{T} \rangle) - \left(x_A \sigma_{AA}^3 \omega(\tilde{T}_{AA}) + x_B \sigma_{BB}^3 \omega(\tilde{T}_{BB}) \right) \end{aligned} \quad (29)$$

The excess Gibbs free energy can be given as

$$\begin{aligned} G^E/kT &= \eta_o(\langle \tilde{T} \rangle) - \left(x_A \eta_o(\tilde{T}_{AA}) + x_B \eta_o(\tilde{T}_{BB}) \right) \\ &\quad - 3 \left(\ln \langle \sigma \rangle - x_A \ln \sigma_{AA} - x_B \ln \sigma_{BB} \right) \end{aligned} \quad (30)$$

where the reduced temperature and reduced volume are defined as:

$$\langle \tilde{T} \rangle = \frac{kT}{\langle \epsilon \rangle}, \quad \tilde{T}_{AA} = \frac{kT}{\epsilon_{AA}}, \quad \omega = \frac{V}{N \langle \sigma^3 \rangle \sqrt{2}} \quad (31)$$

2. Two-liquid model

For the two-liquid model it is assumed that the partition function of the mixture is:

$$\begin{aligned} Q(N_A, N_B, V, T) &= \frac{N_A! N_B!}{N_A! N_B!} \langle \sigma_A \rangle^{3N_A} q \left(\langle \tilde{T}_A \rangle, \langle \tilde{v}_A \rangle \right)^{N_A} \langle \sigma_B \rangle^{3N_B} \\ &\quad q \left(\langle \tilde{T}_B \rangle, \langle \tilde{v}_B \rangle \right)^{N_B} \end{aligned}$$

with $\langle \tilde{T}_A \rangle = kT / \langle \epsilon_A \rangle$, $V = N_A \langle \sigma_A \rangle^3 \langle \tilde{v}_A \rangle + N_B \langle \sigma_B \rangle^3 \langle \tilde{v}_B \rangle$

Here the two kinds of average potentials are:

$$\begin{aligned} \langle u_A(r) \rangle &= x_A u_{AA}(r) + x_B u_{AB}(r) = \langle \epsilon_A \rangle f\left(\frac{r}{\langle \sigma_A \rangle}\right) \\ \langle u_B(r) \rangle &= x_A u_{AB}(r) + x_B u_{BB}(r) = \langle \epsilon_B \rangle f\left(\frac{r}{\langle \sigma_B \rangle}\right) \end{aligned} \quad (33)$$

with the averaged force parameters given for Lennard-Jones (12, 6) potential as

$$\langle \epsilon_A \rangle = \frac{(x_A \epsilon_{AA} \sigma_{AA}^6 + x_B \epsilon_{AB} \sigma_{AB}^6)^2}{(x_A \epsilon_{AA} \sigma_{AA}^{12} + x_B \epsilon_{AB} \sigma_{AB}^{12})^{12}} \quad (34)$$

$$\langle \sigma_A \rangle = \left(\frac{x_A \epsilon_{AA} \sigma_{AA}^{12} + x_B \epsilon_{AB} \sigma_{AB}^{12}}{x_A \epsilon_{AA} \sigma_{AA}^6 + x_B \epsilon_{AB} \sigma_{AB}^6} \right)^{1/6} \quad (35)$$

with similar expressions for $\langle \epsilon_B \rangle$ and $\langle \sigma_B \rangle$.

The excess functions are expressed as:

$$\begin{aligned} V^E &= x_A \left(\langle \sigma_A \rangle^3 \omega(\langle \tilde{T}_A \rangle) - \sigma_{AA}^3 \omega(\tilde{T}_{AA}) \right) + \\ & x_B \left(\langle \sigma_B \rangle^3 \omega(\langle \tilde{T}_B \rangle) - \sigma_{BB}^3 \omega(\tilde{T}_{BB}) \right) \end{aligned} \quad (36)$$

and

$$\begin{aligned} G^E/kT &= x_A \left(\eta_O(\langle \tilde{T}_A \rangle) - \eta_O(\tilde{T}_{AA}) \right) + x_B \left(\eta_O(\langle \tilde{T}_B \rangle) - \eta_O(\tilde{T}_{BB}) \right) \\ & - 3 \left(x_A \ln(\langle \sigma_A \rangle / \sigma_{AA}) + x_B \ln(\langle \sigma_B \rangle / \sigma_{BB}) \right) \end{aligned} \quad (37)$$

Here the two-liquid model was taken from Prigogine's refined version, where V is shared unequally between molecules A and B by minimizing the free energy of the system with respect to $\langle \tilde{v}_A \rangle$ and $\langle \tilde{v}_B \rangle$ taking account of the constraint of V in Equation 32.

3. Three-liquid model

In this model, the mixture is considered to be made up of three non-interacting liquids. Prigogine and co-workers did not give this version. However, based on the idea given by Scott [68], the following relations can be obtained. For the excess volume:

$$V^E = \left(x_A^2 \sigma_{AA}^3 \omega(\tilde{T}_{AA}) + 2x_A x_B \sigma_{AB}^3 \omega(\tilde{T}_{AB}) + x_B^2 \sigma_{BB}^3 \omega(\tilde{T}_{BB}) \right) - \left(x_A \sigma_{AA}^3 \omega(\tilde{T}_{AA}) + x_B \sigma_{BB}^3 \omega(\tilde{T}_{BB}) \right) \quad (38)$$

or

$$V^E = 2x_A x_B \left[\sigma_{AB}^3 \omega(\tilde{T}_{AB}) - \frac{1}{2} \left(\sigma_{AA}^3 \omega(\tilde{T}_{AA}) + \sigma_{BB}^3 \omega(\tilde{T}_{BB}) \right) \right]$$

Similarly for the excess Gibbs free energy:

$$G^E/kT = 2x_A x_B \left[\left(\eta_O(\tilde{T}_{AB}) - 3 \ln \sigma_{AB} \right) - \frac{1}{2} \left(\eta_O(\tilde{T}_{AA}) - 3 \ln \sigma_{AA} \right) - \frac{1}{2} \left(\eta_O(\tilde{T}_{BB}) - 3 \ln \sigma_{BB} \right) \right] \quad (39)$$

where $\tilde{T}_{AB} = kT/\epsilon_{AB}$

Filmed as received

without page(s) 107.

UNIVERSITY MICROFILMS.

4. The one-liquid van der Waals model

Leland, et al. [46,47] proposed a so-called van der Waals approximation which was based on an expansion of the radial distribution function about that of a system of hard spheres and neglecting powers of T^{-1} beyond the first. Calculations in this model were essentially the same as those in the one-liquid model, except that the random mixing was not used. The averaged force parameters are:

$$\langle \epsilon \rangle = \left(\frac{x_A^2 \epsilon_{AA} \sigma_{AA}^3 + 2x_A x_B \epsilon_{AB} \sigma_{AB}^3 + x_B^2 \epsilon_{BB} \sigma_{BB}^3}{x_A^2 \sigma_{AA}^3 + 2x_A x_B \sigma_{AB}^3 + x_B^2 \sigma_{BB}^3} \right) \quad (40)$$

$$\langle \sigma \rangle = \left(x_A^2 \sigma_{AA}^3 + 2x_A x_B \sigma_{AB}^3 + x_B^2 \sigma_{BB}^3 \right)^{1/3} \quad (41)$$

The expressions for the excess functions remain the same as in the one-liquid model.

5. The two-liquid van der Waals model

Leach and Leland [42] and Leland and Chappellear [43] presented a two-liquid van der Waals model applied to multicomponent systems. Their averaged force parameters were derived for a multicomponent mixture divided into two portions. However, these parameters can be readily expressed for a binary system as

$$\langle \epsilon_A \rangle = \left(\frac{x_A \epsilon_{AA} \sigma_{AA}^3 + x_B \epsilon_{AB} \sigma_{AB}^3}{x_A \sigma_{AA}^3 + x_B \sigma_{AB}^3} \right) \quad (42)$$

$$\langle \sigma_A \rangle = (x_A \sigma_{AA}^3 + x_B \sigma_{AB}^3)^{1/3} \quad (43)$$

Similarly $\langle \epsilon_B \rangle$ and $\langle \sigma_B \rangle$ can be obtained from the above equations by interchanging subscripts A and B.

In previous comparisons [6] between the average potential model and the experimental results, various mixing rules for unlike interactions were not tested extensively. Another weak point was that the reduced volume equation obtained by Simon does not include the xenon data, which are of interest in this investigation. In the present APM calculation methods, the following new features are presented:

1. The one-liquid van der Waals model and the two-liquid van der Waals model are used in addition to the previous three models.
2. A more precise reduced volume equation for heavy rare gas liquids was obtained and used in calculations.
3. The various mixing rules for unlike interactions are tested in conjunction with all five models used here for the APM calculations.

A section discussing the extension of the APM by using three parameter principle of corresponding states is included.

Mixing Rules of Force Constants

In order to calculate the unlike interactions between molecules, it is necessary to use mixing rules to express the mixture pair potential force constants in terms of the component pair potential constants. The difference

in configurational Helmholtz free energies of two substances is

$$F_B(T,V) - F_A(T,V) = 3NkT \ln \left(\frac{\sigma_{AA}}{\sigma_{BB}} \right) - kT \ln Q_N \left(\frac{\epsilon_{AA}}{\epsilon_{BB}} \right) T, \left(\frac{\sigma_{BB}}{\sigma_{BB}} \right)^3 V \quad (44)$$

where $Q_N(\tilde{T}, \tilde{V})$ is the configurational partition function. Thus, by knowing the mixing rules of force constants, it follows

$$Q_{\{N\}}(T,V,\{N_i\},\{\epsilon_{st}\},\{\sigma_{st}\}) = Q(T,V,\{N_i\},\{\epsilon_{ss}\},\{\sigma_{ss}\}) \quad (45)$$

The mixing rules used conventionally are the geometric mean rule for the energy constant and the arithmetic mean rule for the length constant, they are:

$$\epsilon_{AB} = \sqrt{\epsilon_{AA} \cdot \epsilon_{BB}} \quad (46)$$

and

$$\sigma_{AB} = \frac{1}{2} (\sigma_{AA} + \sigma_{BB}) \quad (47)$$

It has been pointed out that these rules are not accurate for predicting mixture properties [12,15,16,17,48,66].

It is necessary to examine the various mixing rules for force constants in conjunction with various APM formalisms. The experimental results obtained in this investigation for the simple systems of Ar + Kr, Kr + Xe, and Ar + Xe, plus similar results obtained from the literature should serve as a good foundation for this purpose.

The following mixing rules for force constants are to be examined here in the numerical calculations:

1. Geometric-Arithmetic Mean Rules: Equation 47 and Equation 46, or called Lorentz-Berthelot rules [66].

2. Srivastava and Madan rule for ϵ_{AB} [76]

Arithmetic mean rule for σ_{AB} .

$$\epsilon_{AB} \sigma_{AB}^6 = \frac{\epsilon_{AA} \cdot \epsilon_{BB} (\sigma_{AA}^3 \sigma_{BB}^3)}{\left(\frac{I_{AA} \cdot I_{BB}}{I_{AA} + I_{BB}} \right)} \quad (48)$$

where I is the ionization potential of the pure substance.

3. Srivastava and Madan rule for σ_{AB}

Canfield's rule for ϵ_{AB} [12].

Here the ϵ_{AB} is first calculated with the empirical rule obtained by Canfield and by using the ϵ_{AB} value obtained to calculate σ_{AB} from the Srivastava and Madan rule.

$$\epsilon_{AB} = \xi \cdot \epsilon_{AA} \cdot \epsilon_{BB} \quad (49)$$

$$\xi = a + b \left(\frac{\epsilon_{AA} - \epsilon_{BB}}{\epsilon_{AA} + \epsilon_{BB}} \right) \left(\frac{\sigma_{AA} - \sigma_{BB}}{\sigma_{AA} + \sigma_{BB}} \right) \quad (50)$$

with $a = 1.0$ and $b = -1.95$. These rules were proved to be superior to the Lorentz-Berthelot rules by Canfield in predicting the interaction second virial coefficient for binary systems $N_2 + O_2$, $He + Ne$, $Ne + Ar$, $Ne + N_2$, $He + N_2$, and $He + Xe$.

4. The Kirkwood and Muller rule for ϵ_{AB} [56] is

$$\epsilon_{AB} = \frac{(2 \epsilon_{AA} \epsilon_{BB} / \chi_A \chi_B)}{(\epsilon_{AA} \sigma_{AA}^6 / \chi_A^2) + (\epsilon_{BB} \sigma_{BB}^6 / \chi_B^2)} \left(\frac{\sigma_{AA}^6 \cdot \sigma_{BB}^6}{\sigma_{AB}^6} \right) \quad (51)$$

where χ is the paramagnetic susceptibility. This rule was simplified by Fender and Halsey [25] as:

$$\epsilon_{AB} = \left(\frac{2 \epsilon_{AA} \cdot \epsilon_{BB}}{\epsilon_{AA} + \epsilon_{BB}} \right) \quad (52)$$

This Fender and Halsey rule is to be used with the arithmetic mean rule for σ_{AB} .

5. The geometric mean rule for ϵ_{AB} and the Kreglewski's rule for σ_{AB} [41].

The Kreglewski's rule for σ_{AB} was obtained from examining mixtures of polyatomic molecules.

$$\sigma_{AB} = (1 + k_\sigma) \left(\frac{\sigma_{AA} + \sigma_{BB}}{2} \right) \quad (53)$$

with

$$k_\sigma = \frac{\epsilon_{BB} - \epsilon_{AA}}{\epsilon_{AA} + \epsilon_{BB}} - \left(\frac{\sigma_{AA} - \sigma_{BB}}{\sigma_{AA} + \sigma_{BB}} \right)^2 \quad (54)$$

where $\epsilon_{BB} > \epsilon_{AA}$

It should be pointed out that the above-mentioned rules have been tested for the prediction of the interaction second virial coefficient and/or gas phase transport properties such as diffusion coefficient and viscosity. These rules are tested here for predicting the excess thermodynamic

properties in the liquid phase. The purpose is to establish a set of better mixing rules for predicting fluid mixture properties without resorting to any mixture data in the first place.

Kihara Spherical Core Potential and Three Parameter Principle of Corresponding States

In the course of studying the limitations of the APM approach, it was decided to examine the basic assumption that a two-parameter principle of corresponding states was followed microscopically. There is ample evidence that even for the heavy rare gases, the Kihara potential does better than the Lennard-Jones (12 : 6) potential in predicting gas phase properties. However, it was also pointed out by Rowlinson [66] and others [22,74] that the Lennard-Jones (12 : 6) potential can be viewed as a better "effective" model for liquid phase calculations. Nevertheless, it is worthwhile to digress here to show that substances following the Kihara potential model should follow the three parameter principle of corresponding states. To extend the APM based on Kihara potential does present some problems. The following development follows from Chiu and Canfield [16]. The Kihara spherical core potential is:

$$u(r) = \begin{cases} \infty & r \leq 2a \\ 4\epsilon \cdot \left[\left(\frac{\sigma-2a}{r-2a} \right)^{12} - \left(\frac{\sigma-2a}{r-2a} \right)^6 \right] & r \geq 2a \end{cases} \quad (55)$$

Now it is assumed that the Kihara potential is followed. Starting from the configuration partition function,

$$Q = \frac{1}{N!} \int_V \dots \int_V \exp [-U/kT] d\mathbf{r}_1 \dots d\mathbf{r}_N \quad (56)$$

Let

$$\rho = (r-2a), \quad \sigma^* = (\sigma-2a), \quad a^* = \frac{2a}{(\sigma-2a)} \quad (57)$$

Then,

$$Q = \frac{(4\pi\sigma^{*3})^N}{N!} \int_{v^{1/3}/\sigma^*} \dots \int_{v^{1/3}/\sigma^*} \exp \left[-\frac{\epsilon}{kT} \sum_{i < j} \phi \left(\frac{\rho_{ij}}{\sigma^*} \right) \right] \cdot \left[\frac{(\rho+2a)^2 d\rho}{\sigma^{*3}} \right]_1 \dots \left[\frac{(\rho+2a)^2 d\rho}{\sigma^{*3}} \right]_N \quad (58)$$

or

$$Q = \left[\sigma^{*3} \cdot q \frac{T}{\epsilon/k}, \frac{v}{\sigma^{*3}}, a^* \right]^N, \quad v = \frac{V}{N} \quad (59)$$

It follows that $\tilde{P} = \tilde{P}(\tilde{T}, \tilde{v}, a^*)$

$$\text{with } \tilde{P} = \frac{P \cdot (\sigma^*)^3}{\epsilon/k}, \quad \tilde{v} = \frac{v}{\sigma^{*3}}, \quad \tilde{T} = \frac{kT}{\epsilon}, \quad a^* = \frac{2a}{\sigma^*} \quad (60)$$

A logical extension of the APM approach to more complex systems necessitates using the Kihara potential. The average potential in the case of a Kihara spherical core potential will then be:

$$\langle u(r) \rangle = \epsilon \cdot f \frac{r-2a}{\sigma-2a} = \langle \epsilon \rangle \cdot \left\langle f \frac{r-2a}{\sigma-2a} \right\rangle \quad (61)$$

Further extension should start from here. However, the approach may not be appealing because of the algebraic difficulties in evaluating the average force constants.

Results of the Average Potential Model Calculations

The equations presented in previous sections were used to calculate the excess volume and excess Gibbs function for argon and krypton mixture at 115.77°K and for krypton and xenon mixtures at 161.36°K.

The calculations were done using the molecular force constants derived from the critical properties as given by Simon et al. [6]. These were given in Table 17. First, the reduced equations $\eta(\tilde{T})$ and $\omega(\tilde{T})$ were used in conjunction with the five models to calculate V^E and G^E for composition spacing of 0.1 from $x_1 = 0.1$ to 0.9. The calculations were done for each set of mixing rules. The comparison of mixing rules of force constants is presented in Table 18. The same calculations were done again with the equation of state for liquid molar volume taken from Terry, Staveley, et al. [84] for krypton. Because the equation covers the temperature range from 116°K to 163°K, thus this equation was used as a reference equation for calculating the liquid molar volumes for argon and krypton in the sense of the principle of corresponding states.

The results were compared for equimolar mixtures. These comparisons were given in Tables 19 and 20. As can

TABLE 17

PURE COMPONENTS DATA USED IN THE AVERAGE
POTENTIAL MODEL CALCULATIONS

Substance	$T_c, ^\circ K$	$P_c, \text{atm.}$	$\epsilon/k, ^\circ K$	$r^{*3}, \text{\AA}^3$	I, ev^*
Argon	151.0	48.0	123.2	53.8	15.76
Krypton	209.4	54.3	171.	56.0	14.00
Xenon	289.8	58.0	236.8	85.5	12.13

* Ionization potentials are from Pitzer, K.S., Adv. Chem. Phys. 2, (1959).

TABLE 18

COMPARISON OF MIXING RULES OF FORCE CONSTANTS

$$\xi_\sigma = \sigma_{12}/(0.5(\sigma_{11} + \sigma_{12})), \quad \xi_\epsilon = \epsilon_{12}/(\epsilon_{11} \cdot \epsilon_{22})^{1/2}$$

Mixing Rules (Set No.)		<u>Argon + Krypton</u>		<u>Krypton + Xenon</u>	
		ξ_ϵ	ξ_σ	ξ_ϵ	ξ_σ
(1)	Lorentz-Berthelot	1.0	1.0	1.0	1.0
(2)	ϵ_{12} , S-M Rule σ_{12} , Arithmetic	.99478	1.0	.99188	1.0
(3)	ϵ_{12} , Canfield Rule σ_{12} , S-M Rule	.98921	1.00094	.98643	1.00092
(4)	ϵ_{12} , Fender Halsey σ_{12} , Arithmetic	.98671	1.0	.98690	1.0
(5)	ϵ_{12} , Geometric σ_{12} , Kreglewski Rule	1.0	1.16132	1.0	1.15949

TABLE 19

COMPARISON OF CALCULATION RESULTS FOR EQUIMOLAR LIQUID MIXTURE OF ARGON

AND KRYPTON AT 115.77°K BASED ON AVERAGE POTENTIAL MODEL

APPROACHES (SIMON EQUATION FOR $\omega(\tilde{T})$)

Model	<u>V^E, cm³/gm-mole</u>					<u>G^E, cal./gm-mole</u>				
	Mixing Rules Set No.					Mixing Rules Set No.				
	1	2	3	4	5	1	2	3	4	5
(This Work Experimental)		(-.464)					(19.46)			
APM-1	.437	.490	.584	.572	18.4	48.0	52.0	55.6	58.1	154.
APM-2	.079	.129	.233	.207	19.9	32.4	36.3	40.2	42.5	144.
vdW-1	-.777	-.732	-.638	-.663	8.60	8.93	13.0	17.0	19.3	-43.1
vdW-2	-.534	-.486	-.388	-.411	8.79	12.7	16.8	20.8	23.0	-40.8
Three Liquid	-.285	-.238	-.139	-.162	9.09	16.4	20.5	24.4	26.7	-35.2

TABLE 20

COMPARISON OF CALCULATION RESULTS FOR EQUIMOLAR LIQUID MIXTURE OF KRYPTON
AND XENON AT 161.36°K BASED ON AVERAGE POTENTIAL MODEL
APPROACHES (SIMON EQUATION FOR $w(\tilde{T})$)

Model	<u>V^E, cm³/gm-mole</u>					<u>G^E, cal./gm-mole</u>				
	Mixing Rules	Set	No.			Mixing Rules	Set	No.		
	1	2	3	4	5	1	2	3	4	5
(This Work Experimental)		(-.459)					(24.82)			
APM-1	1.33	1.45	1.56	1.52	23.0	86.4	94.9	99.5	100.	205.
APM-2	.492	.595	.728	.658	25.3	54.9	63.3	68.4	68.5	189.
vdW-1	-.966	-.878	-.760	-.824	10.7	6.76	15.5	21.0	20.8	-64.0
vdW-2	-.662	-.567	-.444	-.507	11.0	14.6	23.3	28.7	28.6	-59.2
Three Liquid	-.350	-.254	-.131	-.194	11.4	22.3	31.0	36.3	36.3	-48.9

be seen that the van der Waals two fluid model gave overall better predictions. This finding was in agreement with those of Leland, Rowlinson, Sather, and Watson [48]. Next, within the framework of the vdW-2 model, the merits of the various mixing rules were examined. It was unnecessary to do a similar comparison for other models because they were shown to be inferior to vdW-2 already. The Krewglewski rule was so bad that the results were excluded from the comparisons. The comparisons of the four other sets of mixing rules results with experimental data were shown in Figure 19 and Figure 20 for V^E and in Figure 21 and Figure 22 for G^E . It can be seen that the vdW-2 model with mixing rules set 3, i.e., the S-M rules for σ_{12} and Canfield rule for ϵ_{12} was the best in predicting the excess properties V^E and G^E for the heavy rare gas liquid mixtures.

The calculation results using the reference equation of state of krypton did not improve the results. It is possible that Simon's equation may be better, because it was obtained from the curve fitting through more substances which follow the principle of corresponding states.

Sometimes it was possible to arbitrarily adjust the mixing rule to force the prediction close to the experimental values. However, this does not serve the purpose of checking the basic weak points of any model. The merit of any specific model should be judged from its

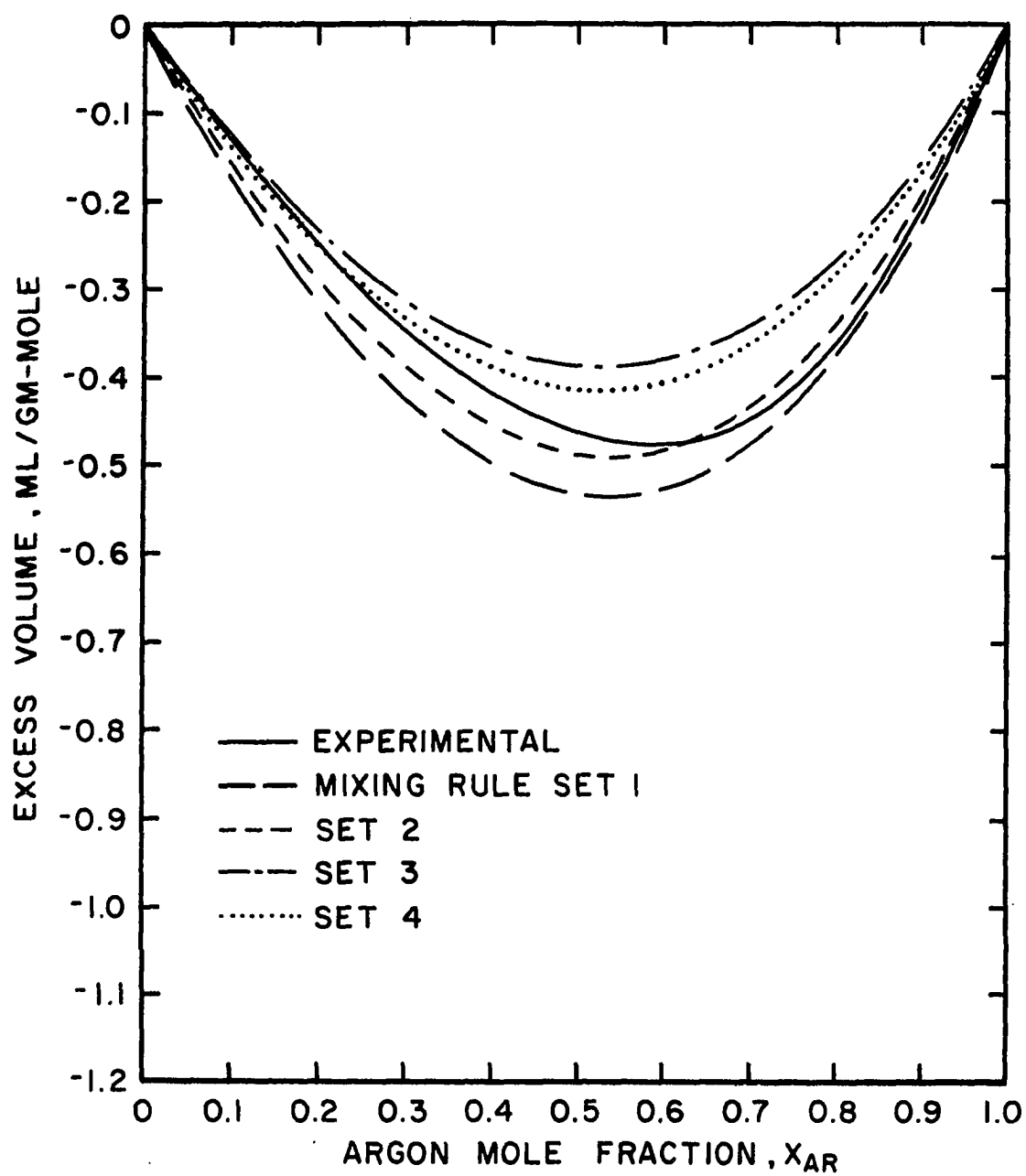


Figure 19. Comparison of Excess Volume Calculated from vdW-2 Model for Ar + Kr at 115.77°K

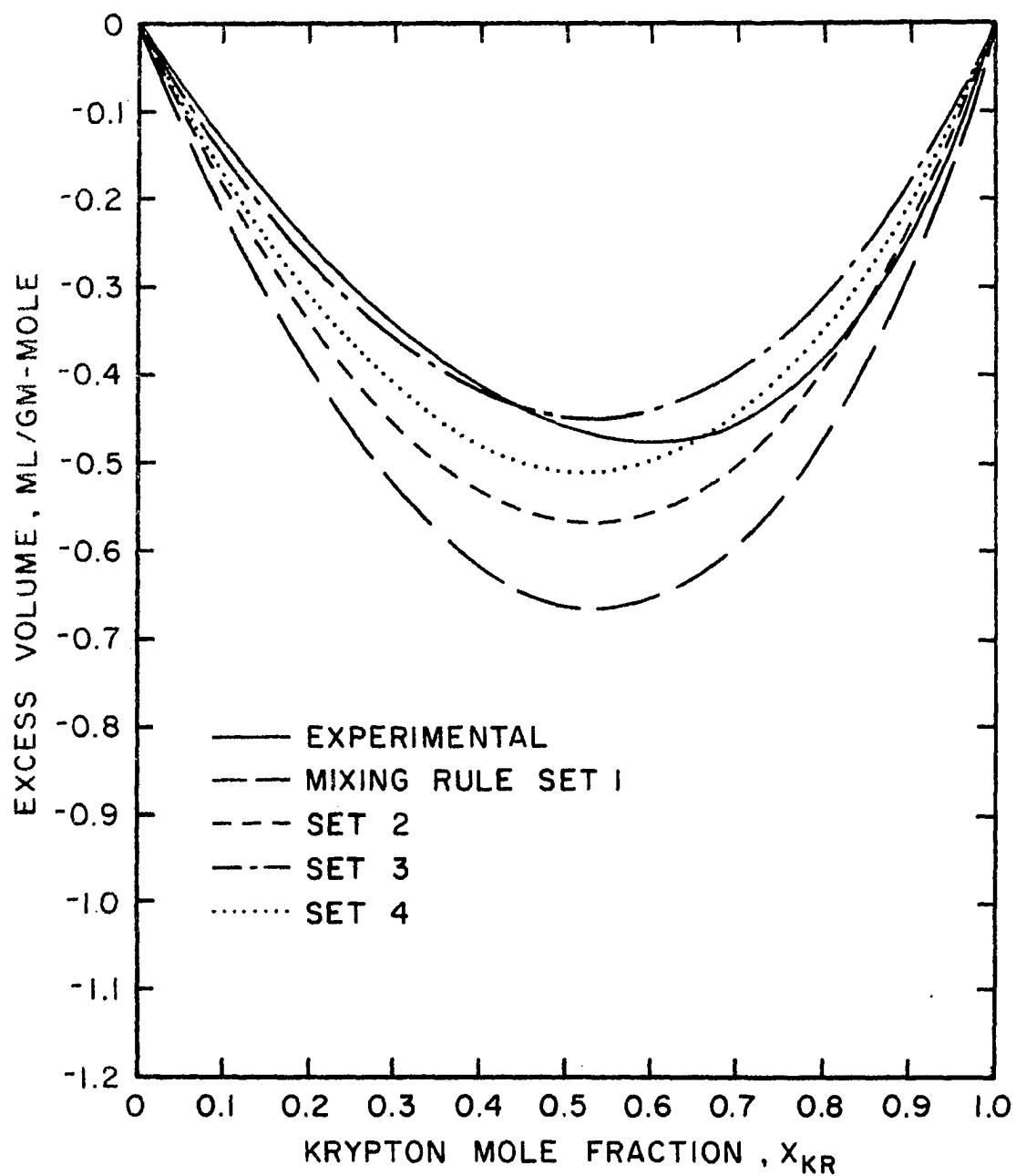


Figure 20. Comparison of Excess Volume Calculated from vdW-2 Model for Kr + Xe at 161.36°K

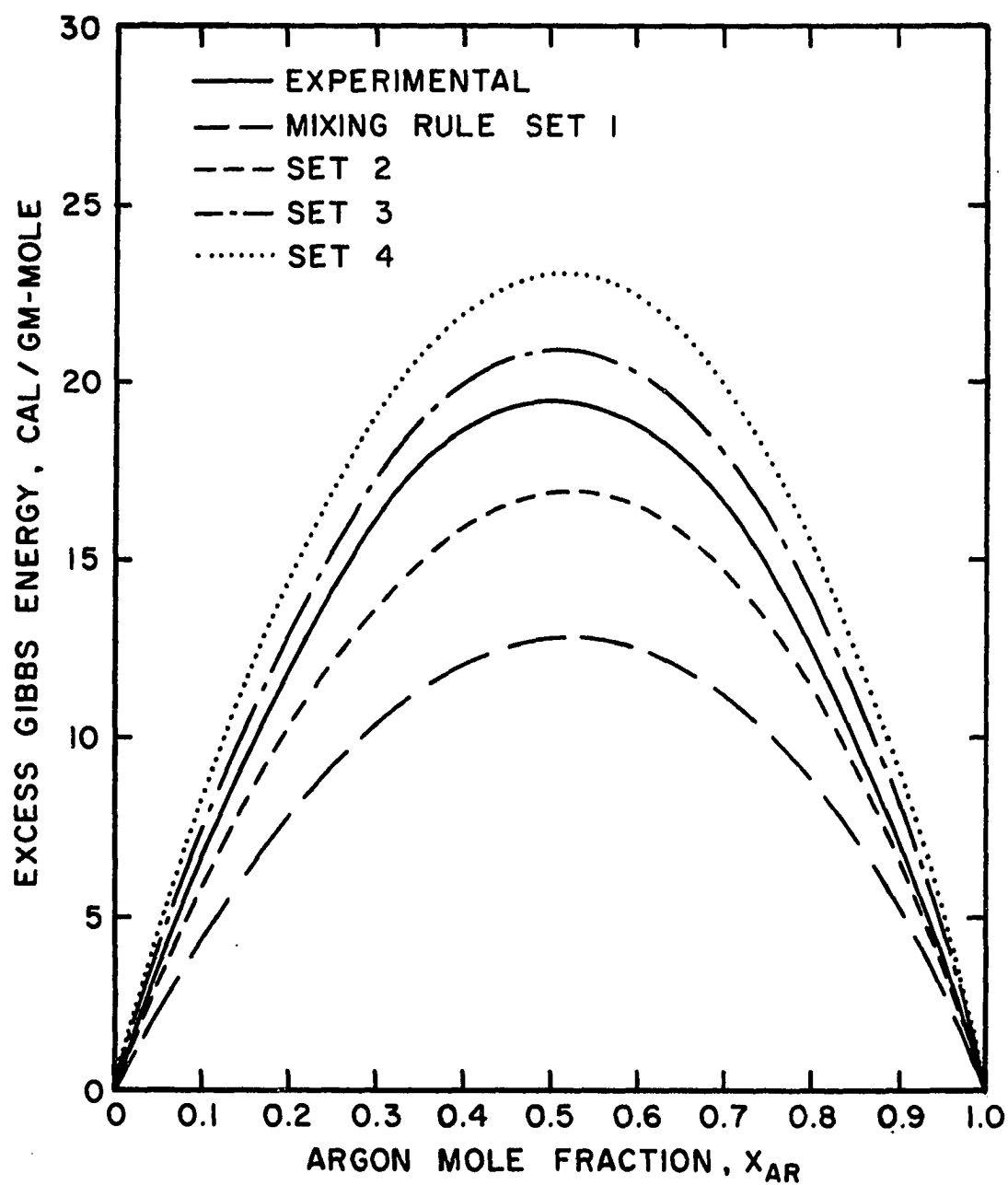


Figure 21. Comparison of Excess Gibbs Energy Calculated from vdW-2 Model for Ar + Kr at 115.77°K

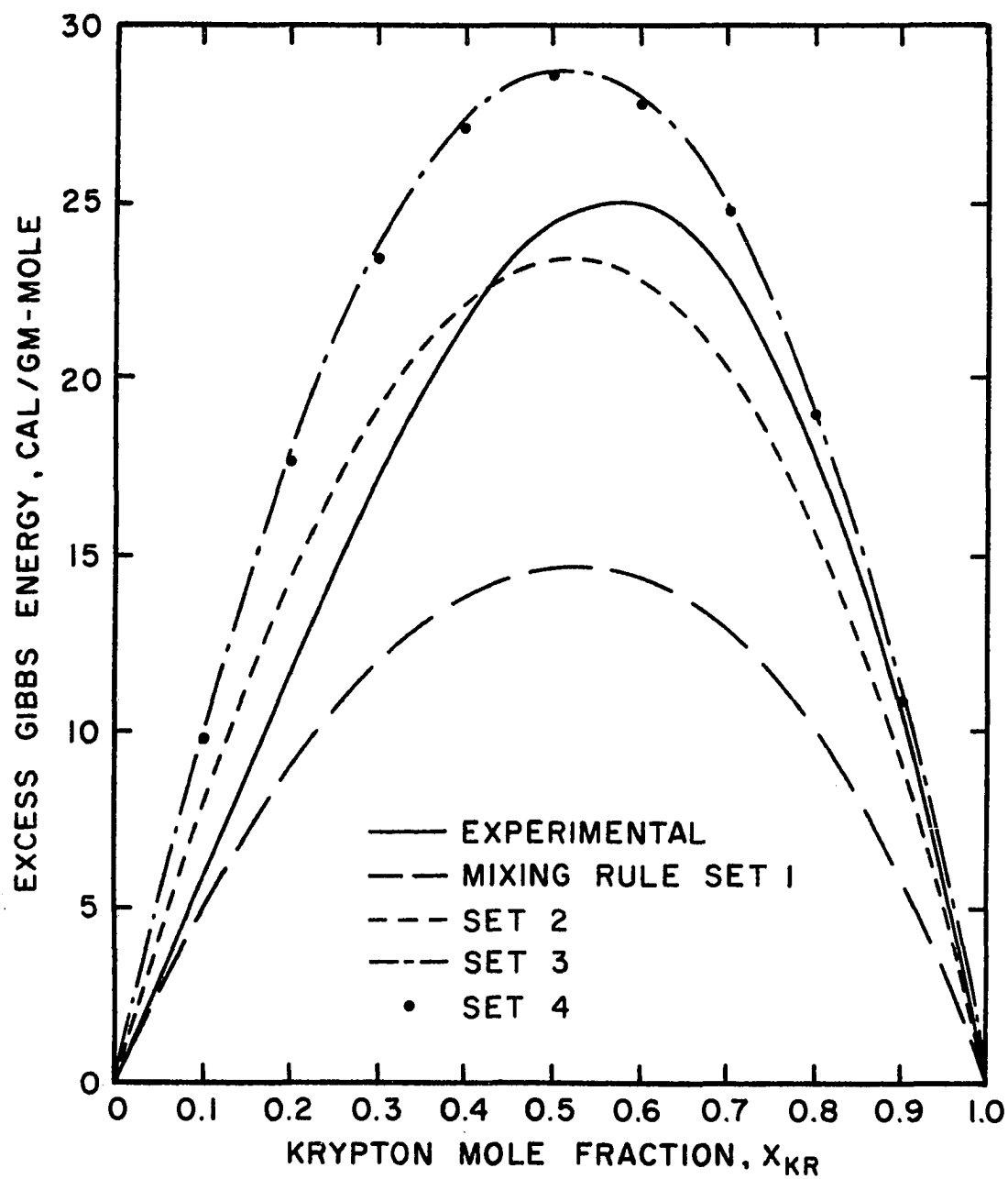


Figure 22. Comparison of Excess Gibbs Energy Calculated from vdW-2 Model for Kr + Xe at 161.36°K

ability to predict both G^E and V^E . The adjustment parameter or "fudge factor" called by R. L. Scott [69] should not be abused as to lose the initial purpose of using it, that is, checking the weakness of theory of solution.

One point that needs emphasis is that the vdW models did predict the very slight asymmetry of the G^E and V^E versus x curves. The equation of state approach in the next chapter also predicts the asymmetry of excess functions. As pointed out by Scott and Fenby [69] any fundamental interpretation consists of three steps:

1. the equation of state for the pure liquids, or the experimental data in the corresponding states theories.
2. a prescription for extension to solutions.
3. assignment of values to ϵ_{12} and σ_{12} .

Thus, an unwise choice at steps 1. and 2. may force choices of ϵ_{12} and σ_{12} meaningless as far as the real intermolecular pair energy is concerned.

It was found that the switch of the reduced equation of state from Simon's equation to the equation based on Staveley's krypton data did not change the value of G^E but changed the value of V^E . As pointed out by Staveley, their experimental data of krypton and xenon follow the same curve of $\Delta(V_c/V)$ versus (T/T_c) . The value $\Delta(V_c/V)$ was $(V_c/V)_{\text{exptl.}} - (V_c/V)_{\text{calc.}}$ where

$$(V_c/V)_{\text{calc.}} = 1 + \frac{3}{4} (1 - T/T_c) + \frac{7}{4} (1 - T/T_c)^{1/3} \quad (62)$$

The curve of argon needs 1% change in its V_c in order to coincide that of krypton and xenon. Thus, it can be seen that the reference equation of state of $w(\tilde{T})$ was important in the quantitative value of V^E .

From the above comparison, it was obvious that both the APM-1 and APM-2 were ineffectual in even the simpler systems encountered, i.e., Ar + Kr and Kr + Xe.

The weakness of APM-1 was pointed out by Rowlinson. This was the assumption of random mixtures, which for $\langle \sigma \rangle$ lead, for the general case of the Lennard-Jones (n,6) potential with a repulsive exponent n approaching infinity, to the absurd result that no intermolecular distance can be smaller than the diameter of the largest molecular present, even if the mole fraction of that species is vanishingly small. As shown by Rowlinson in his recent book that the theory of random mixture badly overestimates the excess free energy of mixtures of different sizes. However, the vdW-2 gave overall better prediction consistent with those findings by Rowlinson, et al. [48]. The three liquid model would lead to too much ordering, it would not predict the "asymmetry" of any excess functions. So far as the frame work of vdW-2 is concerned, the mixing rules set 2, 3, and 4 gave close predictions. The final judgment should wait for

more accurate equation of state for the liquid molar volume. However, it did point out one fact that the so-called Lorentz-Berthelot mixture are not true pictures in these simple systems. It was doubtful that arithmetic mean for σ_{12} was correct even if it was a better approximation than the geometric mean for ϵ_{12} . This was shown in the use of Simon's equation, the Canfield rule for ϵ_{12} in conjunction with S-M rule for σ_{12} gave better prediction.

CHAPTER VIII

PERTURBATION APPROACH BASED ON HARD SPHERE EQUATION OF STATE

In recent years considerable advances have been made in the liquid theory from the radial distribution function approach [3,5,23,26,64]. The model theories of the liquid state suffer from the same weak point [36]: that they all assume that the molecular structure of a liquid may be described by a well-defined spatial arrangement of the molecules. Thus the approach of the radial distribution function, considering the liquid molecular structure from the viewpoint of simple statistics of intermolecular distances, has been explored with revived vigor. This was further supported by x-ray diffraction experiments [26] on liquid structure and exact machine computations, such as the Monte Carlo method and the molecular dynamic method [26,57,63].

In this chapter, an extension of the perturbation approach based on the hard sphere equation of state [5] to a binary liquid mixture is examined. Calculations based on a simplified version are performed for the heavy rare

gas liquid systems studied in this investigation. The esthetic part of a rigorous approach lies in the fact that a prediction method based on first principles can be developed without "a priori" information. Needless to say, chemical engineers in the field of development of the equation of state for fluids and fluid mixtures may have a sound foundation as a starting point.

The Percus-Yevick Equation of State

The hard sphere equation of state is used in both the perturbation approach in the pure component and binary systems derivation. Theories of the distribution function for the liquid state may be found elsewhere [18,24,35,57,64] and are not to be repeated here. A radial distribution function is defined as:

$$g(r) = g^{(2)}(r) = \frac{\rho(r)}{n} = \frac{dn/(4\pi r^2 dr)}{n} \quad (63)$$

where $n = \frac{N}{V}$ is the mean number density, $\rho(r)$ is the local fluid number density, or the number of particles contained per unit volume of the shell.

The local deviation from the mean fluid number density is

$$\rho(r) - n = n \cdot h(r) \quad (64)$$

where $h(r)$ is called total correlation function, which represents some sort of short-range order and

$$h(r) = g(r) - 1 \quad (65)$$

The pressure equation is

$$P = \rho kT - \frac{\rho^2}{6kT} \int_V r \frac{du(r)}{dr} g(r) d\mathbf{r} \quad (66)$$

The compressibility equation is

$$\frac{\partial \rho}{\partial P} kT = \rho \int_V (g(r) - 1) d\mathbf{r} + 1 = \rho \int_V h(r) d\mathbf{r} + 1 \quad (67)$$

or

$$\left(\frac{1}{kT} \frac{\partial P}{\partial \rho} \right)_T = 1 - \rho \int_V c(r) d\mathbf{r} \quad (68)$$

This follows from using the Fourier transform on the Ornstein-Zernike equation [58]:

$$h(r) = c(r) + \rho \int c(|\mathbf{r} - \mathbf{r}'|) h(r') d\mathbf{r}' \quad (69)$$

Theoretically, thermodynamic properties of a liquid may be evaluated by knowing $g(r)$ and $u(r)$. It can be shown that the relation between $g(r)$ and $u(r)$ is:

$$\left[\frac{\partial}{\partial r} \ln g(r) + \frac{u(r)}{kT} \right] = - \frac{1}{kT} \int \frac{\partial u(s)}{\partial s} \cdot \frac{(\mathbf{r} \cdot \mathbf{s})}{rs} p(\mathbf{r}_1, \mathbf{r}_2, \mathbf{r}_3) d\mathbf{r}_3 \quad (70)$$

$$\text{or} \quad g(r) = \exp \left[- \frac{u(r) + w(r)}{kT} \right] \quad (71)$$

$$w(r) = \int_V d\mathbf{r}' \int_V \frac{\partial u(s)}{\partial s} \frac{\mathbf{r}' \cdot \mathbf{s}}{r's} p(\mathbf{r}_1, \mathbf{r}_2, \mathbf{r}_3) d\mathbf{r}_3 \quad (72)$$

The Percus-Yevick equation for evaluating $w(r)$ is

$$\ln g(r) + \frac{u(r)}{kT} = \ln [g(r) - c(r)] = \frac{w(r)}{kT} \quad (73)$$

$$\text{or} \quad c(r) = g(r) \left(1 - e^{u(r)/kT} \right) \quad (74)$$

For a hard sphere potential, Wertheim [94] has solved the PY equation for $c(r)$ as

$$c(r) = - \frac{1}{(1-\eta)^4} \left[(1+2\eta)^2 - 6\eta \left(1 + \frac{\eta}{2} \right)^2 \frac{r}{\sigma} + \frac{\eta}{2} (1+2\eta)^2 \left(\frac{r}{\sigma} \right)^3 \right] \quad \text{for } r < \sigma \quad (75)$$

$$c(r) = 0 \quad \text{for } r \geq \sigma$$

$$\text{where} \quad \eta = \frac{1}{6} \pi \sigma^3 \rho \quad (76)$$

By substituting the above solution into Equation 66 and Equation 68, it follows for the hard sphere equation of state,

$$\frac{P}{\rho kT} = \frac{1+2\eta+3\eta^2}{(1-\eta)^2} \quad \text{(Pressure equation)} \quad (77)$$

$$\frac{P}{\rho kT} = \frac{1+\eta+\eta^2}{(1-\eta)^3} \quad \text{(Compressibility equation)} \quad (78)$$

Ree & Hoover have developed the following Páde approximation [63] from Monte Carlo calculations:

$$\frac{P}{\rho kT} = 1 + \frac{(b\rho) (1+0.063507 (b\rho)+0.017329 (b\rho)^2)}{(1-0.561493 (b\rho)+0.081313 (b\rho)^2)} \quad (79)$$

$$\text{where} \quad b = (2\pi N\sigma^3/3)$$

This is a better hard sphere equation of state; however, in the following derivations and calculations the PY hard sphere compressibility equation is used exclusively.

Perturbation Approach, Single Component

In order to calculate thermodynamic properties from self consistent $u(r)$ and $g(r)$ for a liquid, based on the radial distribution function approach, it is necessary to know $g(r)$ and $u(r)$ very precisely [23]. Up to now, this has not been possible. Another way of looking at a liquid is to consider it as hard sphere molecules with attractive force as a perturbation [40,50,75,96]. Barker and Henderson [4,5] have developed, based on ideas of Zwanzig [103] and Rowlinson [66], a perturbation equation of state. The Helmholtz free energy is

$$\begin{aligned} \frac{F}{NkT} = & \left(\frac{F}{NkT} \right)_0 + 2\pi\rho\beta \int_0^\infty g_0(R;\rho) u(R) R^2 dR \\ & - \rho\pi\beta \left(\frac{\partial \rho}{\partial P} \right)_0 \frac{\partial}{\partial \rho} \left[\int_0^\infty g_0(R;\rho) u^2(R) R^2 dR \right] \end{aligned} \quad (80)$$

where $u(r) = u_0(R) + u_s(R)$

$$\begin{aligned} u_0(R) &= \infty, R < d; u_0(R) = 0, R \geq d; u_s(R) = 0, R < d; \\ u_s(R) &= f(R), R \geq d \end{aligned} \quad (81)$$

The hard sphere cut-off diameter d is temperature dependent:

$$d = \int_0^\sigma \left[1 - \exp\left(-\frac{u(z)}{kT}\right) \right] dz = c \cdot \sigma \quad (82)$$

where subscript "o" denotes hard sphere, and "s" denotes the "soft" potential.

The corresponding pressure equation is:

$$\begin{aligned} \frac{PV}{NkT} = & \left(\frac{PV}{NkT} \right)_o + \rho \frac{\partial}{\partial \rho} \left[2\pi\beta\rho \int_{\sigma}^{\infty} g_o(R;\rho) u(R) R^2 dR \right] \\ & - \rho \frac{\partial}{\partial \rho} \left[\pi\rho\beta \left(\frac{\partial \rho}{\partial P} \right)_o \frac{\partial}{\partial \rho} \rho \int_{\sigma}^{\infty} g_o(R;\rho) u^2(R) R^2 dR \right] \end{aligned} \quad (83)$$

where the hard sphere part is given by the Percus-Yevick compressibility equation result:

$$\left(\frac{PV}{NkT} \right)_o = \frac{1 + \frac{1}{6} \pi N(c\sigma)^3 \rho + \left(\frac{1}{6} \pi N(c\sigma)^3 \rho \right)^2}{\left(1 - \frac{1}{6} \pi N(c\sigma)^3 \rho \right)^3} \quad (84)$$

The significance of the above equations is that they indicate a physical picture of liquids similar to that originally envisioned by van der Waals. The pressure of the liquid may be viewed as being contributed by the hard sphere repulsion, the mean background attraction field, and higher order perturbation terms. Now $g_o(R;\rho)$ is the hard sphere radial distribution function obtained from the Percus-Yevick equation and has been evaluated both analytically [94] and numerically [86].

Kozak and Rice [40] used the following perturbation equation of state for a pure component:

$$\frac{P}{\rho kT} = \left(\frac{P}{\rho kT} \right)_o + \frac{A}{T} + \sum_{m=2}^{\infty} f_m^* D^{*m-1} \quad (85)$$

where

$$A = \frac{\rho}{k} \frac{\partial}{\partial \rho} \left[2\pi\rho \int_0^\infty R^2 u(R) g_0(R; \rho) dR \right] \quad (86)$$

The third "terms" on the right hand side are called the fluctuation terms. The hard sphere cut-off parameter, c , was evaluated by minimization of the Helmholtz free energy at constant T and V . It was found that c^3 is density dependent instead of temperature dependent as shown by Barker and Henderson.

Longuet-Higgins and Widom [50] used the following equation instead:

$$\frac{P}{\rho kT} = \left(\frac{P}{\rho kT} \right)_0 - \frac{a\rho}{kT} \quad (87)$$

and a is considered to be constant. It should be mentioned that in the more elaborate forms presented by Barker and Henderson and Kozak and Rice, the first order perturbation term is the same. However, both their second order term involve approximations with unknown uncertainties introduced. As pointed out by Graben [30] and Sinanoglu [74], the triplet potential may be significant in liquid state calculations. Thus, although the Longuet-Higgins and Widom equation of state considers " a " as a constant, the last term tends to lump together all the perturbation effects due to attraction forces.

Perturbation Approach for Mixtures

The perturbation approach should be extended to mixture application in order to have a predictive theory for liquid mixtures. First, a brief review on the state of the art is given.

There is, up to the present writing, no perturbation approach for real liquid mixtures based on the equation of state of the Barker and Henderson type.

Throop and Bearman [87] have investigated the numerical results for the Percus-Yevick equation by using the Lennard-Jones (12 : 6) potential. They found that the combination rule of σ_{12} has quite an effect on the shape of the radial distribution function and is not given correctly by $\frac{1}{2}(\sigma_{11} + \sigma_{22})$.

Snider and Herrington [75] have applied the Longuet-Higgins and Widom [50] equation of state to liquid mixtures. Encouraging results were obtained. For instance, the calculated V^E for the argon-krypton liquid mixture showed a minimum at 0.6 mole fraction of argon, which is the experimentally observed position of the minimum by Staveley and co-workers [21]. The van der Waals type configurational internal energy is used:

$$\frac{U}{N} = - (a_{11}x_1^2 + 2a_{12}x_1x_2 + a_{22}x_2^2) \rho_m \quad (88)$$

where a_{12} is either obtained by fitting one theoretical point to experimental value of G^E or by assuming that

$$a_{12} = \left(a_{11} \cdot a_{22} / r_1^3 \cdot r_2^3 \right)^{1/2} \left(0.5 (r_1 + r_2) \right)^3 \quad (89)$$

They found that a_{12} evaluated in the above two methods checked well. The hard sphere Percus-Yevick equation for mixture was taken from those derived by Lebowitz [45].

Fundamental Equations for Hard Sphere Model
of Binary Liquid Mixtures

The Longuet-Higgins and Widom equation of state for a pure component liquid can be written as:

$$\frac{PV}{RT} = \chi(y) - \frac{a}{VRT} \quad (90)$$

where χ is $\frac{(1+y+y^2)}{(1-y)^3}$, y is $\frac{1}{6} \pi r^3 \rho$, r is the hard sphere diameter and ρ is the number density.

For binary mixture, the generalization [45] is:

$$\chi_m(y_m, x) = \frac{1+y_m+y_m^2}{(1-y_m)^3} - \frac{3y_m}{(1-y_m)^3} \cdot \frac{x_1 \cdot x_2}{x_1 r_1^3 + x_2 r_2^3} \cdot (r_1 - r_2)^2 \left(r_1 + r_2 + y_m r_1 r_2 \cdot \frac{x_1 r_1^2 + x_2 r_2^2}{x_1 r_1^3 + x_2 r_2^3} \right) \quad (91)$$

where x_1 and x_2 are the mole fractions of the components, y_m is $\frac{\pi}{6} x_1 r_1^3 + x_2 r_2^3 \rho_m$ resulted from assuming $r_{12} = .5(r_1 + r_2)$, and ρ_m is the liquid density of the binary mixture at composition x . For a binary liquid mixture, the equation of state is:

$$\frac{PV_m}{RT} = \chi_m(y_m, x) - \frac{(a_{11} \cdot x_1^2 + 2a_{12} \cdot x_1 x_2 + a_{22} x_2^2)}{V_m \cdot RT} \quad (92)$$

Defining the standard state of the substance as the ideal gas limit, then it follows for coexisting vapor and liquid:

$$(H^L - H^*)/RT = (Z^L - 1) - U^L/RT \quad (93)$$

$$(H^V - H^*)/RT = (Z^V - 1) - U^V/RT \quad (94)$$

where H, Z, U are enthalpy, compressibility factor, and internal energy respectively. For the model under consideration, the internal energy is [50]:

$$U = -a/V \quad (95)$$

Thus, at the normal boiling point, assuming $\chi^V = 1$ then the heat of vaporization is

$$\frac{\Delta H^V}{RT} = \frac{(H^V - H^L)}{RT} = \chi(y) + 1 + 2 \cdot (Z^V - 1 - Z^L) \approx \chi(y) + 1 \quad (96)$$

This relation can also be derived by assuming that the vapor phase at normal boiling point is ideal gas.

Pure component parameter r can be obtained from Equation 96 at normal boiling point. Constant "a" can then be determined from the equation of state by knowing r.

The excess properties of the binary liquid mixture can be shown to be [75]:

$$V^E = \frac{1}{6} \pi N \sum_{i=1}^2 x_i r_i^3 (y_m^{-1} - y_i^{-1}) \quad N = \text{Avogadro Number} \quad (97)$$

$$\frac{H^E}{RT} = \sum_{i=1}^2 x_i \left[\left(\frac{2P_m V_m}{RT} - \chi_m(y_m, x) \right) - \left(\frac{2P_i V_i}{RT} - \chi_i(y_i) \right) \right] \quad (98)$$

where P_m is the saturation total vapor pressure of mixture, P_i is the saturation vapor pressure of pure component i at temperature T . The excess Gibbs energy is:

$$\begin{aligned} G^E/RT = & \sum_{i=1}^2 x_i \left[\frac{2P_m V_m}{RT} - \chi_m(y_m, x) - \ln \frac{V_m(1-y_m)}{V_i(1-y_i)} + \frac{3}{2} y_m \frac{(2-y_m)}{(1-y_m)^2} \right. \\ & \left. - \left(\frac{2P_i V_i}{RT} - \chi(y_i) + \frac{3}{2} y_i \frac{(2-y_i)}{(1-y_i)^2} \right) \right] \\ & - \frac{3}{2} \frac{y_m}{(1-y_m)^2} \frac{x_1 x_2}{(x_1 r_1^3 + x_2 r_1^3)} (r_1 - r_2)^2 \cdot \\ & \left(2(r_1 + r_2) - y_m \frac{x_1 r_1^4 + x_2 r_2^4}{x_1 r_1^3 + x_2 r_2^3} \right) \end{aligned} \quad (99)$$

The above equations can be used for calculating excess properties at saturation pressures.

Calculation of Excess Properties for Binary
Liquid Mixtures of Argon + Krypton, and
Krypton + Xenon

The parameters used for calculation are given in Table 22. The parameters for xenon were determined in this work based on the pure component properties at the normal boiling point given in Table 22.

TABLE 21

EQUATION OF STATE PARAMETERS FOR
THE PURE AR, KR, AND XE

Substance	Constants Set A		Constants Set B	
	r, Å	$a \times 10^{-5}$, J-cc/mole ²	r, Å	$a \times 10^{-5}$, J-cc/mole ²
Argon	3.360	1.67	3.356	1.66
Krypton	3.575	2.74	3.583	2.79
Xenon	---	---	3.900	5.01

- Note: 1. Constants for argon and krypton were obtained from Snider and Herrington [75].
2. Constants Set A were determined by Snider and Herrington from

$$\frac{\Delta H_v}{RT} = \ln \left(\frac{PV}{RT} \right) - \ln(1-y) + \frac{3}{2} y \frac{(2-y)}{(1-y)^2}$$

$$\text{and } \frac{PV}{RT} = \frac{1+y+y^2}{(1-y)^3} - \frac{a}{VKT}$$

TABLE 22

NORMAL BOILING TEMPERATURE DATA FOR THE PURE
COMPONENTS IN EQUATION OF STATE STUDY

Substance	Normal Boiling Temperature, °K	Heat of Vaporization, ΔH_v , J/mole	Pure Liquid Volume, $\text{cm}^3/\text{gm-mole}$
Argon	87.29	6,516.6	28.66
Krypton	119.8	9,029.1	34.73
Xenon	165.02 ^a	12,635.7 ^a	44.50 ^b
Nitrogen	77.35	5,59.49	34.67
Oxygen	90.19	6,825.0	28.02
Methane	111.67 ^c	8,171.4 ^c	38.11 ^d
CO	81.63	6,040.0	35.41

- Note: 1. Unless indicated otherwise, the constants were taken from Table I of Snider and Herrington [75].
2. N_2 , O_2 , CH_4 , CO data were used in the generalized equation of state study in Chapter IX.
3. a. Ziegler, W.T., et al. [101],
 b. Bewilogua, L. and Gladun, C. [8],
 c. Ziegler, W.T., et al. [100]
 d. Terry, M.J., et al. [84].

For argon and krypton mixtures at 115.77°K, the calculations were done first with the first set of parameters given by Snider and Herrington. These parameters are slightly different from those determined from Equation 96 and Equation 90. In calculating a_{12} , Equation 89 was used. The Newton-Raphson method was used to calculate the liquid density of the binary mixture by using the experimental total vapor pressure versus composition data. First, an initial liquid mixture density was assumed at a given set of (P, x) , then the revised guess was calculated from:

$$(\rho_m)_{j+1} = (\rho_m)_j - \frac{(P_{\text{calc.}} - P_{\text{exptl.}})_j}{(dP/d\rho_m)_j} \quad (100)$$

When the difference between two successive calculations j and $j+1$ was negligibly small, say, 10^{-6} , the calculated density was accepted as the converged value.

The calculations were then performed for G^E , V^E , and H^E , all at the saturation pressures, for the two binary mixtures. The Srivastava and Madan rule for ϵ_{12} and the arithmetic mean rule for r_{12} were used in calculating a_{12} . The results are presented in Table 23 and Table 24. The following conclusions were obtained from these calculations:

1. Contrary to Snider and Herrington's findings, the predicted H^E were bad. The calculated H^E were negative for both binary systems. It was estimated [36] that for equimolar mixture of argon and krypton at 115.77°K, H^E

TABLE 23

EXCESS PROPERTIES AND LIQUID DENSITY OF ARGON AND KRYPTON

MIXTURE AT 115.77°K ACCORDING TO THE LONGUET-HIGGINS,

WIDOM, AND LEBOWITZ EQUATION OF STATE

Pressure, Psia	Mole Fraction, Argon, x_{Ar}	V^E ml./gm-mole	G^E cal./gm-mole	H^E cal./gm-mole	ρ_m gm/ml.
10.588	0.0	0.0	0.0	0.0	2.464
28.5098	.12148	-.302	6.016	.048	2.312
27.7404	.11581	-.289	5.764	.050	2.319
39.5163	.20235	-.478	9.349	.024	2.209
52.0518	.2997	-.657	12.600	-.048	2.083
55.5254	.3280	-.701	13.369	-.077	2.046
62.5402	.38495	-.780	14.694	-.134	1.971
75.2300	.49377	-.883	16.225	-.272	1.825
68.0918	.42999	-.830	15.511	-.177	1.911
78.1956	.51899	-.897	16.390	-.300	1.790
87.9592	.60171	-.913	16.372	-.379	1.677
101.3297	.71569	-.846	14.742	-.451	1.519
101.8520	.71963	-.842	14.654	-.449	1.513
110.8478	.79409	-.726	12.390	-.441	1.408
124.2571	.90064	-.438	7.237	-.317	1.256
138.0606	1.0	0.0	0.0	0.0	1.111

TABLE 24

EXCESS PROPERTIES AND LIQUID DENSITY OF KRYPTON AND XENON

MIXTURE AT 161.36°K ACCORDING TO THE LONGUET-HIGGINS,

WIDOM, AND LEBOWITZ EQUATION OF STATE

Pressure, Psia	Mole Fraction, Krypton, x_{Kr}	V^E ml./gm-mole	G^E cal./gm-mole	H^E cal./gm-mole	ρ_m gm/ml.
11.987	0.0	0.0	0.0	0.0	2.992
28.000	.10	-.314	7.553	-.079	2.903
44.000	.20	-.591	14.050	-.167	2.810
45.297	.21056	-.618	14.625	-.203	2.800
55.402	.27629	-.774	18.128	-.286	2.737
59.200	.30	-.825	19.273	-.304	2.714
74.500	.40	-1.007	23.159	-.419	2.613
88.900	.50	-1.125	25.382	-.564	2.508
102.800	.60	-1.165	25.722	-.696	2.398
113.500	.68217	-1.126	24.308	-.800	2.304
116.000	.70	-1.107	23.808	-.802	2.283
129.000	.80	-.923	19.237	-.817	2.162
131.826	.82509	-.852	17.548	-.827	2.130
143.000	.90	-.574	11.530	-.609	2.034
159.505	1.0	0.0	0.0	0.0	1.899

was about 11. cal/gm-mole, while the calculated value was about -.27 cal/gm-mole.

2. The predictions on G^E were good. The theory also predicted the slight asymmetry of G^E versus x_1 curve, with the maximum of G^E situated at $x_1 = 0.6$.

3. The theory predicted the asymmetry in the v^E versus x_1 curves.

Finally it was conjectured that the temperature dependency in the parameters may be responsible for some of the weakness in the present prediction ability.

As can be seen in Figure 23 and Figure 24, the equation of state predicted a similar non-ideality in the density versus composition curve. Prediction of the liquid density of the more volatile component was bad as the parameters of this substance were determined at the normal boiling temperature which is not too close to the system temperature.

In Figure 25 and in Figure 26 the excess Gibbs energy was compared. Even though the experimental pressure versus composition data were used in calculating G^E by using the Longuet-Higgins - Widom - Lebowitz equation, the agreement between the calculated and experimental values were good. This also pointed out the soundness of the mixing rules adopted. It can be shown that $a \propto r^3 \cdot (\epsilon/k)$ [75,55]. Thus, again the geometric mean of ϵ_{12} was proven in error.

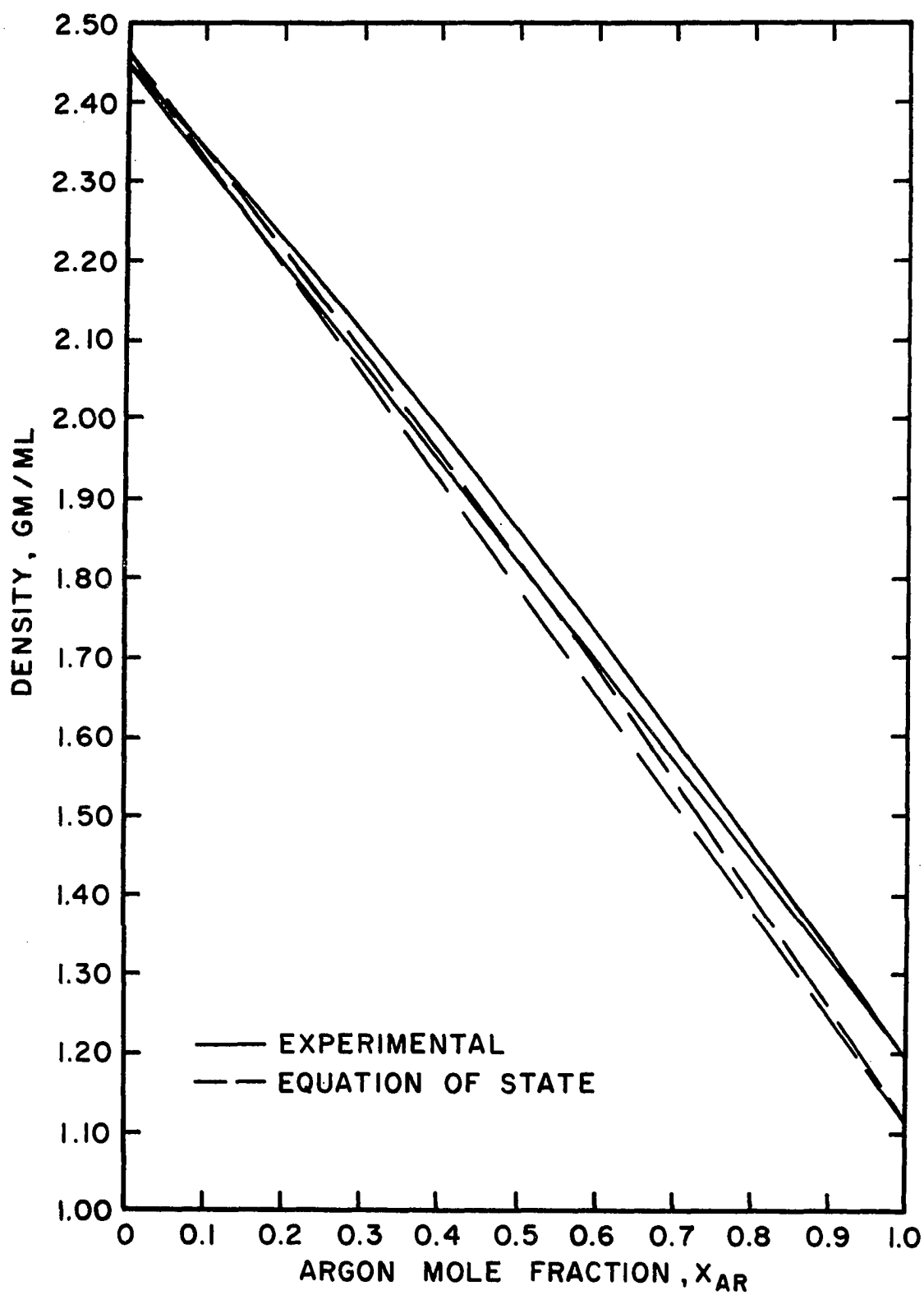


Figure 23. Comparison of Saturated Liquid Density of Ar + Kr at 115.77°K

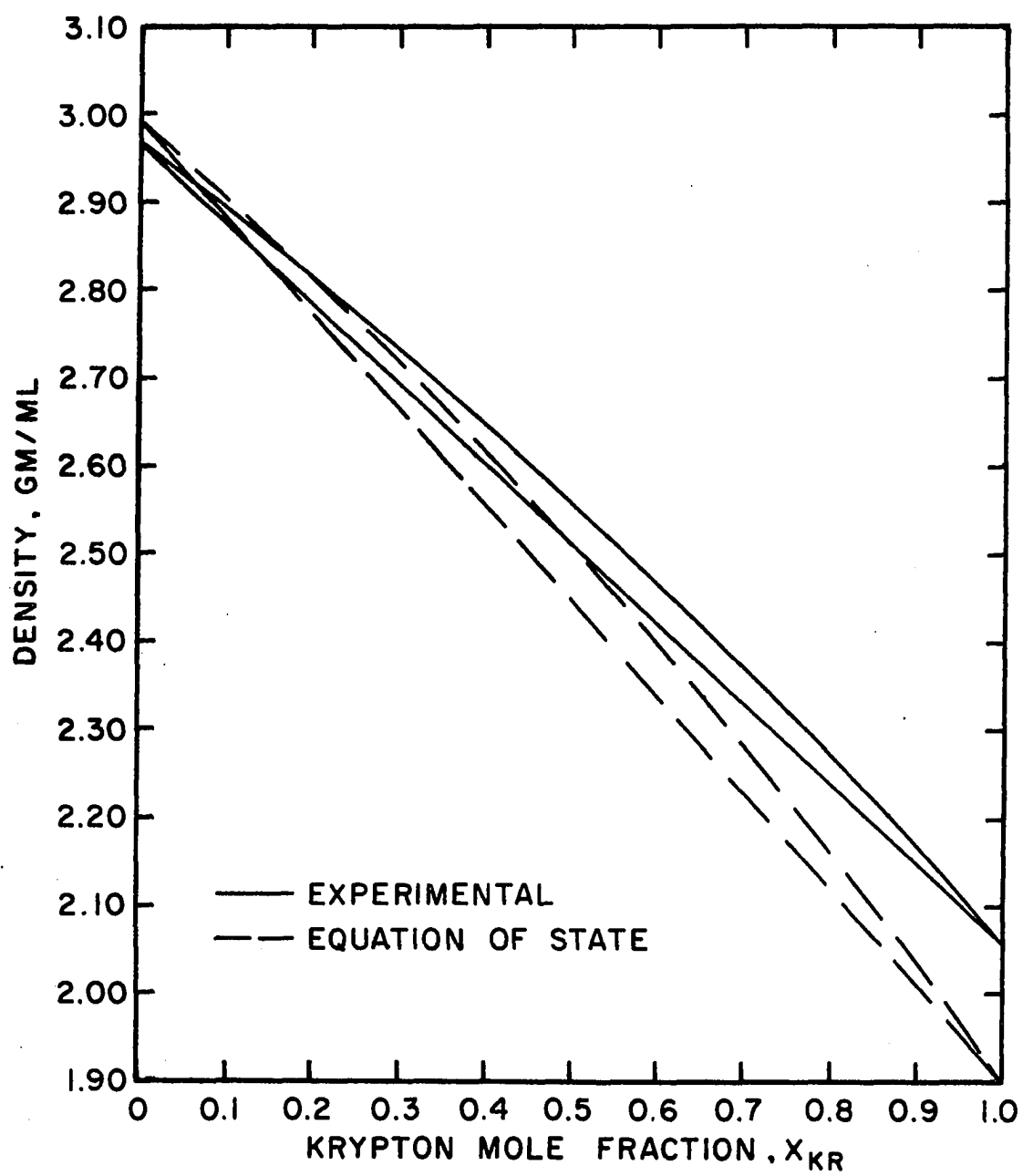


Figure 24. Comparison of Saturated Liquid Density of Kr + Xe at 161.36°K

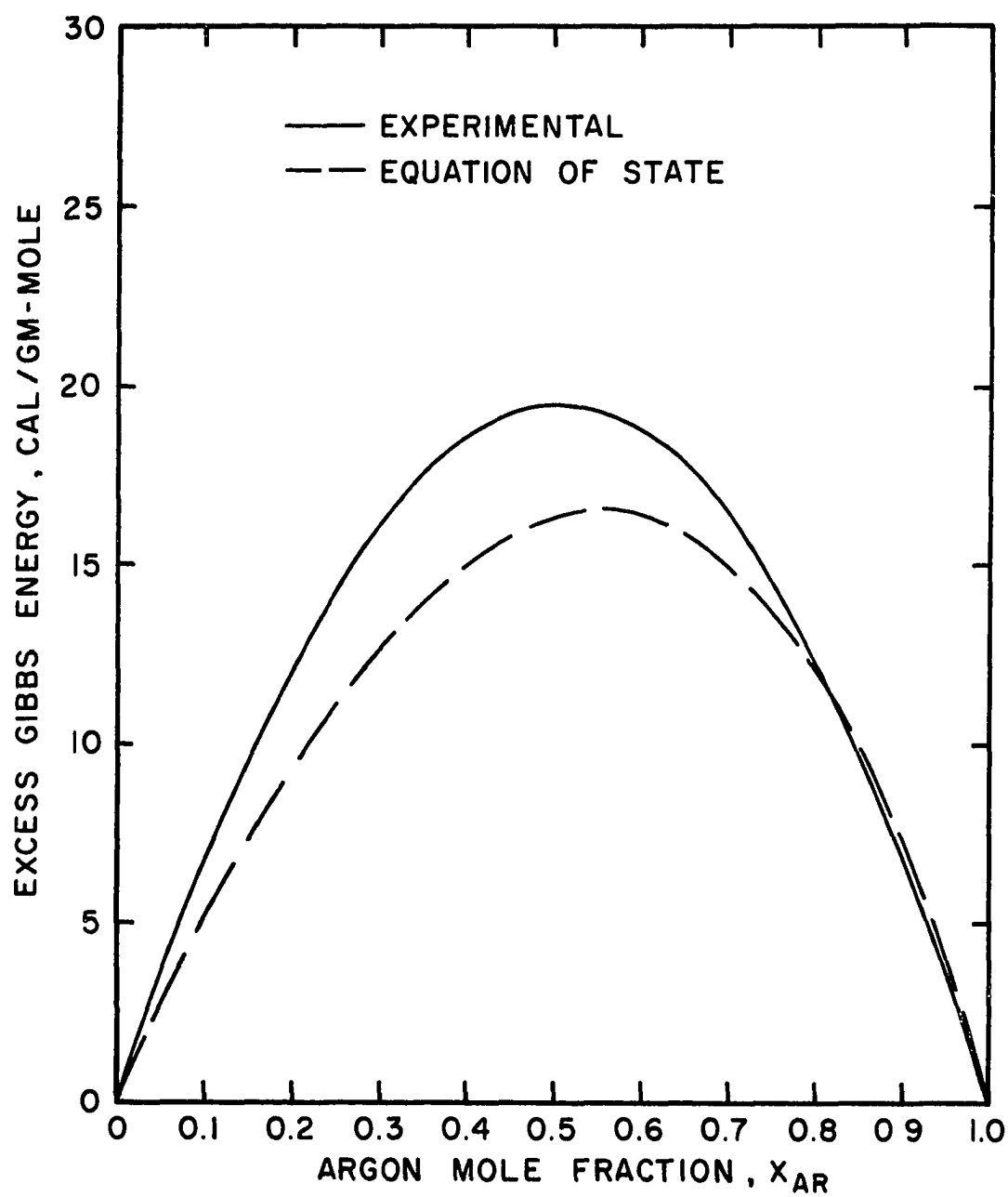


Figure 25. Comparison of Excess Gibbs Energy of Ar + Kr at 115.77°K

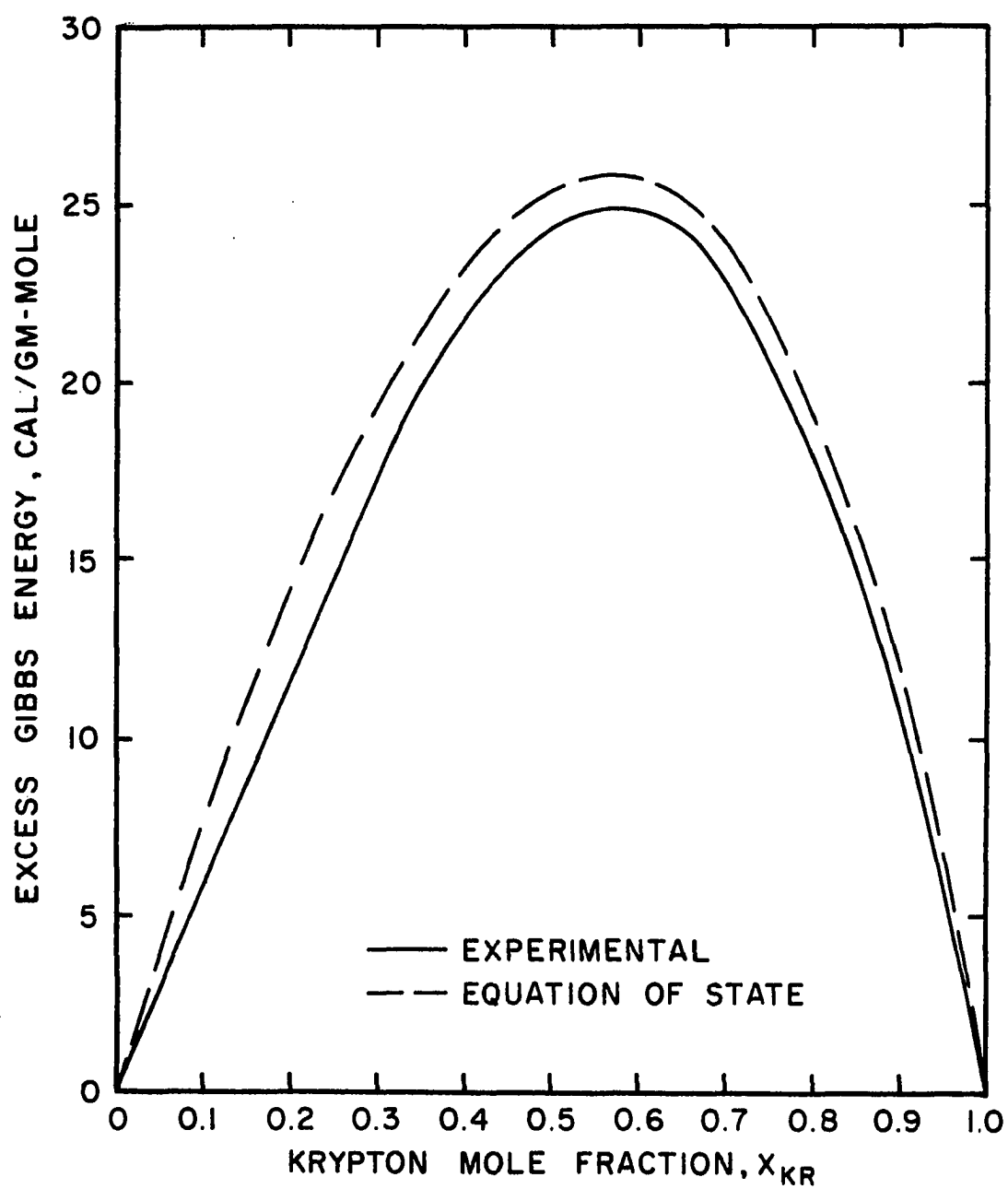


Figure 26. Comparison of Excess Gibbs Energy of Kr + Xe at 161.36°K

CHAPTER IX

CALCULATION OF THE BINARY LIQUID MIXTURE PROPERTIES BASED ON THE GENERALIZED EQUATION OF STATE

The success of the one fluid model based on the hard sphere perturbation equation of state proposed by Snider and Herrington suggested that one fluid model based on similar equation of state may be successfully applied to binary mixtures. Although, in engineering applications, the Redlich-Kwong equation of state has been used in this sense for a while, it has not been used to calculate the excess thermodynamic properties at zero pressure for liquids. Recently, McGlashan [55] has applied this approach by using the van der Waals equation and the Guggenheim equation [32]. Better results have been claimed over the Leland, Rowlinson, and Sather [47] approach, which does not base itself on any explicit equation of state. The approach of Snider and Herrington was based on the Longuet-Higgins and Widom equation which assumes the hard sphere part can be represented by the Percus-Yevick compressibility equation (P-Y, c). However, it is known that the Percus-Yevick compressibility equation

(P-Y, c) or the Percus-Yevick pressure equation (P-Y, p) is approximate at best. Even so, the theory that produces the pure component P-Y equation can also give the P-Y multi-component equation for the multicomponent case. On the other hand, this is not so for some empirical equations of state for hard spheres, such as those given by Páde approximation and by Carnahan and Starling [13]. Thus, it is obvious that the equation of state based on the perturbation of a hard sphere equation, or, consisting of a hard sphere repulsive part and a uniform background potential term should be exploited in the sense of the McGlashan approach. There are two more reasons for so doing. First, a generalized equation of state can be presented and examined. Second, the empiricism on the part of the hard sphere repulsion can be used. It has been shown that the empiricism of Carnahan has given a hard sphere equation of state most closely agrees with the "computer experiments" of the hard sphere equation [13].

In this section, a generalized equation of state is proposed. This equation will be examined based on the one fluid approach for liquid mixtures. By varying the two parameters, the generalized equation can generate the various equations of state. It is proper to examine this generalized equation and compare the relative merits of the various equations in the sense of one fluid model approach of the principle of corresponding states.

The generalized equation of state can be written as:

$$PV = RT \left(\frac{1 + y + y^2 + w_1 y^2 + w_2 y^3}{(1 - y)^3} \right) - \frac{a}{V} \quad (101)$$

where $y = b/4V$

The various equations of state can be written in a form similar to the above generalized equation. For the van der Waals equation:

$$PV = RT \left(\frac{1}{1 - 4y} \right) - \frac{a}{V} \quad (102)$$

the term $(1 - 4y)^{-1}$ can be written as

$$\begin{aligned} (1 - 4y)^{-1} &= (1-y)^{-3} [(1-y)^3 / (1-4y)] \\ &= (1-y)^{-3} (1+y+y^2+6y^2+27y^3+\dots) \end{aligned} \quad (103)$$

Thus, by neglecting the higher order terms in the above equation, the van der Waals equation is:

$$(vdW): \quad PV = RT \left(\frac{1+y+y^2+6y^2+27y^3}{(1 - y)^3} \right) - \frac{a}{V} \quad (104)$$

that is $w_1 = 6, \quad w_2 = 27$

For the Guggenheim equation:

$$PV = RT \left[\frac{1}{(1-y)^4} \right] - \frac{a}{V} \quad (105)$$

the term $(1-y)^{-4}$ can be rewritten as

$$(1-y)^{-4} = (1-y)^{-3} \left[\frac{1}{(1-y)} \right] = (1-y)^{-3} (1+y+y^2+y^3+\dots) \quad (106)$$

Thus, by neglecting the higher order terms in the Guggenheim equation, it can be written as

$$(G): \quad PV = RT \left[\frac{1+y+y^2+y^3}{(1-y)^3} \right] - \frac{a}{V} \quad (107)$$

that is $w_1 = 0, \quad w_2 = 1$

For the Longuet-Higgins and Widom equation:

$$(LH,W): \quad PV = RT \left[\frac{1+y+y^2}{(1-y)^3} \right] - \frac{a}{V} \quad (108)$$

The two parameters in the generalized equation are

$$w_1 = 0, \quad w_2 = 0$$

If we use the (P-Y,p), i.e., the Percus-Yevick pressure equation for the hard sphere part, we have

$$PV = RT \left[\frac{1+2y+3y^2}{(1-y)^2} \right] - \frac{a}{V} \quad (109)$$

Let us denote this equation as (PYP,vdW). The (PYP,vdW) can then be rewritten as

$$(PYP,vdW): \quad PV = RT \left[\frac{1+y+y^2-3y^3}{(1-y)^3} \right] - \frac{a}{V} \quad (110)$$

which corresponds to the generalized equation with

$$w_1 = 0, \quad w_2 = -3$$

Finally, by using the Carnahan-Starling equation for the hard sphere part, the equation of state can be written as

$$(CS,vdW): \quad PV = \left[\frac{1+y+y^2-y^3}{(1-y)^3} \right] - \frac{a}{V} \quad (111)$$

which corresponds to the generalized equation with

$$w_1 = 0, \quad w_2 = -1$$

The above classification of the various forms of the equation of state can be summarized in the following table.

TABLE 25
CHARACTERIZATION OF THE GENERALIZED EQUATION
OF STATE

Equivalent to	w_1	w_2
vdW	6.	27.
G	0.	1.
LH,W	0.	0.
CS, vdW	0.	-1.
PYP, vdW	0.	-3.

In order to apply the one fluid principle of corresponding states, it is necessary to determine the pertinent set of constants "a" and "b" for each set of w_1 and w_2 . This can be done by solving the following equations:

$$\left(\frac{\partial P}{\partial Y}\right)_{T_c} = 0, \quad \left(\frac{\partial^2 P}{\partial Y^2}\right)_{T_c} = 0 \quad (112)$$

Without referring to any experimental values, the two reduced parameters $(a/RT_c V_c)$ and (b/V_c) may thus be obtained. In the following calculations argon is chosen

to compare a and b obtained from the generalized equation of state by varying (w_1, w_2) .

Characteristic Constants of the Generalized Equation of State

The generalized equation of state can be written as:

$$P = \left(RT \frac{4}{b} \right) f_1(y, w_1, w_2) - f_2(y) \left(\frac{16a}{b^2} \right) \quad (113)$$

$$\text{where } f_1(y, w_1, w_2) = y(1-y)^{-3}(1+y+y^2+w_1y^2+w_2y^3) \quad (114)$$

$$f_2(y) = y^2 \quad (115)$$

By applying the conditions at the critical point:

$$\left(\frac{\partial P}{\partial y} \right)_{T_c} = \left(RT \frac{4}{b} \right) \left(\frac{\partial f_1}{\partial y} \right)_{T_c} - \left(\frac{16a}{b^2} \right) \left(\frac{\partial f_2}{\partial y} \right)_{T_c} = 0 \quad (116)$$

$$\left(\frac{\partial^2 P}{\partial y^2} \right)_{T_c} = \left(RT \frac{4}{b} \right) \left(\frac{\partial^2 f_1}{\partial y^2} \right)_{T_c} - \left(\frac{16a}{b^2} \right) \left(\frac{\partial^2 f_2}{\partial y^2} \right)_{T_c} = 0 \quad (117)$$

By eliminating constants a and b from the above two equations, the value of "y" at the critical point, y_c , is to be obtained by finding the root of the equation:

$$\begin{aligned} h(y) &= A_1 + A_2 y + A_3 y^2 + A_4 y^3 + A_5 y^4 + A_6 y^5 = 0 \\ &= A_1 + y \cdot (A_2 + y \cdot (A_3 + y \cdot (A_4 + y \cdot (A_5 + A_6 \cdot y)))) = 0 \end{aligned} \quad (118)$$

$$\begin{aligned} \text{with } A_1 &= 1. \\ A_2 &= -5. \end{aligned}$$

$$\begin{aligned}
A_3 &= -20. - 3w_1 \\
A_4 &= -8. - 3w_1 - 8w_2 \\
A_5 &= -5w_2 \\
A_6 &= w_2
\end{aligned}$$

The Newton-Raphson method is applied to solve the $h(y) = 0$ for y_c . That is, by evaluating

$$\begin{aligned}
\frac{dh(y)}{dy} &= A_2 + 2A_3y + 3A_4y^2 + 4A_5y^3 + 5A_6y^4 \\
&= A_2 + y \cdot (2A_3 + y \cdot (3A_4 + y \cdot (4A_5 + 5A_6 \cdot y)))
\end{aligned} \tag{119}$$

assuming $y_c = y_j$, and evaluating

$$y_{j+1} = y_j - \left[\frac{h(y_j) - 0.}{\left(\frac{dh}{dy}\right)_{y=y_j}} \right] \tag{120}$$

$$\text{if } |y_{j+1} - y_j| < 10^{-7} \tag{121}$$

the value of y_{j+1} is accepted as y_c . With the value of y_c thus obtained, the reduced parameters can be obtained from:

$$\frac{a}{RT_c V_c} = \left[y \left(\frac{\partial f_1}{\partial y} \right) \cdot \left(\frac{\partial f_2}{\partial y} \right)^{-1} \right] \tag{122}$$

$$\frac{b}{V_c} = [4y]_{y=y_c} \tag{123}$$

The equation for evaluating $\frac{a}{RT_c V_c}$ is

$$\frac{a}{RT_c V_c} = \left[(0.5) (1-y)^{-4} (B_1 + y \cdot (B_2 + y \cdot (B_3 + y (B_4 + B_5 y)))) \right]_{y=y_c} \quad (124)$$

where

$$\begin{aligned} B_1 &= 1. \\ B_2 &= 4. \\ B_3 &= 4. - 3 w_1 \\ B_4 &= 4 w_2 \\ B_5 &= - w_2 \end{aligned}$$

It is emphasized here that, since y is a small number ($y < 1.0$), it is necessary to calculate the various values by the "grouping" shown in the above equations. A computer program was written to do the calculations. With the initial guess of " y " taken from Guggenheim's book [32], the convergence is fast. The calculated results are presented in Table 26, where a_r and b_r were calculated after $(a/RT_c V_c)$ and (b/V_c) were calculated from Equation 123 and Equation 124.

Derivations of the Equations for Calculating
Excess Thermodynamic Functions from
Equation of State

Consider a binary liquid mixture at negligible pressure, then at constant temperature

$$dG = VdP \approx -PdV \quad (125)$$

$$\therefore d(PV) = d(ZRT) = RTdZ \approx 0. \quad (126)$$

The change of Gibbs energy from an ideal state with no hard sphere repulsion and no background potential field is

TABLE 26

COMPARISON OF EQUATION OF STATE PARAMETERS

BASED ON CRITICAL CONDITIONS

Parameter	PYP, vdW $w_2 = -3$	CS, vdW $w_2 = -1$	LH, w $w_2 = 0$	G $w_2 = 1$	vdW $w_2 = 6$
y_c	.13550	.13132	.12947	.12777	.09309
V_c/y_c	1.8450	1.9038	1.9309	1.9567	2.6854
$a_r = \frac{a}{R^2 T_c^2 / P_c}$.41517	.40693	.40337	.40009	.35609
$b_r = \frac{b}{RT_c / P_c}$.15843	.15354	.15139	.14939	.10885
(Z_c) calc.	.35406	.35654	.35758	.35852	.35779
(Z_c) exptl. (argon)	(.29231)				
$a \times 10^{-6}$ (argon)	1.3224	1.2962	1.2848	1.2744	1.1342
b (argon)	40.813	39.552	38.997	38.484	28.040

$$G - G^* = - \int_{V^*}^V P dV_i \quad (a_m=0, b_m=0) \quad (127)$$

Similar expression applied to the pure component

$$G_i^{\circ} - G_i^* = - \int_{V_i^*}^{V_i} P dV_i \quad (a_i=0, b_i=0) \quad (128)$$

where

$$G_i^* = G^*, \quad \therefore \sum_i x_i G_i^* - G^* = 0 \quad (129)$$

Thus, by subtracting the molar sum of G_i° from the molar Gibbs energy of the mixture, it follows

$$\Delta G_m = \left(G - \sum_i x_i G_i^{\circ} \right) = - \left(\int_{V^*}^V P dV_m \right) + \left(\sum_i x_i \int_{V_i^*}^{V_i} P dV_i \right) \quad (130)$$

Let the integral be

$$\begin{aligned} [\int P dV]_m &= g(a_m, b_m, V_m) = g_m \\ [\int P dV_i] &= g(a_i, b_i, V_i) = g_i \end{aligned} \quad (131)$$

The evaluation of the ideal state limit is

$$\begin{aligned} g(0,0,V_m^*) - \sum_i x_i g(0,0,V_i^*) \\ = RT \ln V_m - RT \sum_i x_i \ln V_i &= RT \sum_i x_i \ln \left(\frac{P_i}{P} \right) \\ = RT \sum_i x_i \ln x_i \end{aligned} \quad (132)$$

Thus, it follows the Gibbs energy of mixing is given by

$$\begin{aligned}\Delta G_m &= -g(a_m, b_m, V_m) + \sum_i x_i g(a_i, b_i, V_i) \\ &\quad + RT \sum_i x_i \ln x_i\end{aligned}\quad (133)$$

From the definition of G^E , the knowing that

$$\Delta G_m^{\text{ideal}} = RT \sum_i x_i \ln x_i \quad (134)$$

then

$$\begin{aligned}G^E &= \Delta G_m - \Delta G_m^{\text{ideal}} = -g(a_m, b_m, V_m) \\ &\quad + \sum_i x_i g(a_i, b_i, V_i)\end{aligned}\quad (135)$$

At low pressure ($P \rightarrow 0$), the excess enthalpy function is

$$\begin{aligned}H^E &= U^E = U - \sum_i x_i U_i \\ &= \frac{-a_m}{V_m} + \sum_i x_i \left(\frac{a_i}{V_i} \right)\end{aligned}\quad (136)$$

For the excess volume, it is

$$V^E = V_m - \sum_i x_i V_i \quad (137)$$

Excess Function According to the Generalized Equation of State

In order to calculate the excess thermodynamic functions according to the generalized equation of state,

the basic assumption that these functions are evaluated at negligible pressure is used. Thus, for liquid or liquid mixture at $P \rightarrow 0$, it can be shown that

$$d(PV) = 0. \quad - PdV = VdP \quad (138)$$

The generalized equation of state for binary mixtures is

$$\frac{PV_m}{RT} = \frac{(1 + y_m + y_m^2 + w_1 \cdot y_m^2 + w_2 \cdot y_m^2)}{(1 - y_m)^3} - \frac{a_m}{V_m \cdot RT} \quad (139)$$

$$\text{where } a_m = x_1^2 \cdot a_{11} + 2 \cdot x_1 (1 - x_1) a_{12} + (1 - x_1)^2 \cdot a_{22}$$

$$y_m = b_m / 4V$$

$$b_m = x_1^2 \cdot b_{11} + 2 \cdot x_1 (1 - x_1) b_{12} + (1 - x_1)^2 \cdot b_{22}$$

In the following calculations, it is assumed that

$$T_{c12} = \xi \sqrt{T_{c11} \cdot T_{c22}} \quad (140)$$

$$v_{c12}^{1/3} = \frac{1}{2} \left(v_{c11}^{1/3} + v_{c22}^{1/3} \right) \quad (141)$$

where ξ is a deviation factor from the geometric mean rule for T_{c12} . For the first round of calculations ξ is set equal to 1. The arithmetic mean rule for $v_{c12}^{1/3}$ is consistent with the hard sphere assumption. It follows that the excess thermodynamic functions may be given as:

$$\begin{aligned}
\frac{G^E}{RT} = & \left[\ln \left(\frac{y_m}{1-y_m} \right) + \frac{1}{(1-y_m)} + \frac{1}{(1-y_m)^2} + (1+w_1) \left(\frac{1}{2(1-y_m)^2} + \frac{1}{(1-y_m)} \right) \right. \\
& + w_2 \left(\frac{1}{2(1-y_m)^2} - \frac{2}{(1-y_m)} - \ln(1-y_m) \right) \left. - \frac{4a_m y_m}{RT b_m} \right. \\
& - \sum_{i=1}^2 x_i \left\{ \ln \left(\frac{y_i}{1-y_i} \right) + \frac{1}{(1-y_i)} + \frac{1}{(1-y_i)^2} \right. \\
& + (1+w_1) \left(\frac{1}{2(1-y_i)^2} + \frac{1}{(1-y_i)} \right) \\
& \left. \left. + w_2 \left(\frac{1}{2(1-y_i)^2} - \frac{2}{(1-y_i)} - \ln(1-y_i) \right) - \frac{4a_i y_i}{RT b_i} \right\} \right]
\end{aligned} \tag{142}$$

$$H^E = -\frac{a_m}{V_m} + \sum_{i=1}^2 x_i \frac{a_i}{V_i} \tag{136}$$

$$V^E = V_m - \sum_{i=1}^2 x_i V_i \tag{137}$$

It is obvious that in order to calculate these excess functions, the prospective molar volume at $P = 0$ must be used. The Newton-Raphson method was again used to solve for the relevant root of the generalized equation of state by using input information supplied as: $(T_{ci}, V_{ci}, T, W_1, W_2, x_i)$.

Results of Calculation and the Temperature
Dependency of Parameters

The critical constants in Table 27 were used in determining the pure components. Nitrogen, oxygen, methane, and carbon monoxide were included in the study of the temperature dependence of parameters besides argon, krypton, and xenon.

The reduced parameters a_r and b_r given in Table 26 were defined as:

$$a_r = a / (R^2 T_c^2 / P_c) \quad (143)$$

$$b_r = b / (RT_c / P_c) \quad (144)$$

They were calculated from the critical conditions and are characteristic to each specific equation of state. As given in Equation 122 and Equation 123, it can be seen that $a/(RT_c V_c)$ and (b/V_c) are functions of y_c only. While y_c is a characteristic constant of a specific equation of state. Thus the constants a_r and b_r as defined by Equation 143 and Equation 144 involved Z_c implicitly, and are not constants from substance to substance when their Z_c are different. The parameters a and b can then be obtained by knowing a_r , b_r and using the critical properties. These a and b parameters were then used in conjunction with the generalized equation of state to calculate the pure component liquid molar volumes. The results were compared in Table 28. The values of y obtained from solving the equation of state at

TABLE 27

CRITICAL CONSTANTS USED IN THE GENERALIZED
EQUATION OF STATE CALCULATIONS

Substance	$T_c,$ $^{\circ}\text{K}$	$P_c,$ atm	$V_c,$ $\text{cm}^3/\text{gm-mole}$
Argon	150.7	48.0	75.3
Krypton	209.4	54.3	92.3
Xenon	289.8	58.0	118.8
Nitrogen	126.2	33.5	90.1
Oxygen	154.8	50.08	78.0
Methane	190.6	45.8	98.7
Carbon Monoxide	133.0	34.5	93.1

TABLE 28

COMPARISON OF CALCULATED LIQUID MOLAR VOLUMES OF ARGON,
 KRYPTON, AND XENON BASED ON PARAMETERS
 OBTAINED AT CRITICAL CONDITIONS

Calculated Values,	Equation of State				
V in cm ³ /gm-mole	PYP, vdW	CS, vdW	LH, W	G	vdW
<u>Krypton at 115.77°K, V_{exptl.} = 34.2089</u>					
V _{calc.}	27.269	28.282	28.635	28.927	30.253
y	.45864	.42855	.41733	.40767	.28402
<u>Argon at 115.77°K, V_{exptl.} = 33.3411</u>					
V _{calc.}	30.137	30.934	31.238	31.501	33.522
y	.33857	.31965	.31210	.30542	.20912
<u>Krypton at 161.36°K, V_{exptl.} = 40.7291</u>					
V _{calc.}	37.104	38.082	38.456	38.778	41.276
y	.33707	.31827	.31076	.30411	.20816
<u>Xenon at 161.36°K, V_{exptl.} = 44.2166</u>					
V _{calc.}	35.654	36.563	37.018	37.395	39.123
y	.45654	.42666	.41551	.40591	.28269

temperature concerned were also presented. These values were used in the liquid mixture properties calculations.

It must be remembered that the van der Waals and the Guggenheim equations used in the present calculations are not one to one correspondence to their original equations respectively. It can be seen that the prediction of liquid molar volume deteriorated when the temperature became further lower than the critical temperature.

The excess functions were calculated for equimolar liquid mixtures for Ar + Kr and Kr + Xe using the equations derived in the previous section. From strict predictive point of view, and in the context of the Lorentz - Berthelot mixture, the results in Table 29 clearly indicated that the Longuet-Higgins and Widom equation fared better in predicting G^E . On the other hand, the predictions of V^E did not vary significantly by varying the equation of state.

The temperature dependency of the parameters was confirmed by the following calculations. The parameters a and b were recalculated with the normal boiling point data given in Table 21 by using Equation 96, where $\chi(y)$ was now given by $(1+y+(1+W_1)y^2+W_2y^3)/(1-y)^3$. The results for a_r are seen to be independent of any specific set of (W_1, W_2) . This was the case because by assuming the liquid is in equilibrium with an ideal gas at the normal boiling temperature, it can be shown that for the model concerned:

TABLE 29

EXCESS PROPERTIES OF EQUIMOLAR LIQUID MIXTURE OF
 AR + KR, AND OF KR + XE CALCULATED BASED ON
 PARAMETERS OBTAINED AT CRITICAL CONDITION

<u>Mixture Properties</u>	<u>Experimental Values</u>	<u>Calculated from Equation of State</u>				
		<u>PYP, vdW</u>	<u>CS, vdW</u>	<u>L-H, W</u>	<u>G</u>	<u>vdW</u>
<u>Argon + Krypton at 115.77°K</u>						
G^E , cal./gm-mole	19.46	45.213	28.879	21.487	14.570	-65.416
V^E , cm ³ /gm-mole	-.464	-1.116	-1.118	-1.121	-1.124	-1.244
Y_m		.4109	.3197	.3121	.3054	.2091
<u>Krypton + Xenon at 161.36°K</u>						
G^E , cal./gm-mole	24.82	61.465	37.391	26.425	12.269	-101.085
V^E , cm ³ /gm-mole	-.459	-1.367	-1.372	-1.376	-1.380	-1.527
Y_m		.4097	.3845	.3748	.3664	.2534

$$\Delta H^V = RT - U^L - P \cdot V^L = RT - U^L - V^L \quad (P \text{ in atm.}) \quad (145)$$

$$\therefore a_r = \frac{P_c V_c^L}{R^2 T_c^2} (RT - V^L - \Delta H^V) \quad (146)$$

The values of y_m were presented with the reduced parameters a_r and b_r in Table 30. As can be seen that for the heavy rare gases with the same Z_c of .292, the variation of a_r was from .415 at the critical temperature to about .510 at the normal boiling temperature. The variation of b_r was from .158 to about .195 at the normal boiling temperature. If all the substances in Table 30 follow the same two parameter principle of corresponding states, the reduced a_r , b_r should be the same for all the substances within each specific equation of state. This was obviously not the case. Further, the equation of state as given in the present forms all predicted Z_c at between .354 to .358 as shown in Table 26, which were about 1.5 times higher than the heavy rare gas value of .292. Even though the equation of state approach showed some potential in predicting excess properties, the question of the exact form of temperature dependency of parameters still await future work.

TABLE 30

REDUCED PARAMETERS FOR THE GENERALIZED
EQUATION OF STATE BASED ON NORMAL
BOILING TEMPERATURE DATA

<u>Substance</u>	<u>a_r</u>	<u>b_r</u>				
		<u>PYP, vdW</u>	<u>CS, vdW</u>	<u>L-H, W</u>	<u>G</u>	<u>vdW</u>
Argon	.5139	.1972	.1886	.1851	.1821	.1349
Krypton	.5062	.1954	.1868	.1834	.1804	.1336
Xenon	.5072	.1946	.1860	.1826	.1796	.1330
Nitrogen	.5290	.1956	.1875	.1841	.1811	.1343
Oxygen	.5173	.1955	.1869	.1835	.1805	.1337
Methane	.5098	.1959	.1875	.1841	.1811	.1342
Carbon Monoxide	.5424	.1976	.1890	.1856	.1826	.1353

CHAPTER X

CONCLUSIONS AND RECOMMENDATION FOR FURTHER WORK

Conclusions are presented in this chapter. Where further improvements are required, recommendation is offered.

Conclusions

An experimental apparatus with novel design modifications was constructed. The saturated density and total vapor pressure of argon and krypton liquid mixture at 115.77°K, and of krypton and xenon liquid mixture at 161.36°K were determined. One exploratory point of argon and xenon mixture was also measured.

The accuracy of the liquid density data was established by an error analysis.

The excess volume and the excess Gibbs energy functions were extracted from the experimental data. The slight asymmetry in both these excess properties versus composition plots were confirmed. Comparisons of the present work with other investigations were given.

The statistical thermodynamics of the binary rare gas liquid mixtures were studied. In the average potential model approach, the van der Waals two liquid model in

conjunction with mixing rules of force constants seems to be superior in the overall predictive abilities.

A study in the perturbation equation of state indicated that the Longuet-Higgins - Widom - Lebowitz equation of state was able to predict the asymmetry in both (V^E, x) and (G^E, x) curves. However, the prediction of the liquid density of the more volatile component requires further study in the equation of state parameters. The S-M rule was shown again to be superior than the geometric mean for ϵ_{12} .

Further study in a generalized equation of state, which accommodated the empiricism on the hard sphere compressibility factor part of the equation of state, showed that the temperature dependency of the equation of state parameters still existed. In the context of Lorentz - Berthelot mixture, the Longuet-Higgins - Widom equation of state still fared better in its predictive ability.

Recommendation for Further Work

Experimentally, a better way of measuring the total vapor pressure versus composition data in the present pycnometer method should be sought. As theoretical study on liquid mixture being at its growing stages, further accurate data on the high pressure liquid density data should be determined.

Although the cryogenic periscope was used in this experiment, it is necessary to refine the method of taking the liquid volume readings.

A fool-proof method of detecting the leakage of gas during the experiment run is still a necessity.

On the theoretical part, the van der Waals two liquid model should be further studied with more accurate reduced volume equation of the reference substance. Mixing rules of force constants should be studied from the experimental liquid mixture data in conjunction with the statistical thermodynamics of liquid mixture.

The perturbation equation of state approach should be studied and extended to liquid mixtures in a more exact manner than presently available. In engineering application, the temperature dependency of the equation of state parameters should be examined from the experimental data.

The generalized equation of state proposed in this work should be studied further in the sense of multi-fluid principle of corresponding states.

Another point of interest is to study the equation of state of liquid by focusing the attention on the internal pressure of the liquid.

BIBLIOGRAPHY

1. Arp, V., Wilson, J. H., Winrich, L. and Sikora, P., Cryogenics 2, 230 (1958).
2. Barieau, R. A., Private Communication to F.B. Canfield, (1963).
3. Barker, J. A., Australian J. Chem. 6, 207 (1953).
4. Barker, J. A., and Henderson, D., J. Chem. Education, 45, 2 (1968).
5. Barker, J. A. and Henderson, D., J. Chem. Phys., 47, 2856, 4714 (1967).
6. Bellemans, A. Mathot, V. and Simon, M., Adv. Chem. Phys., 11, (1967). Editor, I. Prigogine, Interscience Publishers, New York.
7. Bellemans, A. and Vilcu, R., Bull. Soc. Chem. Belges, 76, 316 (1967).
8. Bewilogua, L. and Gladun, C., Contemp. Phys. 9, 277 (1968).
9. Blancett, A. L., Ph.D. Dissertation, University of Oklahoma, Norman, Oklahoma (1966).
10. Bowman, D. H., Aziz, R. A. and Lim, C.C., Canadian J. of Phys. 47, 267 (1969).
11. Byrne, M. A., Jones, M. R., and Staveley, L. A. K., Trans. Faraday Soc. 64, 1747 (1968).
12. Canfield, F. B., Ph.D. Thesis, Rice University, Houston, Texas (1962).
13. Carnahan, N.F., and Starling, K.E., J. Chem. Phys. 51, 635 (1969).

14. Chappuis, P., Bureau International des Poids et Mesures, Travous et Memoires, 13, D1 (1907).
15. Chiu, C.-h., and Canfield, F. B., Advan. Cryog. Eng., 12, 741 (1967).
16. Chiu, C.-h., and Canfield, F. B., Ind. Eng. Chem. Fundamentals, 7, 320 (1968).
17. Chiu, C.-h., Research Proposal, University of Oklahoma, Norman, Oklahoma, April (1968).
18. Cole, G. H. A., "An Introduction to the Statistical theory of Classical Simple Dense Fluids" Pergamon Press (1967).
19. Cook, G. A., Editor, "Argon, Helium and the Rare Gases" Vol. I. and Vol. II, Interscience Publishers, New York (1961).
20. Davenport, A. J., Rowlinson, J. S., and Saville, G., Trans. Faraday Soc. 62, 322 (1966).
21. Davies, R. H., Duncan, A. G., Saville, G., and Staveley, L. A. K., Trans. Faraday Soc. 63, 855 (1967).
22. Discussions of the Faraday Society, No. 43, "The Structure and Properties of Liquids", The Faraday Society, London (1967).
23. Egelstaff, P. A., "An Introduction to the Liquid State", Academic Press (1967).
24. El Hardi, Z. E. H. A., Durieux, M., and Van Dijk, H., Physica 41, 289 (1969).
25. Fender, E. F. and Halsey, Jr., G. D., J. Chem. Phys., 36, 1881 (1962).
26. Frisch, H. L. and Salsburg, Z. W., Editor, "Simple Dense Liquids", Academic Press, New York (1968).
27. Fuks, S. and Bellemans, A., Physica 32, 594 (1966).
28. Fuks, S., and Bellemans, A., Bull. Soc. Chim. Belges 76, 290 (1967).
29. Garside, D. H., and Smith, B. L., Physica 37, 369 (1967).

30. Graben, H. W., Phys. Rev. Letters, 20, 529 (1968).
31. Guggenheim, E. A., "Applications of Statistical Mechanics", Clarendon Press, Oxford (1966).
32. Guggenheim, E. A., "Thermodynamics", Fifth Revised Edition, North-Holland Publishing Co., Amsterdam (1967).
33. Hamrin, C. E., and Thodos, G., J. Chem. Phys. 35, 899 (1961).
34. Heastie, R., and Lefebvre, C., Proc. Phys. Soc. (London) 76, 180 (1960).
35. Hill, T. L., "Statistical Mechanics", Chapter 6, McGraw-Hill, (1956).
36. Höcker, H., and Flory, P. J., Trans. Faraday Soc. 64, 1188 (1968).
37. Kell, G. S., J. Chem. Eng. Data, 12, 66 (1967).
38. Knobler, C. M. and Pings, C. J., J. Chem. Eng. Data, 10, 129 (1965).
39. Kohler, W., Dissertation, University Gottinger (1964).
40. Kozak, J. J. and Rice, S. A., J. Chem. Phys., 48, 1226 (1968).
41. Kreglewski, A., J. Phys. Chem., 71, 2860 (1967).
42. Leach, J. W., and Leland, T. W., Proc. Natl. Gas. Proc. Assn. 45, 8 (1966).
43. Leland, T. W., and Chappellear, P. S., Ind. Eng. Chem. 60, 15 (1968).
44. Leadbetter, A. J., and Thomas, H. E., Trans. Faraday. Soc. 61, 10 (1965).
45. Lebowitz, J. L., Phys. Rev., 133, A895 (1964).
46. Leland, T. W., Chappellear, P. S., and Gramson, B. W., A.I.Ch.E. Journal 8, 482 (1962).
47. Leland, T. W., Rowlinson, J. S. and Sather, G. A., Trans. Faraday Soc., 64, 1447 (1968).

48. Leland, T. W., Rowlinson, J. S., Sather, G. A., and Watson, I. D., Trans. Faraday Soc. 65, 2034 (1969).
49. Longuet-Higgins, H. C., Proc. Roy. Soc., A205, 247 (1951).
50. Longuet-Higgins, H. C. and Widom, B., Mol. Phys., 8, 549 (1964).
51. Mastinu, G., J. Chem. Phys., 47, 338 (1967).
52. Mathias, E., Onnes, H. K., and Crommelin, C. A., Commun. Phys. Lab. University Leiden, 131A (1912).
53. Mathias, E., Crommelin, C. A.; Bijleveld, W. G.; Grigg, P. P., Comm. Kamerlingh Onnes Lab. Leiden, 221B (1932).
54. Mathot, V., Staveley, L. A. K., Young, J. A., and Parsonage, N. G., Trans. Faraday Soc., 52, 1488 (1956).
55. McGlashan, M. L., Trans. Faraday Soc., 66, 18 (1970).
56. Muller, A., Proc. Roy. Soc. (London), A154, 624 (1936).
57. Munster, A. in "Physics of High Pressures and the Condensed Phase", p. 241, Editor A. Van Itterbeek, North-Holland Publishing Company, Amsterdam (1965).
58. Orstein, L. S. and Zernike, F., Proc. Akad. Sci. (Amsterdam), 17, 793 (1914).
59. Patterson, R. H., Cripps, R. S., and Whytlaw-Gray, R., Proc. Roy. Soc., A86, 579 (1912).
60. Pontius, P. E., "Report of Calibration Test No. G35659", National Bureau of Standards, U. S. Department of Commerce, Washington, D. C., April (1965).
61. Pool, R. A. H., Saville, G., Herrington, T. M., Shields, B. D. C., and Staveley, L. A. K., Trans. Faraday Soc., 58, 1692 (1962).
62. Prigogine, I., Bellemans, A. and Mathot, V., "The Molecular Theory of Solution", North-Holland Publishing Company, Amsterdam (1957).
63. Ree, F. H. and Hoover, W. G., J. Chem. Phys., 40, 939 (1964).
64. Rice, S. A. and Gray, P., "The Statistical Mechanics of Simple Liquids", Interscience Publishers, New York (1965).

65. Rowlinson, J. S., Mol. Phys., 8, 107 (1964).
66. Rowlinson, J. S., "Liquids and Liquid Mixtures", 2nd Edition, Butterworth, London (1969).
67. Schmidt, H. Z., Phys. Chem. Frankf. Ausg. 24, 265 (1960).
68. Scott, R. L., J. Chem. Phys., 25, 193 (1956).
69. Scott, R. L., and Fenby, D. V., Ann. Rev. Phys. Chem., 20, 111 (1969).
70. Seemeyer, D., Dissertation, University of Gottingen (1965).
71. Shana'a, M. Y., Ph.D. Dissertation, University of Oklahoma, Norman, Oklahoma (1966).
72. Shana'a, M. Y., and F. B. Canfield, Trans. Faraday Soc., 64, 2281 (1968).
73. Simon, M., These de Licence, University of Brussels, (1958).
74. Sinanoglu, O., "Intermolecular Forces", Adv. Chem. Phys., 12, 282 (1967).
75. Snider, N. S. and Herrington, T. M., J. Chem. Phys., 47, 2248 (1967).
76. Srivastava, B. N. and Madan, M. P., Proc. Phys. Soc., (London), A66, 278 (1953).
77. Staveley, L. A. K., Private Communication (1970).
78. Stratton, S. W., "Design and Test of Standards of Mass", Circular of the Bureau of Mines, No. 3, 3rd. Ed., 53 (1918).
79. Streett, W. B., and Staveley, L. A. K., J. Chem. Phys., 47, 2449 (1967).
80. Streett, W. B., J. Chem. Phys., 46, 3282 (1967).
81. Streett, W. B., and Staveley, L. A. K., Advan. Cryog. Eng. 13, 363 (1968).
82. Streett, W. B., and Staveley, L. A. K., J. Chem. Phys., 50, 2302 (1969).
83. Streett, W. B., Cryogenics, 8, 88 (1968).

84. Terry, M. J., Lynch, J. T., Bunclark, M., Mansell, K. R., and Staveley, L. A. K., J. Chem. Thermodynamics, 1, 413 (1969).
85. Theeuwes, F. and Bearman, R., J. Chem. Thermodynamics, 2, 171 (1970); 2, 179 (1970). Also: Trans. Kansas Acad., 72, 342 (1969).
86. Throop, G. J. and Bearman, R., J. Chem. Phys., 42, 2408 (1965).
87. Throop, G. J. and Bearman, R., J. Chem. Phys., 44, 1423 (1966).
88. Tilton, L. W., and Taylor, J. K., J. Res. Natl. Bur. Stds., 18, 205 (1937).
89. Van Ness, H. C., "Classical Thermodynamics of Non-Electrolyte Solutions", Pergamon Press, New York (1964).
90. Van Witzenburg, W. and Stryland, J. C., Canadian J. Phys., 46, 811 (1968).
91. Vilcu, R. and Bellemans, A., Bull. Soc. Chim. Belges, 76, 325 (1967).
92. Walling, J. F., and Halsey, G. D., J. Phys. Chem., 62, 752 (1958).
93. Weir, R. D., Wynn Jones, I., Rowlinson, J. S. and Saville, G., Trans. Faraday Soc., 63, 1320 (1967).
94. Wertheim, M. S., J. Math. Phys., 5, 643 (1964).
95. Wheeler, J. D. and Smith, B. D., AIChE Journal, 13, 303 (1967).
96. Widom, B., Science, 157 (3787), 375 (1967).
97. Wilhelm, G. and Schneider, G. Z., Phys. Chem. Frankf. Ausg., 32, 62 (1962).
98. Yunker, W. H., and Halsey, G. D., J. Phys. Chem., 64, 484 (1960).
99. Ziegler, W. T., Mullins, J. C. and Kirk, B. S., Technical Report No. 2, Proj. A-460, Engineering Experiment Station, Georgia Institute of Technology, Atlanta, Georgia, Contract No. CST-7238, National Bureau of Standards, June 15, 1962.

100. Ziegler, W. T., Mullins, J. C., and Kirk, B. S., Technical Report No. 3, Proj. A-460, Engineering Experiment Station, Georgia Institute of Technology, Atlanta, Georgia, Contract No. CST-7238, National Bureau of Standards, August 31, 1961.
101. Ziegler, W. T., Mullins, J. C., and Berquist, A. R., Technical Report No. 3, Proj. A-764, Engineering Experiment Station, Georgia Institute of Technology, Atlanta, Georgia, Contract No. CST-1154, National Bureau of Standards, April 29, 1966.
102. Ziegler, W. T., Yarbrough, D. W., and Mullins, J. C., Technical Report No. 1, Proj. A-764, Engineering Experiment Station, Georgia Institute of Technology, Atlanta, Georgia, Contract No. CST-1154, National Bureau of Standards, July 15, 1964.
103. Zwanzig, R. W., J. Chem. Phys., 8, 107 (1964).

APPENDIX A

CALIBRATION OF PYCNOMETER

The volume of the high pressure pycnometer used in this work were calibrated by two different methods. First, the Pyrex high pressure pycnometer was calibrated at temperatures slightly above room temperature by differential weighing with de-ionized air-free distilled water. Second, the Pyrex high pressure pycnometer was calibrated at operating temperatures against the low pressure quartz pycnometer by measuring the liquid density of the same material at its saturation pressures. Incidentally, the low pressure quartz pycnometer was recalibrated by this investigator to serve as a standard. Briefly the equation of state for calculating water density will be described first.

The Density of Liquid Water

The density of air-free liquid water should be known accurately for calibration. The method of linear interpolation as used by Shana'a on data obtained from tabulated values of Chappuis [14] is both tedious and may involve errors for calculations. Therefore, it is desirable to have an accurate equation of state for the density of liquid water to be used in computer calculations. Recently, the density of ordinary

air-free water from 0° to 150°C was well represented by a rational function with seven parameters by Kell [37]. The density data observed by Chappuis [14] and presented by Tilton and Taylor [88] were used for the range from 0° to 42°C. Thus densities obtained from the equation agree with the tabulated values to six places, except for five entries with difference of 1×10^{-6} gram per ml. Kell chose a rational function $R_{nm}(t)$:

$$R_{nm}(t) = \frac{P_n(t)}{(1+b_1t+b_2t^2+\dots+b_mt^m)} = \frac{(a_0+a_1t+a_2t^2+\dots+a_nt^n)}{(1+b_1t+b_2t^2+\dots+b_mt^m)} \quad (A-1)$$

of $n+m+1$ parameters with $P = R_{51}$ which gives the lowest standard error of 0.21 ppm. Thus, with the equation of state as

$$\rho_w = R_{51}(t) = \frac{(a_0+a_1+a_2t^2+a_3t^3+a_4t^4+a_5t^5)}{(1+b_1t)} \quad (A-2)$$

the coefficients are given by

$$\begin{aligned} a_0 &= 0.9998396 \text{ gm/cc} \\ 10^3 a_1 &= 18.224944 \text{ gm/cc} \\ 10^6 a_2 &= -7.922210 \text{ gm/cc} \\ 10^9 a_3 &= -55.44846 \text{ gm/cc} \\ 10^{12} a_4 &= 149.7562 \text{ gm/cc} \\ 10^{15} a_5 &= -393.2952 \text{ gm/cc} \\ 10^3 b_1 &= 18.159725 \text{ gm/cc} \end{aligned}$$

Standard error in the temperature range from 30° to 40°C was estimated at 1 ppm. To convert gm/cc to gm/ml, the relation

1 ml = 1.000028 cc was used. In computer calculations for pycnometer calibration, Equation (A-2) was used as a function which can be used to give the density, or the specific volume of water by just calling the defined function for liquid water density with a specified temperature, which is between 30°C to 40°C.

Calibration of Pycnometer by Differential Weighing
with Distilled Water

The pycnometer that was used in measuring the liquid density of light hydrocarbons was recalibrated by the present investigator. Because this quartz pycnometer has a set of linear thermal expansion data provided by the U. S. Bureau of Standards [71], it was desirable to recalibrate it and use the calibration as a standard calibration. First, the equation used for calibration will be derived. Let the notation ρ denote density; W, water; M, mass; V, volume; the subscripts PF, full pycnometer; PE, empty pycnometer; S, stirrer; g, glass; r, room temperature; a, air. By differential weighing of distilled water in the pycnometer, the following relations lead to the desired equation for calibration:

$$\begin{aligned} M_W &= M_{PF} - M_{PE} + M_a \\ &= M_{PF} - M_{PE} + \rho_a \cdot (V_p)_{tr_0} \end{aligned} \tag{A-3}$$

where tr_0 denotes the room temperature where the pycnometer containing air was weighed.

Since

$$(V_P)_{t_r} = \frac{M_W}{(\rho_W)_{t_r}} \quad (A-4)$$

from Equations (A-3) and (A-4)

$$(V_P)_{t_r} = \frac{(M_{PF} - M_{PE})}{\left[(\rho_W)_{t_r} - \rho_a \cdot \frac{(\rho_W)_{t_r}}{(\rho_W)_{t_{r0}}} \right]} \quad (A-5)$$

where the water density $(\rho_W)_{t_r}$ can be obtained from Equation (A-2) as $(\rho_W)_{t_r} = R_{51}(t_r)$. In order to obtain the pycnometer volume at a given height reading at any operation temperature, t_{op} , a correction term due to the thermal shrinkage of the glass and the nickel stirrer should be included. Thus, we have

$$(V_P)_{t_{op}} = (V_P)_{t_r} + \left[(\Delta V)_P - (\Delta V)_S \right]_{t_r \rightarrow t_{op}} \quad (A-6)$$

where $[\Delta V_P]_{t_r \rightarrow t_{op}}$ = volume change of pycnometer from t_r down to t_{op} .

$[\Delta V_S]_{t_r \rightarrow t_{op}}$ = volume change of nickel stirrer from t_r down to t_{op} .

Let α_T denote the linear thermal expansion coefficient of glass,

$$\alpha_T = \left(\frac{L_T - L_{T0}}{L_{T0}} \right) \quad (A-7)$$

$$\begin{aligned} [\Delta V_P]_{t_r \rightarrow t_{op}} &= (V_P)_{t_o} (1 + 3\alpha_{t_{op}}) - (V_P)_{t_o} (1 + 3\alpha_{t_r}) \\ &= (V_P)_{t_o} \cdot 3(\alpha_{t_{op}} - \alpha_{t_r}) \end{aligned}$$

$$[\Delta v_P]_{t_r \rightarrow t_{op}} = (V_P)_{t_r} \frac{3(\alpha_{t_{op}} - \alpha_{t_r})}{(1 + 3\alpha_{t_r})} \quad (A-8)$$

Since α_{t_r} is of the order of 10^{-6} , the denominator can be approximated by 1.0, then

$$[\Delta v_P]_{t_r \rightarrow t_{op}} = (V_P)_{t_r} \cdot 3(\alpha_{t_{op}} - \alpha_{t_r}) \quad (A-9)$$

However, in computer calculations, Equation (A-8) will be adopted. Similarly, for nickel stirrer

$$[\Delta v_s]_{t_r \rightarrow t_{op}} = (V_s)_{t_q} \frac{3(\alpha'_{t_{op}} - \alpha'_{t_r})}{(1 + 3\alpha'_{t_q})} \quad (A-10)$$

where t_q is the temperature at which the nickel stirrer volume was determined by weighing.

Recalibration of Fused-Quartz Pycnometer.

The fused-quartz pycnometer was recalibrated in the same cryostat which was used in the low temperature experimental run. This had the advantage that a more accurate temperature control was possible. In previous calibration [71] the pycnometer was immersed in a constant temperature bath with the graduated part of the pycnometer staying outside the thermostat bath. Further, the platinum thermometer was placed inside a metal tube filled with vacuum oil to measure the bath temperature.

The calibration procedure can be best described in the following way.

1. The constant temperature thermostat:

The constant temperature thermostat was prepared by using the cryostat with Deep Rock Napoleum 100-S, a cleaning liquid manufactured by the Kerr-McGee Corporation, as a bath fluid. This fluid has a closed cup flash point of 41.1°C. This limited the calibration temperature. Originally carbon tetrachloride was used. It was replaced mainly because it is toxic and corrosive to metal. Water was used initially to flow into and out of the outer dewar. This did not give good control. Compressed air passed through a regulator set at about 3 psig served to cool the cryostat by flowing through the outer dewar. The temperature control in the region of the calibration temperature, 31°C to 38°C was established to within $\pm 0.002^\circ\text{C}$.

2. Filling the Pycnometer with De-ionized

Air-Free Distilled Water:

De-ionized distilled water with impurities less than 2 ppm obtained from Materials Science laboratory was used to fill the pycnometer. The pycnometer was thoroughly cleaned and immersed in a constant temperature water bath with the temperature controlled close to 31°C. The de-ionized distilled water was fed into the pycnometer from a reservoir by first evacuating the connecting line and the pycnometer. The reservoir valve was then opened to allow the water to flow into the pycnometer. The water in the pycnometer was then degassed. A hypodermic syringe equipped with a long needle was used for adjusting the water to a specific level.

3. Weighing of the Pycnometer:

The pycnometer was weighed with and without the de-ionized, air-free, distilled water before it was placed into the cryostat. After the calibration run, which lasted about 3.5 days, the pycnometer was reweighed. It was found that the weight of the pycnometer with water stayed constant before and after the calibration run.

4. The Calibration Run:

The calibration was performed in two ways. First, the readings were taken with increasing bath temperature. Each temperature interval was such that the water level changed about 2 divisions. Usually it took about one hour to stabilize the temperature. After the level reached the highest mark, the cryostat was cooled down and a series of readings were taken. The calibration data are presented as follows:

Pycnometer hanger weight

Analytical Balance Reading $M_h = 12.2216$ gm

True mass from class M standards (C.M.S.) used
to balance $M_h = 12.2218$ gm

Empty Pycnometer Data

Analytical Balance Reading of (pycnometer +
hanger + air) $M_{pe} + M_h = 106.4953$ gm

Temperature of Balance during weighing process
= 24.82°C

Barometric Pressure = 28.872 in. Hg at 77°F

Pressure Correction = 0.126 in. Hg

Corrected Barometric Pressure = 28.746 in. Hg

at 0°C, or 0.96073 atm.

True Mass from C.M.S. used to Balance

$$M_{pe} + M_h = 106.4968 \text{ gm}$$

True Mass of the Pycnometer with Air

$$(M_{pe} + M_h) - M_h = 94.2749 \text{ gm}$$

Full Pycnometer Data

Analytical Balance Reading of (pycnometer +

hanger + water) $M_{pf} + M_h = 136.4332 \text{ gm}$

Temperature of Balance during Weighing

Process = 24.04°C

Barometric Pressure = 28.922 in. Hg at 76.9°F

Pressure Correction = 0.126 in. Hg

Corrected Barometric Pressure = 28.796 in Hg

at 0°C or 0.97270 atm

True Mass from C.M.S. used to Balance

$$M_{pf} + M_h = 136.4334 \text{ gm}$$

True Mass of the Pycnometer with Water

$$(M_{pf} + M_h) - M_h = 124.2116 \text{ gm}$$

In order to use the equations given in the previous section, information concerning the thermal expansion of the fused quartz and of the nickel-A metal were required. The linear thermal expansion data of annealed fused quartz (G.E. type 204) sample C, which had the same thermal history as that of the quartz pycnometer, in the room temperature region of from 293°K to 300°K may be represented by

$$\text{quartz: } \alpha_{t_r} = [(-105.15) + (0.393)t_r]10^{-6} \quad (\text{A-11})$$

The thermal expansion coefficient of quartz at the operating temperature $\alpha_{t_{op}}$ was obtained from the National Bureau of Standards calibration [71]. For nickel-A metal, the thermal expansion data obtained from Arp, et al. [1] may be represented by

$$\text{Nickel-A: } \alpha_{t_r} = [-346.3 + 1.182t_r]10^{-5} \quad (\text{A-12})$$

The thermal expansion data of Nickel-A at the operating temperature was interpolated from the tabulated values.

A computer program was written for converting the original experimental data of temperature versus scale division on graduated portion of capillary stem to volumes versus scale division. This program also fitted the data to a straight line. The calculated results for the volume of the pycnometer at -165°C do not agree with those obtained by previous investigator. The temperature versus the division readings are presented in Table A-1.

As mentioned before, the recalibration results for the quartz pycnometer do not agree with the previous calibration. In a comparison plot, the maximum difference between the two calibration lines (pycnometer volume versus pycnometer height plot) was 0.005 ml at the division 69. At the opposite end of the scale at division 4, the difference was 0.002 ml. These two lines cross at division 23 with the present calibration line having a higher slope. These differences were outside

TABLE A-1

CALIBRATION READINGS OF THE FUSED QUARTZ PYCNOMETER

Temperature of Pycnometer, °C	Division on Graduated Portion of Capillary Stem	Temperature of Pycnometer, °C	Division on Graduated Portion of Capillary Stem
Heating-up Data			
31.5299	3.00	34.3500	34.00
31.6819	4.85	34.5363	36.00
31.9161	7.10	34.6890	37.78
31.9597	7.65	34.8798	40.00
32.2034	10.15	34.9809	41.20
32.3416	11.65	34.2039	43.90
32.4104	12.50	34.3323	45.45
32.6917	15.50	35.4642	47.00
32.5966	14.55	35.6857	49.50
32.7947	16.77	35.8176	51.00
32.9681	18.41	35.9971	53.00
33.1429	20.50	36.1417	54.90
33.2400	21.55	36.2851	56.53
33.3802	23.00	36.4274	58.10
33.5030	24.50	36.5167	59.35
33.5729	25.17	36.7284	61.85
33.7654	27.38	36.8911	63.70
33.8932	28.81	37.0458	65.53
34.0348	30.30	37.1971	67.40
34.1918	32.10	37.3503	69.22
Cooling-down Data			
36.7350	61.80	32.7331	15.40
35.9742	52.75	32.5510	13.50
34.8337	39.30	32.1791	9.48
34.0506	30.45	31.8359	6.00
33.5793	25.00	31.7597	5.00
33.1914	20.85	31.5433	2.85

the range of accuracy expected. Explanations for the discrepancies are given as follows:

1. The measurement of temperature with a platinum resistance thermometer via the vacuum oil and copper tube results in a lower temperature reading when temperature increases. Errors resulting from this measurement technique explain the lower slope of the previous calibration line.
2. In the previous calibration, the graduated portion of the pycnometer was located outside the constant temperature bath. Water contained in this portion of the pycnometer was then at a temperature lower than that of the bath. Hence the overall density of the water in the pycnometer was higher than the density corresponding to the temperature indicated by the platinum thermometer.

Though these explanations were plausible, more quantitative information was desired. Thus, a method of checking the volume of the graduated portion of the capillary was devised. A seventeen-inch length of 0.41 mm O.D. 304 stainless steel needle tubing was silver soldered to a Beckman VB 22400 Liquid Sampler hypodermic syringe. The liquid volume introduced could be set ranging from 0.005 cc to 0.05 cc with reproducibilities of $\pm 0.1\%$ to $\pm 0.05\%$. The pycnometer was filled with distilled water to some initial level as recorded with a

cathetometer. Next, a precisely gauged volume of water was introduced by means of the syringe. Then the liquid level was again determined with the cathetometer. Thus the volume of the graduated portion between division 0 to division 70 was determined as equal to 0.062 cc. The corresponding volume obtained from the present calibration was 0.063 cc, while that obtained from the previous calibration was 0.055 cc. Therefore, it was concluded that the present calibration results should be used as the standard.

Calibration of the Pyrex Pycnometer

The calibration procedure for the Pyrex pycnometer was essentially the same as that for the fused quartz pycnometer. One difference was that this time the distilled water was introduced into the pycnometer by using a hypodermic syringe with a long stainless steel needle. Care was taken to eliminate bubbles within the pycnometer. The other difference was that the liquid level readings were taken by using the cryogenic periscope in conjunction with the cathetometer. Thermal expansion data for Corning Pyrex 7740 was used in the calibration calculations. The different design of the Pyrex pycnometer permitted weighing of the pycnometer on the analytical balance pan without using a metal hanger. The following are the calibration results of the Pyrex pycnometer:

Mass of the Nickel-A Stirrer

Analytical Balance Reading, Ms = 0.7242 gm

Temperature of Balance during weighing process	=	23.03°C
Barometric Pressure	=	28.744 in. Hg at 73°F
Corrected Barometric Pressure	=	28.629 in. Hg at 0°C
True Mass from C.M.S. used to balance M_s	=	0.7227 gm

Empty Pycnometer Data

Analytical Balance Reading of (pycnometer + air) M_{pe}	=	122.1782 gm
Temperature of Balance during weighing process	=	22.44°C
Humidity during weighing process	=	54.0%
Barometric Pressure	=	28.894 in. Hg at 72°F
Corrected Barometric Pressure	=	28.780 in. Hg at 0°C
True Mass from C.M.S. used to balance M_{pe}	=	122.1790 gm

Full Pycnometer Data

Analytical Balance Reading of (pycnometer + water), M_{pf}	=	141.396 ² gm
Temperature of Balance during weighing process	=	22.95°C
Humidity during weighing process	=	46.0%
Barometric Pressure	=	28.854 in. Hg
Corrected Barometric Pressure	=	28.738 in. Hg
True Mass of the Pycnometer with water from C.M.S. used to balance M_{pf}	=	141.3973 gm

In order to convert the M-2 bridge resistance readings into temperature, the following corrections were applied:

10 Ω decade correction at dial position 2,

$$10_2 = +.0003_3 \Omega$$

1 Ω decade correction at dial position 8, $1_8 = +.0001_3$

Zero point of the bridge = $0.0000_6 \Omega$ (to be added to the bridge reading).

With the above corrections made on the temperature readings, the calibration results of Pyrex pycnometer are presented in Table A-2.

Calibration of Pyrex Pycnometer at Operation
Temperatures Against the Quartz Pycnometer

Pure ethane was used as the calibration material. The dead volumes of the two pycnometer setup were determined as described in Appendix D. Ethane density was determined at the operation temperature 115.77°K and 161.36°K in both pycnometers.

The calibration results presented in previous sections and in Table A-1 and Table A-2 can be treated to yield the following relations:

$$V_p = A + B \cdot H \quad \text{where } H \text{ is the graduation reading of the pycnometer stem}$$

with

	<u>A</u>	<u>B x 10⁴</u>
Quartz pycnometer		
108.15°K	30.11127	8.973558
115.77°K	30.11091	8.973461
161.36°K	30.10957	8.973128
Pyrex pycnometer		
115.77°K	19.28214	9.532540
161.36°K	19.28765	9.535372

TABLE A-2

CALIBRATION READINGS OF THE PYREX PYCNOMETER

Temperature of Pycnometer, °C	Division on Graduated Portion of Capillary Stem	Temperature of Pycnometer, °C	Division on Graduated Portion of Capillary Stem
29.1664	6.32	34.1960	38.00
29.5671	8.50	34.5795	40.50
29.8551	10.30	34.9046	42.60
30.1458	12.00	35.2218	44.90
30.4660	14.00	35.5498	47.00
30.8836	16.50	35.8880	49.30
31.2044	18.41	36.1885	51.60
31.5094	20.50	36.4661	53.50
31.8579	22.50	36.7418	55.40
31.1838	24.70	37.0691	57.70
32.4621	26.50	37.3687	59.73
32.7916	28.70	37.5790	61.30
33.0999	30.50	37.9163	64.00
33.4171	33.00	38.3023	66.40
33.7520	35.00	38.5880	68.50

The liquid density of ethane was determined in each run by using the above calibration results. The computer calibration results of ethane density are presented in Table A-4. These data were fitted to separate straight lines and the corresponding density of ethane at the operation temperatures were obtained and compared in Table A-4.

TABLE A-3
THERMAL EXPANSION DATA OF VARIOUS MATERIALS
RELATED TO PYCNOMETER CALIBRATIONS

	$10^5 \cdot \alpha_{t_{op}}$ Nickel A	$10^6 \cdot \alpha_{t_{op}}$ Quartz Pycnometer	$10^6 \cdot \alpha_{t_{op}}$ Pyrex Pycnometer
108.15°K	-197	-11.6	----
115.77°K	-192	-15.2	-421
161.36°K	-150	-27.6	-322
α vs t_r^* between 30°C and 40°C	A = -346.3 B = 1.182	A = -105.2 B = 0.393	A = -846.8 B = 3.1

*where $10^6 \alpha_{t_r} = (A+B t_r)$ for glass, t_r in °K

$10^5 \alpha_{t_r} = (A+B t_r)$ for Nickel A, t_r in °K

In the above calculations and in the calculations for quartz pycnometers at -165°C, the following correction terms were used. The titles were so arranged for clarity purpose.

TABLE A-4

ETHANE DENSITIES AT 161.36°K and at 115.77°K DETERMINED BY
USING QUARTZ PYCNOMETER AND BY USING PYREX PYCNOMETER

Pycnometer, and constants in $\rho = A + B \cdot t$	Tempera- ture, t °C	Pressure, psia	Density, ρ , gm/ml	Deviation $\times 10^5$ (Exptl.-Calc.)
Quartz, A=0.438956 B=-(0.119146) $\cdot 10^{-2}$	-112.104	3.360	0.572511	-1.109
	-111.980	3.391	0.572374	-0.032
	-111.865	3.420	0.572248	+1.052
	-111.770	3.449	0.572132	+0.729
	-111.620	3.491	0.571945	-0.127
	-111.508	3.522	0.571813	-0.044
	-111.349	3.566	0.571623	-0.090
	-111.219	3.599	0.571465	-0.379
	<u>-111.790</u>		<u>0.572149</u>	
Pyrex, A=0.438087 B=-(0.119725) $\cdot 10^{-2}$	-113.943	2.965	0.574506	+0.114
	-113.692	3.050	0.574202	-0.346
	-113.335	3.128	0.573784	+0.715
	-113.187	3.166	0.573596	-0.497
	-112.936	3.224	0.573298	-0.045
	-112.732	3.289	0.573055	+0.054
	-112.617	3.338	0.572917	+0.006
	<u>-111.790</u>		<u>0.571927</u>	
Quartz, A=0.459087 B=-(0.104693) $\cdot 10^{-2}$	-157.719	0.064	0.604210	+0.157
	-157.495	0.075	0.623970	-0.279
	-157.331	0.090	0.623802	+0.059
	-157.088	0.098	0.623548	+0.063
	<u>-157.380</u>		<u>0.623853</u>	
Pyrex, A=0.446052 B=-(0.112781) $\cdot 10^{-2}$	-159.537	0.070	0.625981	+0.255
	-159.237	0.086	0.625640	+0.006
	-158.970	0.095	0.625337	-0.179
	-158.672	0.118	0.625003	+0.009
	-158.442	0.139	0.624740	-0.406
	-158.156	0.149	0.624419	-0.201
	-157.975	0.163	0.624221	+0.413
	-157.893	0.175	0.624125	+0.103
	<u>-157.380</u>		<u>0.623546</u>	

Quartz Pycnometer:

Q1, at -165°C (108.15°K)

$$(\Delta Vp)_{t_r \rightarrow t_{op}} = \left[\frac{3(\alpha_{t_{op}} - \alpha_{t_r})}{1 + 3\alpha_{t_r}} \right] \quad (\text{A-13})$$

From values as shown in Table A-3, it follows

$$(\Delta Vp)_{t_r \rightarrow 108.15^{\circ}\text{K}} = (Vp)_{t_r} \cdot \left[\frac{3 \cdot (93.55 - 0.393t_r) \cdot 10^{-6}}{1 + 3 \cdot (-105.2 + 0.393t_r) \cdot 10^{-6}} \right] \quad (\text{A-14})$$

also for the Nickel A Stirrer

$$\therefore \alpha_{t_q} = 4.7 \times 10^{-5}$$

$$\therefore (\Delta Vs)_{t_r \rightarrow t_{op}} = (Vs)_{t_o} \cdot 3 \cdot (\alpha_{t_{op}} - \alpha_{t_r})$$

$$(Vs)_{t=23.6^{\circ}\text{C}} = 0.1792 \text{ ml}, T_o = 293^{\circ}\text{K}$$

$$(Vs)_{t_q=23.6^{\circ}\text{C}} = (Vs)_{T_o} (1 + 3\alpha_{t_q}) \quad (\text{A-15})$$

$$(Vs)_{t_r} = (Vs)_{t_o} (1 + 3\alpha_{t_r})$$

$$(Vs)_{t_{op}} = (Vs)_{t_o} (1 + 3\alpha_{t_{op}})$$

$$(Vs)_{t_o} = \left[\frac{(Vs)_{t_q=23.6^{\circ}\text{C}}}{1 + 3\alpha_{t_q}} \right] = \left(\frac{0.1792}{1 + 0.000141} \right)$$

$$\therefore (\Delta Vs)_{t_r \rightarrow t_{op}} = \left(\frac{0.1792}{1.000141} \right) \cdot (3) \cdot (\alpha_{t_{op}} - \alpha_{t_r}) \quad (\text{A-16})$$

Using the relation for α_{t_r} in Table A-3

$$\therefore (\Delta Vs)_{t_r \rightarrow 108.15^{\circ}\text{K}} = \left(\frac{0.1792}{1.000141} \right) \cdot (3) \cdot (149.3 - 1.182 \cdot t_r) \cdot 10^{-5} \quad (\text{A-17})$$

Q2, at -157.38°C (115.77°K)

$$(\Delta Vp)_{t_r \rightarrow 115.77^{\circ}\text{K}} = (Vp)_{t_r} \cdot \left[\frac{3 \cdot (89.95 - 0.393 \cdot t_r) \cdot 10^{-6}}{1 + 3 \cdot (-105.2 + 0.393 \cdot t_r) \cdot 10^{-6}} \right] \quad (\text{A-18})$$

$$(\Delta v_p)_{t_r \rightarrow 115.77^\circ K} = \left(\frac{0.1792}{1.000141} \right) \cdot (3) \cdot (+154.3 - 1.182 \cdot t_r) \cdot 10^{-5} \quad (A-19)$$

Q3, at $-111.79^\circ C$ ($161.36^\circ K$)

$$(\Delta v_p)_{t_r \rightarrow 161.36^\circ K} = (v_p)_{t_r} \left[\frac{3 \cdot (77.55 - 0.393 \cdot t_r) \cdot 10^{-6}}{1 + 3 \cdot (-105.2 + 0.393 \cdot t_r) \cdot 10^{-6}} \right] \quad (A-20)$$

$$(\Delta v_s)_{t_r \rightarrow 161.36^\circ K} = \left(\frac{0.1792}{1.000141} \right) \cdot (3) \cdot (+196.3 - 1.182 \cdot t_r) \cdot 10^{-5} \quad (A-21)$$

Pyrex Pycnometer:

P1, at $-157.38^\circ C$ ($115.77^\circ K$)

$$(\Delta v_p)_{t_r \rightarrow 115.77^\circ K} = (v_p)_{t_r} \left[\frac{3 \cdot (-419 - 3.1 \cdot (t_r - 273.15)) \cdot 10^{-6}}{1 + 3 \cdot (-1.5 + 3.1 \cdot (t_r - 273.15)) \cdot 10^{-6}} \right] \quad (A-22)$$

$(\Delta v_s)_{t_r \rightarrow 115.77^\circ K}$ is the same as that given in Q2.

P2, at $-111.79^\circ C$ ($161.36^\circ K$)

$$(\Delta v_p)_{t_r \rightarrow 161.36^\circ K} = (v_p)_{t_r} \left[\frac{3 \cdot (-320 - 3.1 \cdot (t_r - 273.15)) \cdot 10^{-6}}{1 + 3 \cdot (-1.5 + 3.1 \cdot (t_r - 273.15)) \cdot 10^{-6}} \right] \quad (A-23)$$

$(\Delta v_s)_{t_r \rightarrow 161.36^\circ K}$ is the same as that given in Q3.

The ethane densities determined in both the quartz pycnometer and the Pyrex pycnometer are presented in Table A-4 along with a least square curve fitted values. Also the values of ethane density at the temperature $115.77^\circ K$ and at the temperature $161.36^\circ K$ were obtained by either interpolation or extrapolation of the experimental data, using their best fitted equations presented in the same table.

A close examination of the values of ethane density presented in Table A-4 reveals that a linear relation between $\Delta\rho = (\rho_g - \rho_p) t_{op}$ (where ρ_g is the ethane liquid density determined by using quartz pycnometer at t_{op} , and ρ_p by using Pyrex pycnometer at t_{op}) versus the operation temperature t_{op} . By considering that the room temperature calibrations of both pycnometer should yield no error and that the density determined in the quartz pycnometer is the ultimate correct one, the above linear relation of $\Delta\rho$ vs. T actually crosses the point of $\Delta\rho = 0$ at around room temperature within the experimental accuracy expected in the error analysis. However, a sensitivity check shows that it would require an error of about 50% in the thermal expansion data of the Pyrex glass to produce the above calibration discrepancies. Because the Pyrex thermal expansion characteristics may be altered by the thermal history sustained during the pycnometer fabrication process and also because reliable thermal expansion data of Pyrex were unavailable, it was concluded that the ultimate standard of the quartz pycnometer calibration be adopted for all data reduction in this investigation.

The calculation results which gave the variation of the pycnometer volume with respect to temperatures can be expressed as:

at temperature around 161.36°K

$$V_p = V_p \cdot (2. - (.438956 - .00119146 t) \cdot (.438087 - .00119725 t)^{-1})$$

(A-24)

$$V_p = V_p \cdot (2. - (.45087 - .00104693t) \cdot (.446052 - .00112781t)^{-1}) \quad (A-25)$$

where t was in degree centigrade.

Pressure Effect on Pycnometer Volume

The variation of the pycnometer volume with its internal pressure can be derived from the working equations given by Blancett [9] as:

$$\frac{\Delta V_p}{V_p} = \left(\frac{2 + 2 \frac{R_i}{L}}{1 + \frac{4}{3} \frac{R_i}{L}} \right) \frac{\Delta R_i}{R_i} + \left(\frac{1}{1 + \frac{4}{3} \frac{R_i}{L}} \right) \frac{\Delta L}{L} \quad (A-26)$$

with

$$\frac{\Delta R_i}{R_i} = \frac{P_i}{E} \left\{ \frac{R_i^2 (1-2\mu) + R_e^3 [1+\mu+(\mu-2)(P_e/P_i)]}{R_e^2 - R_i^2} \right\} \quad (A-27)$$

$$\frac{\Delta L}{L} = \frac{P_i}{E} \left\{ \frac{R_i^2 (1-2\mu) + R_e^2 [2\mu-1](P_e/P_i)]}{R_e^2 - R_i^2} \right\} \quad (A-28)$$

For the Pyrex pycnometer:

L = length of cylindrical bulb = 72.2 mm.

R_i = the inside radius of bulb = 8.7 mm.

μ = Poisson's ratio for Pyrex No. 7740 = 0.20.

E = modulus of elasticity of borosilicate
= 6.2 x 10⁵ atm.

R_e = the outside radius of bulb = 12.7 mm.

P_i = the internal pressure of pycnometer, atm.

P_e = the external pressure of pycnometer = 1.14 atm.

The effect of the internal pressure on the pycnometer volume can then be expressed as:

$$\Delta V_p = 1.035 \cdot P_i \cdot 10^{-5} \quad (\text{A-29})$$

At 161.955°K, with $P_i = 166.152$ psia, the increase in the pycnometer volume was 0.00196 cm^3 .

APPENDIX B

TEMPERATURE MEASUREMENT AND MASS MEASUREMENT

The calibration and other information concerning the temperature measurement and mass measurement are presented here for ready reference.

Temperature Measurement

The Leeds and Northrup platinum resistance thermometer used in this experiment, which was calibrated by the National Bureau of Standards, was certified as follows:

Thermometer Series Number 1628421

Test Number G36351

Completed January 28, 1966

$$\alpha = 0.003926634$$

$$\delta = 1.49222$$

$$\beta = 0.11007 \text{ (t below } 0^{\circ}\text{C)}$$

$$= 0 \text{ (t above } 0^{\circ}\text{C)}$$

$$R_0 = 25.5772 \text{ Abs. ohms.}$$

Where R_0 was redetermined by Shana'a [71] at the ice point with the conjunction of the G-2 bridge used here to give a value of 25.5775 ohms.

The following two equations were used to relate the resistance of the thermometer to the international temperature scale as defined in the range from 630.5°C to -182.97°C.

The Callender Equation ($t > 0^\circ\text{C}$):

$$t (^{\circ}\text{C}) = \frac{R_t - R_0}{\alpha R_0} + \delta \left(\frac{t}{100} - 1 \right) \frac{t}{100} \quad (\text{B-1})$$

The Callender - Van Dusen Equation ($t < 0^\circ\text{C}$):

$$t (^{\circ}\text{C}) = \frac{R_t - R_0}{\alpha R_0} + \delta \left(\frac{t}{100} - 1 \right) + \beta \left(\frac{t}{100} - 1 \right) \left(\frac{t}{100} \right)^3 \quad (\text{B-2})$$

The constants were determined from the calibrations at the boiling points of sulfur, steam, ice and oxygen (oxygen was included for B-2).

The G-2 Mueller Bridge was used to measure the resistance of thermometer. Equation (B-2) can be written also in the form

$$R_t = R_0 + \alpha R_0 \left[(1+\delta) 10^{-2} T - \delta 10^{-4} T^2 + \beta 10^{-6} T^3 - \beta 10^{-8} T^4 \right] \quad (\text{B-3})$$

A calibration table computer programmed by using Equation (B-3) gives resistance versus temperature output for handy use. The zero point of the bridge was checked before experiment and calibration of the 10 ohm decades and 1 ohm decades were used for room temperature measurements.

Mass Measurement

The mass measurement was done by using a Right-A Weigh analytical balance with a set of class M mass standards,

Serial No. 29876. The calibration of this set of standards was done by the National Bureau of Standards [60]. The standards were manufactured from three materials with densities different from stainless steel, while the built-in weights of the analytical balance were made of stainless steel. This necessitated a buoyancy correction [78] for each group of standards. The calibration and the buoyancy corrections are presented in Table B-1.

TABLE B-1

CALIBRATION OF CLASS-M STANDARDS			
<u>Class M Standards</u>	<u>True Mass Correction (MG)</u>	<u>True Mass of Standards (G)</u>	<u>True Mass of Stainless Steel Weights (G)</u>
(Correction Factor to Stainless Steel Weights = 1.00001)			
100G	-0.273799	99.999729	100.000726
50G	-0.046178	49.999954	50.000454
30G	0.057515	30.000058	30.000358
20G	-0.144462	19.999856	20.000056
10G	0.022679	10.000023	10.000123
5G	-0.038297	4.999962	5.000012
3G	-0.016081	2.999984	3.000014
2G	-0.014886	1.999985	2.000005
1G	0.003517	1.000004	1.000014
(Correction Factor to Stainless Steel Weights = 1.000078)			
500MG	-0.047850	0.499952	0.499991
300MG	-0.023315	0.299977	0.300000
200MG	-0.016153	0.199984	0.200000
100MG	-0.006843	0.099993	0.100001
50MG	-0.002293	0.049998	0.050002
30MG	-0.001582	0.029998	0.030000
(Correction Factor to Stainless Steel Weights = 0.999718)			
20MG	0.010037	0.020010	0.020004
10MG	0.003766	0.010004	0.010001
5MG	0.010083	0.005010	0.005009
3MG	0.001105	0.003001	0.003000
2MG	-0.000842	0.001999	0.001998
1MG	0.014019	0.001014	0.001014

In the previous method [71] the Right-A-Weigh analytical balance was first calibrated in the weighing range near the weight of the bomb. Then applied the difference between the balance reading and the Class M standards needed to "match" the reading was applied to all weighings. It was found that the difference between the nominal balance reading (N.B.R.) and the Class M standards needed to obtain that same reading was not a constant. Therefore, in this investigation, the method of substituting weighing was adopted. The weighing procedure is as follows:

1. The balance was properly leveled. The zero point of the balance was checked and recorded.

2. The sample bomb was weighed. The nominal balance reading (N.B.R.) was taken. Care must be exercised for closing the side panel of the balance barricade. The following readings were then recorded: the barometric pressure, the temperature inside the barricade, the humidity inside the barricade.

3. The sample bomb was removed from the balance. The zero point was checked again. The class M standards (C.M.S.) were then put on the weighing pan of the balance to reproduce the balance reading in step 2. A reading was taken which gave the nominal balance reading (N.B.R.) less than the N.B.R. in 2. Additional weight, usually a 1 mg. C.M.S. was added which will give a N.B.R. higher than the N.B.R. in 2. The weight of the C.M.S. and the corresponding

N.B.R. reading were recorded. The zero point of the balance was checked and recorded. These readings were used in a computer sub-routine to calculate the true "mass" reading.

The Effect of the Variations in the Buoyancy Correction

The equation that was used for calculating the air density was taken from Barieau [2]. The compressibility factor of air was given as:

$$Z = 1. - (6.02 + 25.4y + 758.y^2) \cdot 10^{-4} \cdot P + (1.05 + 1.31y + 131.y^2) \cdot 10^{-5} \cdot (t) \cdot (P) \quad (B-4)$$

$$M = 28.968 - 10.952 \cdot y \quad (B-5)$$

$$\rho_A = \frac{P \cdot M}{Z \cdot R \cdot T} \quad (B-6)$$

where: Z = compressibility of air
 y = mole fraction of water vapor in air
 P = barometric pressure, atm.
 t = air temperature inside the balance barri-
 cade, °C.

The relative humidity reading H was taken to calculate y .

$$y = \left(\frac{H}{100 \cdot P} \right) \cdot \left(\frac{1.43 \cdot t - 11.065}{760.0} \right) \quad (B-7)$$

The equation, in which the air buoyancy corrections were taken into consideration, for calculating the mass of gas charged from the weighing bomb is:

$$M_g = \left(\rho_{AF} \cdot V_{BF} + M_{SF} \left(1 - \frac{\rho_{AF}}{\rho_S} \right) \right) - \left(\rho_{AE} \cdot V_{BE} + M_{SE} \left(1 - \frac{\rho_{AE}}{\rho_S} \right) \right) \quad (B-8)$$

where the subscription F denotes weighing at full bomb condition, E denotes weighing at the end of gas-charging.

M_g = mass of gas charge

M_S = mass of class M standards needed to balance the bomb's nominal balance reading

ρ_A = density of air

ρ_S = density of standards

V_B = volume of the bomb

It must be emphasized that the weighing procedure in this investigation was different from that adopted by Shana'a who subtracted a constant calibration number from N.B.R. instead of following the substitution weighing process as described in this section. The computation was done by a subroutine in the data treatment program.

APPENDIX C

ERROR ANALYSIS

The absolute errors in the experimental data are established in this analysis. All the errors incurred in the measurements of variables contribute to the resultant experimental errors in the liquid density.

The experimental liquid density data were determined by the following variables: temperature t , mass m , volume V , pressure P , and composition x . Thus, it can be stated as

$$\rho = \rho(t, m, V, P, x) \quad (C-1)$$

The first order terms in a Taylor expansion of ρ about the true value of density ρ_0 can be expressed as

$$\Delta\rho = \left(\frac{\partial\rho}{\partial t}\right) \Delta t + \left(\frac{\partial\rho}{\partial m}\right) \Delta m + \left(\frac{\partial\rho}{\partial V}\right) \Delta V + \left(\frac{\partial\rho}{\partial P}\right) \Delta P + \left(\frac{\partial\rho}{\partial x}\right) \Delta x \quad (C-2)$$

Because the propagation of errors does not usually result in cancellation of errors, equation (C-2) is rewritten as

$$E(\rho) = \left| \frac{\partial\rho}{\partial t} E(t) \right| + \left| \frac{\partial\rho}{\partial m} E(m) \right| + \left| \frac{\partial\rho}{\partial V} E(V) \right| + \left| \frac{\partial\rho}{\partial P} E(P) \right| + \left| \frac{\partial\rho}{\partial x} E(x) \right| \quad (C-3)$$

In the above expression $E(\rho)$ denotes the estimated error in density ρ ; similar meanings apply to $E(m)$, etc. Thus $E(\rho)$ is the sum of the absolute values of the various error terms incurred in an experimental run.

Estimation of the Partial Derivatives

The various partial derivatives were estimated by using the inherent instrument accuracies. The various term can be illustrated in Table C-1.

The effect of pressure on the density can be estimated from the compressibility data. For argon $\beta = \frac{1}{V} \left(\frac{\partial V}{\partial P} \right)_T$ was $5.5 \times 10^{-4} \text{ atm}^{-1}$ and for krypton it was $1.9 \times 10^{-4} \text{ atm}^{-1}$ at 115.77°K [21]. For krypton and xenon at 161.36°K they are assumed to be $5.5 \times 10^{-4} \text{ atm}^{-1}$ and $1.9 \times 10^{-4} \text{ atm}^{-1}$ also. The various partial derivatives for the pure component runs are presented in Table C-2.

The estimations on the partial derivatives for the binary mixture runs are presented in Table C-3. The errors in the individual instrument measurements are presented in Table C-4. In order to evaluate the partial $\left(\frac{\partial \rho}{\partial x} \right)$ the experimental data of liquid mixture density were fitted to a least square program to a quadratic function of x .

$$\rho = a_1 + a_2 + a_2x + a_3x^2 \quad (\text{C-4})$$

Estimation of Errors Incurred in Each Individual Measurement

The estimation of the errors in each individual measurement were done essentially as before [71]. The

TABLE C-1

PARTIAL DERIVATIVES FOR THE ERROR ANALYSIS

Variable, W	$\rho = \rho(W)$	Partial Derivative ($\partial\rho/\partial W$)
Temperature, t, in °C	$a+b\cdot t$	b
Mass, m, in gm.	m/V	$1/V$
Volume, V, in cm ³	m/V	$-\rho/V$
Pressure, P, in atm	$(\beta = -\frac{1}{V^2} \frac{\partial V^2}{\partial P})$	$-\beta\rho V$
Composition, x = x ₁	<u>Ar + Kr at 115.77°K</u>	
(x ₁ is the mole fraction of the more volatile component)	$2.45241 - 1.11774 x$	-1.11774
	$-.138803 x^2$	-.277606 x
	<u>Kr + Xe at 161.36°K</u>	
	$2.96816 - .728441 x$	-.728441
	$-.179159 x^2$	-.358318 x

TABLE C-2

EVALUATION OF THE PARTIAL DERIVATIVES
FOR THE PURE COMPONENT RUNS

Component	$b \times 10^2$	$(1/V) \times 10^2$	$-(\rho/V) \times 10^2$	$-\beta \rho V \times 10^2$
Argon, 115.77°K	-.779	5.19	6.21	1.27
Krypton, 115.77°K	-.734	5.19	12.7	.898
Krypton, 161.36°K	-1.03	5.18	10.7	2.18
Xenon, 161.36°K	-.675	5.18	19.4	1.09

TABLE C-3

EVALUATION OF THE PARTIAL DERIVATIVES
FOR THE BINARY MIXTURE RUNS

Mixture	x_1	$b \times 10^2$	$(1/V) \times 10^2$	$-(\rho/V) \times 10^2$	$-\beta \rho V \times 10^2$	$-(\frac{\partial \rho}{\partial x_1})$
<u>115.77°K</u>						
Argon + Krypton						
	.49377	-.734	5.19	9.67	1.36	1.25
	.71963	-.750	5.19	8.17	1.36	1.32
<u>161.36°K</u>						
Krypton + Xenon						
	.21056	-.872	5.18	14.5	1.44	.803
	.27629	-.717	5.18	14.3	1.54	.827
	.68217	-.733	5.18	12.4	2.00	.972
	.82509	-.925	5.18	11.6	2.12	1.02

TABLE C-4

ERRORS IN INDIVIDUAL MEASUREMENT

Measurement	Estimated Errors	Remarks
Temperature, Δt	$\pm .01^\circ\text{C}$	for platinum resistance thermometer
Pressure, ΔP	$\pm .167 \times 10^{-3}$ atm.	for Texas Instrument Pressure Gauge
Volume, ΔV	$\pm .3 \times 10^{-3}$ ml.	for determining the pycnometer volume and for reading the capillary graduation
Mass, Δm		Considering errors in weighing, in determining transfer line gas, and in air buoyance effect (where P is the system pressure in atm.)
pure component	$.17 \times P \times 10^{-3}$ gm.	
mixture	$.34 \times P \times 10^{-3}$ gm.	
Composition, Δx		
Ar + Kr	<div> <div>Run No. 7</div> <div>Run No. 8</div> </div> <div> <div>$.120 \times 10^{-3}$</div> <div>$.152 \times 10^{-3}$</div> </div>	
Kr + Xc	<div> <div>Run No. 15</div> <div>Run No. 16</div> <div>Run No. 12</div> <div>Run No. 17</div> </div> <div> <div>$.0621 \times 10^{-3}$</div> <div>$.0616 \times 10^{-3}$</div> <div>$.0920 \times 10^{-3}$</div> <div>$.108 \times 10^{-3}$</div> </div>	Calculated from Equation C-5

Note: The dominating error in Δm was the error incurred in determining the quantity of gas trapped in the transfer line, Δm_T . The Δm_T was evaluated from: (MW = molecular wt., Z = compressibility factor)

$$\Delta m_T = \frac{P \cdot MW}{ZRT} \Delta V + \frac{V \cdot MW}{ZRT} \Delta P + \frac{V \cdot P \cdot MW}{Z^2 RT} |(-\Delta Z)| + \frac{VP \cdot MW}{ZRT^2} |(-\Delta T)|$$

only differences that must be considered are the different ways of accounting the transfer line gases. Also because of the pressure range involved, it was necessarily higher in error in the pressure measurement. The situation can be summarized in Table C-4.

It must be emphasized that in estimating the individual errors in ΔP and Δm , the maximum possible errors were estimated in the worst conceivable situation. These values were then applied to each individual run. Thus, the error analysis was done in a conservative way. The same kind of reasoning was applied to the error in composition. The composition part deserved a little more elaboration. Because the mixture molecular weight was also function of mole fraction thus, the final equation for Δx_i is:

$$\Delta x_i = \frac{1.}{n_T} \frac{\Delta M_i}{(MW)} - x_i \Delta \frac{M_T}{(MW)_M} \quad (C-5)$$

The final absolute errors were obtained according to equation C-3. The results are presented in Table C-5.

TABLE C-5

ABSOLUTE ACCURACY OF THE EXPERIMENTAL
LIQUID DENSITY RESULTS

System	Composition, x_1	Accuracy $\times (10^4)$ gm/cm ³
<u>115.77°K</u>		
Argon + Krypton	0.0	1.12
$x_1 = x_{Ar}$.49377	4.09
	.71963	4.86
	1.0	3.07
<u>161.36°K</u>		
Krypton + Xenon	0.0	1.18
$x_1 = x_{Kr}$.21056	3.07
	.27629	3.24
	.68217	5.11
	.82509	5.76
	1.0	4.49

APPENDIX D

TRANSFER LINE GAS CALCULATIONS

In this appendix, two features are to be examined: first, the determination of the volume of the transfer line between the weighing bomb and the pycnometer (this will subsequently be called the transfer line); then, the determination of the sample gas tapped inside the transfer line during actual experimental runs. These two determinations are closely linked to the accuracy of the data. Thus, special attention was exercised in attempting to achieve the highest accuracy possible.

Determination of the Volume of the Transfer Line

The determination of the volume of the transfer line was made by using dry helium in the Burnett-type expansion between the transfer line and the bomb. It is important to note that the exact positions of the valve stems in the valve body affect the volume of the transfer line and were recorded.

The internal volume of each bomb was determined by direct differential weighing with distilled water [71]. Bomb number one has an internal volume of 560.03 cc., bomb number three, 559.92 cc. and bomb number four 559.02 cc.

A critical examination of the way Shana'a [71] obtained his transfer line volume indicates that he based his determination solely on the known volume of the pycnometer. Actually, the pycnometer volume was known only up to the stem graduation but not to the pycnometer valve. By expanding air from the pycnometer, whose volume was in doubt, to an unknown small volume of transfer line, the error involved was uncertain.

In this experiment, two Burnett-type expansions were used to determine the transfer line volume and the volume between the pycnometer valve and the pycnometer bulb. For convenience, the following notation will be used in the ensuing discussion:

B.V.	=	bomb valve
P.V.	=	pycnometer valve
V _l	=	the metering valve
P _i	=	initial pressure before expansion
P _f	=	final pressure after expansion
V _t	=	transfer line volume
V _b	=	bomb volume
V _p	=	pycnometer volume up to the pycnometer valve

Knowing the bomb volume precisely and with the bomb evacuated, two different Burnett-type expansions were then made. First with P.V. closed, a Burnett expansion from the transfer line to the bomb is sufficient to determine the transfer line volume. Next, with an evacuated bomb, a Burnett expansion

from the system including the transfer line and the pycnometer will suffice to determine the volume V_p . To illustrate the situation, consider

1. Determination of V_t :

The transfer line and the bomb were evacuated. The volume between B.V. and P.V. was filled with dry helium to P_i with V_l at two full turns. Expanding the gas into the bomb results in final equilibrium pressure of P_f . Then:

$$\frac{P_i V_t}{T_{t_i}} + \frac{P_i V_g}{T_{g_i}} = \frac{P_f V_t}{T_{t_f}} + \frac{P_f V_g}{T_{g_f}} + \frac{P_f V_B}{T_B}$$

or

$$P_i \left(\frac{V_t}{T_{t_i}} + \frac{V_g}{T_{g_i}} \right) = P_f \left(\frac{V_t}{T_{t_f}} + \frac{V_g}{T_{g_f}} + \frac{V_B}{T_B} \right) \quad (D-1)$$

Thus

$$V_t = \frac{V_g \left(\frac{P_f}{T_{g_f}} - \frac{P_i}{T_{g_i}} \right) + V_B \frac{P_f}{T_B}}{\left(\frac{P_i}{T_{t_i}} - \frac{P_f}{T_{t_f}} \right)} \quad (D-2)$$

where subscript g denotes pressure gauge bourdon tube.

Here at the initial and final conditions, the temperatures of the bourdon tube, of the room, and of the bomb were recorded. The volume of the bourdon tube was obtained from the Texas Instrument as 0.5 cc. The compressibility of helium was implicitly assumed as constant.

2. Determination of V_p :

With the bomb and the system, including the pycnometer and the transfer line, evacuated and the valve V1 at two full turns, P.V. opened at a definite position, B.V. closed, helium gas was charged to the system at P_i . After expanding the gas into the bomb, the pressure of the system was P_f . Then

$$\frac{P_i V_t}{T_{t_i}} + \frac{P_i V_g}{T_{g_i}} + \frac{P_i V_p}{T_{t_i}} = \frac{P_f V_t}{T_{t_f}} + \frac{P_f V_g}{T_{g_f}} + \frac{P_f V_p}{T_{t_f}} + \frac{P_f V_B}{T_B}$$

or

$$P_i \left(\frac{V_t}{T_{t_i}} + \frac{V_g}{T_{g_i}} + \frac{V_p}{T_{t_i}} \right) = P_f \left(\frac{V_t}{T_{t_f}} + \frac{V_g}{T_{g_f}} + \frac{V_p}{T_{t_f}} + \frac{V_B}{T_B} \right) \quad (D-3)$$

$$\therefore V_p = \frac{V_g \left(\frac{P_f}{T_{g_f}} - \frac{P_i}{T_{g_i}} \right) + V_t \left(\frac{P_f}{T_{t_f}} - \frac{P_i}{T_{t_i}} \right) + V_B \frac{P_f}{T_B}}{\left(\frac{P_i}{T_{t_i}} - \frac{P_f}{T_{t_f}} \right)}$$

or

$$V_p = \frac{V_g \left(\frac{P_f}{T_{g_f}} - \frac{P_i}{T_{g_i}} \right) + V_B \frac{P_f}{T_B}}{\left(\frac{P_i}{T_{t_i}} - \frac{P_f}{T_{t_f}} \right)} - V_t \quad (D-4)$$

The transfer line volume V_t and the pycnometer volume V_p up to P.V. were determined for both the fused quartz pycnometer and the pyrex glass pycnometer prior to the low temperature experiment.

The calibration results of the transfer line volume determinations can be presented in two parts. The first part is for the quartz pycnometer and the second part for the Pyrex pycnometer. For each determination, two experimental expansions were made. The accuracy of the transfer line volumes are believed to be within 0.1 ml.

Transfer Line Volumes

$V_t + V_p$, ml		V_t , ml
<hr/>		<hr/>
Quartz Pycnometer	42.300	10.806
Pyrex Pycnometer	30.190	9.071
<hr/>		<hr/>

The reason that there is a slight difference between the two V_t values is because in the low pressure calibration run using the quartz pycnometer it was necessary to branch out a low pressure relief valve line. Thus, the V_t for quartz pycnometer actually included this extra valve line volume.

Determination of the Sample Gas Trapped Inside the
Transfer Line and the Dead-Space in Pycnometer

Determination of the sample gas trapped inside the transfer line and the dead-space in pycnometer was simpler in the case of the one component experiment than in the case of the binary mixture experiment. For a pure component, the information required are the temperatures of the various

parts of the transfer line and the dead-space. These are as follows:

1. The transfer line between B.V. and P.V.
excluding the Bourdon tube volume.
Volume = V_t , Temperature = T_t .
2. The Bourdon tube of the Texas Instrument
pressure gauge, Volume = V_g , Temperature = T_g .
3. The dead-space between P.V. and the liquid
level inside the pycnometer, Volume = V_p ,
Temperature = T_p .

For the binary mixture, it is necessary to consider the nonideality of the gas mixture and also its degree of homogeneity. Considering that there are n_v moles gases trapped in the transfer line and the dead-space, a thermodynamic analysis yields:

$$\mu_i^E = RT \ln \gamma_i = RT \ln \left(\frac{y_i P}{x_i P_i^0} \right) + (V_i^L - B_{ii}) (P - P_i^0) + P \delta_{12} (1 - y_i)^2 \quad (D-5)$$

$$\text{where } \delta_{12} = 2 B_{12} - (B_{11} + B_{22})$$

The effect of including third virial coefficient on G^E is about 0.03 cal/mole as compared to an error of 20 cm³/mole in second virial coefficient will change G^E by 0.02 cal/mole [21]. Further, the third virial coefficient may differ by a factor of 2. These considerations resulted in the exclusion of the third virial coefficient from the analysis. However, the following form of virial equation was adopted:

$$\frac{PV}{RT} = 1. + B \cdot \left(\frac{P}{RT}\right) + (C-B^2) \left(\frac{P}{RT}\right)^2 = 1. + B \left(\frac{P}{RT}\right) - B^2 \left(\frac{P}{RT}\right)^2 \quad (D-6)$$

Following Van Ness [89] the vapor phase activity coefficient can be rederived as:

$$\begin{aligned} \ln \gamma_1^v &= \ln \hat{\phi}_1 - \ln \phi_1 = \ln \phi + y_2 \cdot \left(\frac{\partial \ln \phi}{\partial y_1} - \frac{\partial \ln \phi}{\partial y^2} \right) - \ln \phi_1 \\ &= \left(y_2^2 \delta_{12} \right) \left(\frac{P}{RT} \right) - \frac{1}{2} \left(\frac{P}{RT} \right)^2 \left(2B_M (B_{11} + y_2^2 \delta_{12}) - B_M^2 - B_{11}^2 \right) \end{aligned} \quad (D-7)$$

$$\begin{aligned} \ln \gamma_1 &= \ln \left(\frac{y_1 P}{x_1 P_1^o} \right) - \left\{ \left[\frac{(V_1^L - B_{11}) (P - P_1^o)}{RT} + \frac{B_{11}^2 (P^2 - P_1^{o2})}{2 (RT)^2} \right] \right. \\ &\quad \left. - \frac{y_2^2 \delta_{12} P}{RT} + \frac{y_2^2 \Delta_1 P^2}{2 (RT)^2} \right\} \end{aligned} \quad (D-8)$$

$$\text{or} \quad \gamma_1 = \left(\frac{y_1 P}{x_1 P_1^o \beta_1} \right)$$

$$\begin{aligned} \ln \gamma_2 &= \ln \left(\frac{y_2 P}{x_2 P_2^o} \right) - \left\{ \left[\frac{(V_2^L - B_{22}) (P - P_2^o)}{RT} + \frac{B_{22}^2 (P^2 - P_2^{o2})}{2 (RT)^2} \right] \right. \\ &\quad \left. - \frac{y_1^2 \delta_{12} P}{RT} + \frac{y_1^2 \Delta_2 P^2}{2 (RT)^2} \right\} \end{aligned} \quad (D-9)$$

$$\text{or} \quad \gamma_2 = \left(\frac{y_2 P}{x_2 P_2^o \beta_2} \right)$$

where

$$\begin{aligned} \Delta_1 &= (1. - y_2^2) \delta_{12}^2 + 2B_{22} \delta_{12} + B_{11}^2 + B_{22}^2 \\ \Delta_2 &= (1. - y_1^2) \delta_{12}^2 + 2B_{11} \delta_{12} + B_{11}^2 + B_{22}^2 \end{aligned} \quad (D-10)$$

The expression of the total number of mole of the transfer gas is given by

$$\begin{aligned}
 n_t &= \frac{P}{R} f\left(\frac{V}{T}\right) = \frac{P}{R} \left(f_{\text{gage}} + f_{\text{room temp.}} + f_{\text{pycnom. capillary}} \right) \\
 &= \frac{P}{R} (f_g + f_t + f_\ell)
 \end{aligned} \tag{D-11}$$

where the three f functions are given as:

$$\begin{aligned}
 f_g &= \left(\frac{V_g}{T_g} \right) \cdot \left(1. + B_M(T_g) \cdot \left(\frac{P}{R \cdot T_g} \right) - \left(B_M(T_g) \right)^2 \cdot \left(\frac{P}{RT_g} \right)^2 \right)^{-1} \\
 f_t &= \left(\frac{V_t}{T_t} \right) \cdot \left(1. + B_M(T_t) \cdot \left(\frac{P}{R \cdot T_t} \right) - \left(B_M(T_t) \right)^2 \cdot \left(\frac{P}{RT_t} \right)^2 \right)^{-1} \\
 f_\ell &= \left(\frac{V_t - V_P}{T_\ell} \right) \cdot \left(1. + B_M(T_\ell) \cdot \left(\frac{P}{R \cdot T_\ell} \right) - \left(B_M(T_\ell) \right)^2 \cdot \left(\frac{P}{RT_\ell} \right)^2 \right)^{-1}
 \end{aligned} \tag{D-12}$$

with $T_1 = 0.5 (T_t + (T \text{ of the cryostat}))$, that is, the capillary temperature was assumed to be the average of the room temperature and cryostat temperature.

Now, by assuming that

$$\ln \gamma_i = a(1.-x_1)^2 \rightarrow \gamma_i = 1. + a \cdot (1.-x_i)^2, \quad i = 1, 2 \tag{D-13}$$

The elimination of the constant "a" resulted in

$$(2x_i - 1.) + (1.-x_i) \cdot \frac{P}{P_2^0} \frac{1}{\beta_2} + x_1 y_1 \left(\frac{P}{P_2^0} \frac{1}{\beta_2} - \frac{P}{P_1^0} \frac{1}{\beta_1} \right) - y_1 \left(\frac{P}{P_2^0} \right) \left(\frac{1}{\beta_2} \right) = 0. \tag{D-14}$$

Now from the following mass balance equations:

(1) Total mass balance on component 1:

$$n_t x_1' = n_l \cdot x_1 + n_v \cdot y_1 \quad (D-15)$$

(2) Transfer line gas equation:

$$P \cdot f\left(\frac{V}{T}\right) = R \cdot n_v \quad (D-16)$$

$$\therefore y_1 = \frac{n_t \cdot x_1' \cdot R}{P \cdot f(V/T)} - \frac{n_t \cdot x_1 \cdot R}{P \cdot f(V/T)} + x_1 \quad (D-17)$$

The elimination of y_1 resulted in a quadratic equation of x_1 :

$$A \cdot x_1^2 + B \cdot x_1 + C = 0 \quad (D-18)$$

with

$$A = (P_1^o \beta_1 - P_2^o \beta_2) \cdot \left(\frac{P \cdot f(V/T)}{n_t \cdot R} - 1. \right)$$

$$B = P_1^o \beta_1 \left(1. + \frac{2 \cdot f(V/T)}{n_t \cdot R} \cdot (P_2^o \beta_2 - P) \right) + x_1' (P_1^o \beta_1 - P_2^o \beta_2)$$

$$C = -P_1^o \beta_1 \left(\frac{f(V/T)}{n_t \cdot R} \cdot (P_2^o \beta_2 - P) + x_1' \right)$$

This final form has been given by Staveley, et al. [54]

also. Here, the $f(V/T)$ and β_1 are different from theirs.

In the data treatment, the first approximation of y_1 was obtained by assuming $x_1 = x_1'$ and $y_1 = x_1' P_1^o / P$. where P_1^o was calculated from the Antoine constants obtained in this investigation. The mole fraction x_1 was solved, the corresponding y_1 was calculated from Equation D-17. This value of y_1 was then used to calculate $f(V/T)$. The value

of x_1 was recalculated, and y_1 recalculated. This step was repeated until the change in y_1 was less than 10^{-5} .

The second virial coefficient for argon, krypton, and xenon were obtained by using the equation given by Guggenheim, which is based on the square well potential:

$$\frac{B}{V_c} = 0.440 - 1.40 \cdot \left(1. - \exp\left(0.75 \cdot \frac{T_c}{T}\right) \right) \quad (D-19)$$

with the constants given as

	V_c cm ³ /mole	T_c , °K
argon	75.3	150.7
krypton	92.1	209.4
xenon	100.3	191.1

This equation was used to calculate B_{11} , B_{22} , and B_{12} . For calculating B_{12} , the investigation critical properties were obtained by using the following mixing rules:

$$V_{c12} = \frac{1}{2} (V_{c11} + V_{c22}) \quad (D-20)$$

$$T_{c12} = \sqrt{T_{c11} \cdot T_{c22}} \cdot \left(\sqrt{I_1 \cdot I_2} \cdot \left(0.5 \cdot (I_1 + I_2) \right)^{-1} \right) \quad (D-21)$$

where I is the ionization potential. As shown by Weir, Wyne Jones, Rowlinson and Saville [93], the root-mean-square residuals for the best fit curve based on quantum corrected Lennard-Jones (12:6) potential for argon was 5.6 cm³/mole, and for krypton was 10.3 cm³/mole. From figure 5 of Weir, et al. and from figure 3 of Byrne, Jones, and Staveley [11]

the Guggenheim equation predicted B_{11} for argon at 115.77°K within 4 cm³/mole out of its value of about -145. cm³/mole, and predicted B_{22} for krypton within 4 cm³/mole out of its value of -335. cm³/mole at 115.77°K. The same equation predicted krypton second virial coefficient at 161.36°K within 4 cm³/mole out of its value of about -175 cm³/mole. It was reported by Guggenheim [31] that the equation is good for predicting the second virial coefficient of argon, krypton, and xenon from high T/T_c down to $T/T_c = 0.5$ (82° to 1223°K for argon, 108° to 873°K for krypton). In the case of xenon, there were no experimental data available for comparison at 161.36°K. Thus, the equation given by Guggenheim was adopted in the data treatment.